(2)

A STUDY OF THE BEHAVIOR AND MICROMECHANICAL MODELLING OF GRANULAR SOIL

VOLUME II

AN EXPERIMENTAL INVESTIGATION OF THE BEHAVIOR OF GRANULAR MEDIA UNDER LOAD

by

Emmanuel Petrakis
Ricardo Dobry
Paul Van Laak
Panos Kotsanopoulos

Prepared under Contract No. AFOSR-89-0350
United States Air Force
Office of Scientific Research
Bolling Air Force Base

Department of Civil Engineering
Rensselaer Polytechnic Institute
Troy, NY 12180-3590

May 1991

REPORT DOCUMENTATION PAGE

Form Approved
OMB No. 0704-0188

1. AGENCY USE ONLY (Leave blank)	2. REPORT DATE	3. REPORT TYPE AND DATES COVERED
	May 22, 1991	Final 1/6/89-5/15/91

4. TITLE AND SUBTITLE
A Study of the Behavior and Micromechanical Modelling of Granular Soil
Volume 2

5. FUNDING NUMBERS
Grant AFOSR-89-0350
PR 2302/C1

6. AUTHOR(S)
Emmanuel Petrakis, Ricardo Dobry, Paul Van Laak, Panos Kotsanopoulos, Tang-Tat Ng, and Li Liu

7. PERFORMING ORGANIZATION NAME(S) AND ADDRESS(ES)
Civil Engineering Department
Rensselaer Polytechnic Institute
Troy, NY 12180-3590

8. PERFORMING ORGANIZATION REPORT NUMBER

9. SPONSORING/MONITORING AGENCY NAME(S) AND ADDRESS(ES)
AFOSR/NA
Bldg. 410
Bolling AFB
Washington, DC 20332-6448

10. SPONSORING/MONITORING AGENCY REPORT NUMBER
AFOSR-89-0350

11. SUPPLEMENTARY NOTES

12a. DISTRIBUTION/AVAILABILITY STATEMENT
Approved for Public Release; Distribution Unlimited

12b. DISTRIBUTION CODE

13. ABSTRACT (Maximum 200 words)

A comprehensive research effort has been conducted on constitutive and micromechanical modelling of granular soil. This includes: 1) the development of a new constitutive relation for granular media based on the contact law between two spheres; 2) an experimental investigation on the stress-strain response of a glass bead material with 46 monotonic and cyclic experiments on hollow cylinder specimens, most of them constant mean stress tests to measure deviatoric response and behavior of initial and subsequent yield loci; and 3) numerical simulations of the behavior of granular media using the discrete element method.

The proposed constitutive law captures a number of key aspects of the observed stress-strain behavior of granular soils, and it predicts well the experiments on glass beads. Novel aspects of the proposed model include yield cones parallel to the failure envelope, and a basic relation between the field of elastoplastic moduli and the elastic constants of the material.

14. SUBJECT TERMS	15. NUMBER OF PAGES
Micromechanics; Constitutive Law; Granular Media; Sand; Yield Surface Distortion; Hollow Cylinder Experiment; Discrete Element Simulations; Plasticity	16. PRICE CODE

17. SECURITY CLASSIFICATION OF REPORT	18. SECURITY CLASSIFICATION OF THIS PAGE	19. SECURITY CLASSIFICATION OF ABSTRACT	20. LIMITATION OF ABSTRACT
Unclassified	Unclassified	Unclassified	UL

The report consists of three volumes, as follows:

Volume I: "A Constitutive Law for Granular Materials Based on the Contact Law Between Two Spheres," by R. Dobry and E. Petrakis.

Volume II: "An Experimental Investigation of the Behavior of Granular Media Under Load," by E. Petrakis, R. Dobry, P. Van Laak, and P. Kotsanopoulos.

Volume III: "A Numerical Investigation of the Behavior of Granular Media Using Nonlinear Discrete Element Simulations," by E. Petrakis, R. Dobry, T.-T. Ng, and L. Liu.

TABLE OF CONTENTS

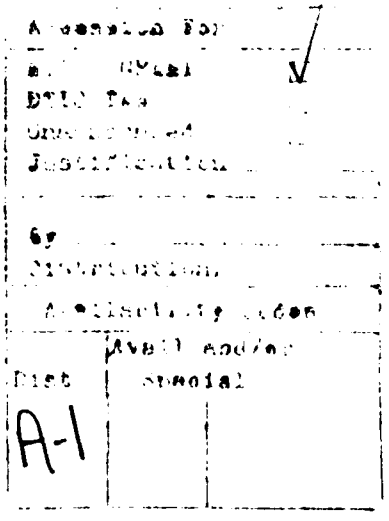

LIST OF SYMBOLS

Greek letters

α	:	intercept of a straight line
β	:	slope of a straight line
γ_{oct}	:	octahedral shear strain
γ_t	:	threshold strain
$\gamma_{z\theta}$	:	shear strain
δ	:	direction angle of distortion strain
ϵ_i	:	principal strains (i = x, y, z)
$\epsilon_{\theta\theta}$	:	circumferential strain
ϵ_{rr}	:	radial strain
ϵ_v	:	volumetric strain
ϵ_{zz}	:	axial strain
ϵ_{11}	:	major principal strain
ϵ_{22}	:	intermediate principal strain
ϵ_{33}	:	minor principal strain
θ	:	angle of shear direction
θ	:	rotation of the specimen relative to the base
ξ	:	dimensionless octahedral shear stress ($\xi = \tau_{oct}/\sigma_m$)
π	:	3.14159
σ_{axial}	:	axial normal stress
$\sigma_{\theta\theta}$	:	tangential normal stress

σ_c : confining pressure

σ_m : mean normal stress

σ_{rr} : radial normal stress

σ_{zz} : axial normal stress

σ_{11} : major principal stress

σ_{22} : intermediate principal stress

σ_{33} : minor principal stress

τ : shear stress

τ_{oct} : octahedral shear stress

$\tau_{z\theta}$: horizontal shear stress

ϕ : friction angle

ω : inclination angle of the major principal stress relative to the direction of specimen deposition

Latin Letters

B : pore pressure parameter

b : parameter reflecting the change of the intermediate principal stress

D_r : relative density

e : void ratio

e_{max} : maximum void ratio

e_{min} : minimum void ratio

F : axial force

H : specimen height

H_i : height of the i layer

i : number of layer

K_f : failure line

m : number of slip directions

N : number of cycles

n : number of slip planes

n : total number of layers

p : mean of major and minor principal stresses ($p = (\sigma_{11}+\sigma_{33})/2$)

q : maximum shear stress ($q = (\sigma_{11}-\sigma_{33})/2$)

R_i : inside radius specimen

R_o : outside radius specimen

T : torque

U_n : undercompaction value of the bottom layer

U_{ni} : undercompaction value of the i layer

U_{nt} : undercompaction value of the top layer

V_a : volumetric strain

ACKNOWLEDGEMENTS

The authors wish to acknowledge the following people and organizations for their valuable assistance in this study:

The Air Force Office of Scientific Research, and especially Lieutenant Colonel Steven C. Boyce for their continued support throughout this research

Professor Felix Darve, of the Institute de Mecanique de Grenoble, Grenoble, France, Director of GRECO, for providing advice on the modelling aspects of the yield surface distortion, information and assistance regarding experiments on sand, exchanging ideas on the subject of testing and modelling granular media

Professor James Jenkins of the Department of Theoretical and Applied Mechanics of Cornell University, Ithaca, NY, for his invaluable discussions and exchange of information regarding the drained behavior of granular media

Professor J. Lanier of the Institute de Mecanique de Grenoble, Grenoble, France for providing information and ideas on the drained behavior of sand

Professor Isao Ishibashi of the Department of Civil Engineering of Old Dominion University, Norfolk, VA for providing information on the drained behavior of granular media

Professor Yehia Bahei El-Din of the Department of Civil Engineering RPI, Troy, NY for his stimulating discussions on the subject of experimentally defining yield surfaces in metals and composite materials

Professor E.H. Lee of the Department of Mechanical, Aeronautical Engineering and Mechanics, of RPI, Troy, NY for his help and advice regarding the yield surface measurements

Professor Erhard Krempl, Chairman, Department of Mechanical, Aeronautical Engineering and Mechanics, of RPI, Troy, NY for his help and advice regarding the experimental aspects of yield surface testing

Professor Dimitri Lagoudas of the Department of Civil Engineering RPI, Troy, NY for stimulating discussions

Professor Elias Aifantis of the Department of Mechanical Engineering, Michigan Technological University, Houghton, MI, for his interest and support, ideas and discussions regarding modelling of local failure in granular media

Professor Yiannis Vardoulakis, of the Department of Applied Mechanics of the National Technical University, Athens, Greece for his stimulating discussions

Professor Adel Saada, Chairman of the Department of Civil Engineering CWRU, for his advice, discussions and exchange of ideas regarding the drained behavior of sand and membrane compliance testing and for sharing his experimental data with us

Dr. Don Helling of Hughes Aircraft, for sharing his experience on investigating the yield surfaces of metals
Dr. Mike Stout of Los Alamos National Laboratories, for his invaluable information on the subject of experimentally defining yield surfaces in engineering materials

The Department of Applied Mechanics of the Aristotelian University of Thessaloniki for the hospitality and facilities provided to E. Petrakis' while Visiting Assistant Professor during 1990.

Group Captain A. Economou, Commander, Squadron Leader N. Vourliotis, of 113 Fighter Wing, Greek Air Force, for their help and support during E. Petrakis' service at 113 Fighter Wing in 1990.

Mr. Victor Taboada and Ms. Min Fan, graduate students in the Department of Civil Engineering at RPI for their assistance in preparing this document.

CHAPTER 1

INTRODUCTION

The main objective of this experimental work is to determine the experimental parameters necessary for formulating a constitutive law for granular media based on micromechanics which is the subject of Volume I of this AFOSR report. These parameters include the hardening7 characteristics of the yield surfaces of the granular medium under various levels of prestrain, and the observed normality and flow rule. For this, a number of experiments was performed under specific stress paths on hollow cylindrical samples of glass beads. Moreover, numerical simulations were performed on random arrays of elastic, rough spheres to provide an insight on the micromechanical phenomena influencing aspects of the macroscopic behavior and are presented in this volume. The underlying concept of the experimental procedure followed is that random packings of equal and quasi-equal spheres have characteristics similar to those of *pressure dependent* polycrystalline aggregates. For example, regular arrays of identical, rough, elastic, spheres have been shown to behave like pressure dependent monocrystals (Petrakis and Dobry, 1986). Furthermore, random arrangements of these regular arrays have been used successfully to predict the small strain behavior of Ottawa sand by means of the Self Consistent and nonlinear Finite Element techniques (Petrakis and Dobry, 1987a, 1987b) Finally, recent distinct element simulations (Petrakis et al 1988) have demonstrated the actual occurrence of crystallization while at the same time being in excellent agreement with the other methods used. Therefore, it is useful, from the viewpoint of development of a constitutive law for granular soil, to review some findings on polycrystalline aggregates such as metals.

1.1 Micromechanical Studies in Polycrystalline Aggregates

Starting in the 1950's, researchers have been simulating the elastic-plastic behavior of polycrystalline aggregates, such as metals, through analytical, semi-analytical, and numerical micromechanical techniques (Hershey 1954, Hill 1967, Budiansky and Wu 1962, Lin and Ito 1965, 1966, Canova et al. 1985). This micromechanical work has not fully supported either of the continuum mechanics hypotheses of kinematic or isotropic strain hardening behavior, but has predicted instead a combined translation and distortion of the yield surfaces in the direction of loading. This micromechanical prediction has been verified by several experiments (Naghdi et al. 1958, Phillips 1968). The micromechanical approach commonly used to analyze the elastic-plastic behavior of polycrystals, is to assume that they are an assemblage of equal isotropic monocrystals (single crystals) randomly oriented in space (Fig. 1). This results in an isotropic polycrystal when the distribution of the orientations is statistically uniform. A monocrystal has n slip planes, with each plane having m slip directions, and with every direction corresponding to a pair of parallel yield planes in stress space. In the limiting case in which an infinite number of possible crystal orientations is assumed, this infinitely sided polyhedron becomes a curved yield surface.

Plastic strain in the aggregate is caused by slip of one of the slip planes occurring in a family of similarly oriented crystals. After slip has occurred in a number of these families, each surface of yield polyhedron mentioned above expands and shifts differently. These slip directions are all more or less parallel to the direction of the plane of the maximum shear stress acting on the

aggregate. As the aggregate is loaded farther beyond the elastic range, more crystals and crystal families slide (slip), and increasingly more yield planes pass through the loading point on the yield surface. These yield planes of different orientations intersect at that point on the yield surface and form a corner or vertex (Fig. 1).

This vertex, which is particularly important for the stress-strain modeling of cyclic loading, is not easily observed during testing. The reason is that the very large number of monocrystal orientations smooths the effect, which appears as a "smooth vertex" or distortion of the yield surface in the direction of loading, instead of a sharp corner. The distortion of the yield surface associated with the vertex reflects the "memory" the material has of the prestraining in the direction of loading. The existence of this yield surface distortion in metals has been observed experimentally by many researchers in several polycrystalline aggregates, including aluminum, aluminum alloys, brass, and magnesium (Naghdi et al. 1958, Phillips 1968, Kelley and Hosford 1968, Phillips et al. 1970, 1972, Shiratori et al. 1976, Helling et al. 1986).

The late Professor Phillips developed a testing procedure to seek and compute the initial and subsequent yield surfaces of aluminum and their motion in stress space. This procedure is now widely used in experimental plasticity studies of metals and metal matrix composites (Dvorak 1987, Dvorak et al. 1988, Stout et al. 1985). The experiments are typically conducted by applying a combination of axial and torsional stresses to a hollow cylindrical specimen, in the sequence shown in Fig. 2 . In these tests, the loading stops and reverses as soon as a point on the yield surface is reached, so that the entire yield surface may be determined. Yielding is defined as the deviation from the linear region of the stress strain curve by a certain amount of offset. The micromechanical mechanism that causes this first deviation from nonlinearity is the first incidence of slip in one of the monocrystals comprising the aggregate. Figure 3 clearly shows the characteristic distortion of the initial yield surface in the direction of loading. While the initial yield surface (for a given temperature) in the τ–σ_a space is an ellipse, the subsequent yield surfaces have distorted and become pointed in the direction of the loading (a), while becoming flatter in the opposite direction (b).

Laboratory results such as these have made possible the linking of the micromechanical theory with experiments (Stout et al. 1985) and have led to a new family of constitutive laws (Phillips and Weng 1975, Eisenberg and Yen 1981, 1984, and Yen and Eisenberg 1987, Voyiadjis and Foroozesh 1990) which incorporate the above findings.

1.2 Micromechanical Behavior of Granular Soil

The behavior of sand aggregate is very similar to that of polycrystals since the individual grain packings within the sand may be considered in first approximation to behave like randomly oriented crystals. However, a main difference is that the properties of these grain packings are now pressure dependent and the amount of slip in each of these packings, in contrast to the polycrystalline aggregates, depends on the normal pressure acting on the slip[1] plane. For

---

[1] Notice that the word "slip" in granular media has a different meaning than "slip" occurring in polycrystalline aggregates. "Slip" in granular media refers to the gradual movement taking place at the edges of the contact annulus between particles which leads to "gross sliding"

example, a simple cubic array of equal spheres (Fig. 4) is a pressure dependent monocrystal with three sliding planes (n=3), and with each plane containing two sliding directions (m=2). Also the sand may experience dilation under shear which is not present in polycrystalline aggregates. Unlike metals (such as those tested by Phillips) soils exhibit nonlinear inelastic stress-strain behavior even at very small strains. Therefore, strictly speaking, a cohesionless aggregate does not have a clear "linear elastic region" defined by an initial yield surface. However, up to the threshold strain (Fig. 5; Dobry et al. 1982), a granular soil exhibits a nondestructive behavior, characterized by inelasticity at the intergranular contacts, but without gross sliding between particles. Therefore, one possible definition of an initial yield surface in a cohesionless soil is the locus of all points in stress space at which gross sliding between particles starts. Since this may be difficult to achieve in the laboratory, the yield surface may be defined as the locus of all points in stress space having a certain value of octahedral shear strain (close to the threshold); this approach has been recently adopted by Peters (1988; see Fig. 6).

1.3 Brief Review of Constitutive Relations in Soils.

Over the past 30 years considerable attention has been given to the development of constitutive laws for engineering materials (Hill 1950, Prager 1955, Mroz 1967, Dafalias and Popov 1976, Drucker and Palgen 1981). Among other formulations the existing models are based on the theories of elasticity, hypoelasticity, plasticity, and viscoplasticity. Despite the large number of models there has been no consensus within the research community on the best approach. However, the models based on the theory of plasticity or viscoplasticity appear to be the most promising.

Some of the most popular and widely used models for sand have been based on the "cap model" of DiMaggio and Sandler (1976). As versatile as "cap" models may be, they have not been successful in accurately modeling monotonic and cyclic conditions. Similar limitations apply to other models (Baladi and Rohani, 1979), and it can be argued that the existing plasticity models of the "cap" type are only adequate for monotonic loading of isotropic soil. In an effort to overcome this, a variety of constitutive laws have been proposed which incorporate a combination of isotropic and kinematic hardening (Mroz 1967), either in a two (Dafalias and Popov 1976) or multiple yield surface context (Mroz 1967, Lade 1977). Although these more recent theories represent a considerable advancement over the "cap" models, they too have drawbacks. These include the use of "a priori" hardening rules, and the inability to take into account either the prestraining effect after load reversals or the inherent, elastic anisotropy of the soil. This elastic (inherent) anisotropy which is most significant for anisotropically consolidated sand, has been measured in sand by Stokoe and his co-workers (Knox et al. 1982, Koppermann et al. 1982), while Dafalias (1979) has discussed its modeling implications. Finally, all of the above existing plasticity models for soils are phenomenological; their formulation depends on the interpretation of the macroscopic results by the researcher and not on micromechanical

---

when the contact fails. Therefore, there is no corresponding term to the interparticle "slip" in polycrystalline aggregates. The term analogous to "slip" in polycrystals is "gross sliding" at the interparticle contacts. This *gross sliding* results in particle motion and is responsible for geometric changes in the fabric of the particulate medium. It manifests itself macroscopically as irreversible volumetric change or pore pressure increase.

principles. As such, they are in need of constant refinement when needed for cases very different from the one the model was originally developed and calibrated for.
The current situation in metal plasticity is quite different. Although it is true that modeling of the nonlinear behavior of metals started on a similar phenomenological basis, there has been a later shift toward formulating the metal response with due consideration to basic micromechanical principles. Recently, this has been enhanced by specific experiments and micromechanical (electron microscopy) measurements (Stout et al. 1985, Helling et al. 1986). The situation is analogous in the modeling of more complex composite materials, where experiments and micromechanical analytical simulations are combined to create the corresponding constitutive law (Dvorak 1987, Dvorak et al. 1988).

Although metal properties are not pressure dependent and their symmetry does not change as much with loading as in soils, the stress-strain behavior of metals and soils is in many respects similar. As a result, most current soil plasticity models are modified versions of popular phenomenological metal models. Notable examples include the Mroz (1967) model for metals and the Prevost (1978) model for undrained loading of clay, as well as the bounding surface model used by Dafalias and Popov (1976) for metals and subsequently adapted to soils by Dafalias and Herrmann (1982). Unfortunately, no plasticity model exists for soils resulting from the combination of specific laboratory experiments and micromechanical principles including numerical simulations of granular arrays.

1.4 Scope and Objective of this Work

The objective of this work is to provide the experimental foundation for a new constitutive law for granular soils, of which the plasticity model presented in Volume I is the first step. For this purpose a series of specific experiments, similar to those described by Phillips et al (1968), and to a lesser extent, to those of Sture et al. (1987), were performed on samples composed of glass beads. Since the concept of the yield surface, or yield function, is central to plasticity theory, the shapes of the initial yield surfaces were defined and measured on distinct, but identical specimens. As a second step, the motion and shape of these yield surfaces after prestraining was also obtained by a series of cyclic experiments on the same specimen. Thus, the effect of stress induced anisotropy could be measured. It is believed that micromechanical interactions are responsible for the macroscopic behavior of granular media, through mechanisms which are similar to those in polycrystalline aggregates such as metals.

CHAPTER 2

TEST EQUIPMENT

2.1 General

The purpose of this experimental work is to investigate the deformation characteristics of granular media under load necessary for the development of a micromechanically based constitutive law. For this, experiments are performed on long, thin, hollow cylindrical specimens made out of glass beads. Each specimen is first consolidated isotropically by having the same internal and external pressure, σ_c, and then is subjected to shear by a combination of axial and torsional loads, always under drained conditions. The testing program included tests along proportional and non-proportional stress paths and investigations on the shape of the yield surfaces and their motion, expansion, and distortion in the stress space due to loading. In any given test, the mean stress is kept constant and equal to the consolidation pressure during the shear stage. Therefore all the experimental data from the test are on one π-plane in the stress space.

2.2 The Hollow Cylinder in Experimental Studies

Hollow cylindrical specimens have been tested extensively in materials research. Taylor and Quinney (1931) and Goode and Helmy (1967) tested metal and concrete elements, respectively, under combined axial force and torque. Hollow cylinders of soils were tested first by Cooling and Smith (1936) who subjected unconfined elements to torque. Since then, hollow cylindrical soil specimens have been used by many researchers, employing a greater control of applied stresses and strains and taking advantage of the features hollow cylinder offers, to investigate different aspects of soil behavior.

Kirkpatric (1957) investigated the influence of the confining pressure on the failure of sand. Whitman and Luscher (1962) studied the strength characteristics of hollow cylinders of sand, and Broms and Jamal (1965) and Ersig and Bembem (1965) investigated the failure conditions in sands. Different aspects of strength and deformation of clays have been examined. Broms and Ratnam (1963) studied the effect of anisotropic consolidation, Broms and Casbarian (1965) investigated the effect of confining pressure and direction of principal stress on strength. Tensile deformations was examined by Suklje and Drnovesk (1965), and the effect of anisotropy was studied by Saada and Baah (1967).

Drnevich (1972) developed a hollow cylinder resonant device and studied the influence of shearing strain on shear modulus and damping of soils. Both Yoshimi and Oh-Oka (1973), and Ishibashi and Sherif (1974) used in their studies shorter hollow cylindrical specimens having different heights at the outside and inside diameters to generate uniform shear strains. More recently, Hight, Gens, and Symes (1983) designed and built a hollow cylinder test apparatus to investigate the effect of principal stress rotation in sands and clays. Ladd and Silver (1975) noted that, because the shearing stresses on each boundary are not the same, all initial stresses cannot be uniform throughout the specimen. Wright, Gilbert, and Saada (1978) discussed the

potential development of radial forces and shearing stresses on the surfaces of hollow cylindrical samples whenever there is a tendency of changing volume or height at constant volume.

Based on St. Venant's principle for isotropic elastic materials, the extent of these radial shear forces decreases with the distance from the surfaces of the specimen. Wright et al. (1978) proposed the following criteria, which were also verified by a linear finite element study by DeNatale et al. (1981), for selecting a specimen configuration in which exists a central zone free from end effects:

$$R_i / R_o > 0.65 \qquad (2.1)$$

$$H \geq 5.44\sqrt{R_o^2 - R_i^2} \qquad (2.2)$$

where R_i is the inside radius, R_o is the outside radius, and H is the height of the specimen.

Concluding, the thin, long, hollow cylinder subjected to a combination of axial and torsional stresses in addition to spherical stresses is a valuable tool in material studies when rotation of principle stresses is necessary. When both inner and outer pressure are equal, the thin walls practically guarantee (away from the ends) the equality of radial, σ_{rr}, and tangential, $\sigma_{\theta\theta}$, stress to the cell pressure, σ_c, across the specimen thickness. The shearing stress due to torsion does vary across the thickness, but this variation can be minimized by making the walls as thin as possible; thus a uniform distribution of the shear stresses can be reasonably assumed. End effects can be minimized by using long cylinders.

2.3 Stresses and Strains in Hollow Cylindrical Specimens

All experiments were performed on hollow cylindrical specimens having the same inner and outer pressures, σ_c. In this case, the axial stress, σ_{zz} (Fig. 7), is given by :

$$\sigma_z = \frac{F}{\pi(R_o^2 - R_i^2)} + \sigma_c \qquad (3.3)$$

in which F is the axial force, R_o is the outside radius, and R_i is the inside radius. The other normal stresses, i.e. the radial, σ_{rr}, and tangential, $\sigma_{\theta\theta}$, are always equal to the cell pressure, σ_c:

$$\sigma_{rr} = \sigma_{\theta\theta} = \sigma_c \qquad (2.4)$$

If the torsional shear stress is assumed to increase linearly with increasing specimen radius, the average shear stress, $\tau_{z\theta}$, over the cross-section of the specimen is given by:

$$\tau_{z\theta} = \frac{3T}{2\pi(R_o^3 - R_i^3)} \qquad (2.5)$$

in which T is the applied torque.

The shear strain (Fig. 7) also increases linearly with the radius. The average shear strain is obtained by:

$$\gamma_{z\theta} = \frac{2\theta(R_o^3 - R_i^3)}{3H(R_o^2 - R_i^2)} \qquad (2.6)$$

where θ is the rotation of the specimen relative to the base and H is the specimen height.

2.4 Loading and Measuring Systems

The available cyclic loading equipment is located in the Class 1933 Earthquake Engineering and Cyclic Loading Laboratory. This laboratory houses an MTS electro-servohydraulic closed loop testing system connected to an axial/torsional frame and a modified NGI Direct Simple Shear testing device. The computer system is a MACSYM-2 computer made by Analog Devices. It is built around the 8086 Intel processor and uses a 16-bit bus and the Intel 8087 co-processor for computing. At the front end of it has an Intel 8088 chip for fast data acquisition and control from the ten available channels. Figure 8 sketches the configuration of this computer controlled axial/torsional testing system.

The axial/torsional MTS system can perform cyclic tests in both axial and torsional modes, alone or combined. Each mode can be applied either monotonically (increasing or decreasing) or cyclically, in stress or strain control. In either mode, the load or displacement may be held constant while the loading is varied in the other mode. In addition, if a combined cyclic axial-torsional triaxial test is desired, the two modes (axial and torsional) may be used at the same frequency with an arbitrary phase shift which can be anywhere between 0 and 360 degrees.

The applied axial load is monitored by a load cell and changes in the axial force of order of 4.45×10^{-3} KN can be measured. Vertical (axial) deformation in the specimen is measured by LVDT (Linear Variable Differential Transformer) located at the top of the loading piston. The resolution of the LVDT is 6.35×10^{-5} m FSO (Full Scale Output).
The applied torque is measured by a torque load cell which is able to distinguish changes in torque of the order of 0.565×10^{-4} KN-m. The rotation of the specimen is measured by an RVDT (Rotational Variable Differential Transformer) located at the top of the loading piston. The resolution of the RVDT is 0.05 degrees FSO.

Drainage is possible through both the top and bottom platens. Two drainage lines are connected to the top platen and another two to the bottom one. Continuous measurement of volume change during the drained tests is made by measuring the changes in the position of a brass piston incorporating a Bellofram rolling diaphragm of the WF17038 automatic volume change apparatus. The resolution of the device depends on the sensitivity of the indication of the transducer output. Volumetric changes of the order of 0.05 cc can be measured.

The cell pressure is measured by means of a very stiff pressure transducer, which is connected to the cell through high quality stainless steel ball valve at the bottom of the triaxial cell. That

pressure transducer has a resolution equal to 1.03 KPa FSO. The signals from the previously described devices are transmitted, using six different channels, to the MACSYM-2 computer system through an Analog Digital converter. The resolution of the A/D converter, for the particular gain used in these tests, is 4.88 mV. The computer performs all appropriate calculations and sends signals to keep the mean stress constant by changing the cell pressure. This is achieved by transmitting the signals through the Digital / Analog converter to an Electro-Pneumatic Regulator NIT200. The regulator is capable of performing a cell pressure control of 0.14 KPa and handling any pressure between 0 and 120 KPa.

CHAPTER 3

EXPERIMENTAL PROCEDURE

3.1 General

In order to investigate the behavior of granular media under load, a series of experiments was performed on hollow cylindrical specimens made out of glass beads. The methods of sample preparation were consistent with procedures used in the past that have proven to produce high quality results. All experiments were controlled by a computer connected to an MTS servo-hydraulic axial/torsional device which was operating a data acquisition/control software written specifically for this type of experiments. The resulting testing procedure was applied to provide a quantitative characterization of the monotonic and cyclic behavior of granular media, their yield surfaces and their motion and distortion in stress space. The experimental data obtained were compared to results from experiments on other materials such as polycrystalline aggregates, and to results from numerical simulations on of random arrays of rough, elastic spheres. These experiments provide the experimental foundation on which a micromechanically based constitutive relation of a granular material may be built.

3.2 Material Properties of Test Specimens

The material used for the construction of the hollow cylindrical specimens was glass beads. Glass beads were used instead of natural sand to investigate the behavior of granular media, in order to minimize the variability in geometric properties which may influence their behavior and to directly compare with results of numerical simulations on random packings of spheres performed in this study and other studies. The glass beads were manufactured by Potters Industries Inc., New Jersey, and are made from soda-lime glass. The elastic properties of the material used are summarized below:

Table 1. Properties of Glass Spheres

Specific Gravity	2.45 to 2.50
Roundness	Minimum of 70%
Poisson's Ratio, ν_s	0.21
Young's Modulus, E_s	68.97 X 10^6 KPa
Shear Modulus, G_s	28.66 X 10^6 KPa
Dynamic coefficient of friction	0.7 to 0.8
Static coefficient of friction	0.9 to 0.8

3.3 Specimen Preparation

The hollow cylindrical specimens were constructed by using an inner collapsible and outer split mold with nominal dimensions averaging 7.11 cm (2.8 inches) outside diameter, 5.08 cm (2.0

inches) inside diameter, and 13.97 cm (5.5 inches) height, as shown in Figure 9. In addition to the molds, the sample preparation equipment consisted of the top and bottom platens with rough porous stones, designed to function in the triaxial cell made to accommodate the hollow cylinder specimen. During sample preparation, the bottom porous stone is attached to the cell platen and the membranes are mounted and fixed with "O rings". Then, the inner mold is introduced and fixed, the external mold is firmly clamped and vacuum is applied to the membranes in order to ensure good seating between the membranes and the material when eventually the vacuum is released.

Two methods of specimen preparation were used: the first was undercompaction while the second was dry pluviation. At first, undercompaction was used, because it has been known to produce uniform samples. Baziar, (1987), by impregnating sand samples with gelatin and taking measurements by weighing sections of the samples, proved that samples prepared by undercompaction are uniform. Consequently, the first batch of specimens was prepared by the dry tamping undercompaction technique (Ladd, 1978), using eight layers of 1.27 cm (0.5 in) in thickness. The undercompaction value, U_n, of the bottom layer was chosen to be equal to 5%. This value was zero for the top layer and it varied linearly through the layers. Therefore, the undercompaction value, U_{ni}, of each layer was determined by the following expression:

$$U_{ni} = U_n - \frac{i-1}{n-1}(U_n - U_{nt}) \qquad (3.1)$$

in which U_{nt} is the undercompaction value of the top layer, i the number of layer, and n is the total number of layers. Once the undercompaction value of the layer had been calculated, the height, H_i, of that layer after compaction, was determined by:

$$H_i = \frac{i - U_{nt}}{n} H \qquad (3.2)$$

where H is the specimen height.

Each layer was slowly poured into the cavity formed by the membranes, leveled by a flat spoon, and finally compacted by the compactor to the desired height. The rubber membranes used in this study are widely used in triaxial testing. The outside membrane was 0.64 mm (0.025 inches) thick while the inner membrane had a thickness of 0.30 mm (0.012 inches). They are commercially available from Geotest Instrument Corp., Wheeling, Illinois.

Due to the one-dimensional tamping associated with the undercompaction method, the specimens exhibited strong anisotropy along the longitudinal (compaction) axis. This is evident in the results of the monotonic tests presented in the following chapters. Obtaining an initially isotropic granular medium was fundamental to this study, since modelling an inherently anisotropic material was beyond the scope of this work. As a result, this method of sample preparation was abandoned and dry pluviation was used instead. By pluviating the glass beads

under gravity in the absence of moisture, it was expected that there would not be strong anisotropy along the vertical direction. As can be seen from the experimental results in the following chapters, the samples prepared with this method could be considered to be isotropic. This method of sample preparation is very simple: the glass beads were poured continuously into the mold from a given height, and at the end the surface was leveled with a flat spoon.

A small vacuum pressure was applied to the specimen before removing the inner and outer molds. The final arrangement of the triaxial cell and specimen is sketched in Fig. 10. The triaxial cell was filled with deaired water to prevent migration of air through the specimen membrane. After this, the specimen was percolated upwards with carbon dioxide gas (CO_2) to eliminate air, was filled with deaired distilled water and then was connected to the pore pressure transducer, volume change apparatus, and pore pressure regulator. After that, the specimen was back-pressured overnight to ensure a good level of saturation.

The next day, the B parameter, which is a indication of 3-D pore pressure response, was measured to check for the saturation level of the sample. This was done by increasing the confining pressure 34.5 KPa (5 psi) and then checking the pore pressure increase within the specimen. Once a satisfactory B parameter was obtained ($B > 0.94$), the specimen was isotropically consolidated with the desired all-around confining pressure, σ_c. Then the specimen was hooked-up to the MTS testing machine and the test was started. Simultaneously, the data acquisition/control software started to run in the MACSYM-2 computer system. This way, the test was controlled by the computer and all data from the experiment were stored in the computer's hard disk.

3.4 Data Acquisition and Control Software

A data acquisition and control program was developed to run the experiments in this study. This program has been central to this experimental phase, since these experiments can be accomplished only under computer control. This program not only drives the MTS servohydraulic device along the prescribed stress path, but it also corrects in real time for membrane and torsional compliance effects discussed in detail in Chapter 5. The input of the program consists of the specimen height, inside and outside radii, area of the loading piston rod, back pressure, and any changes in height and volume of the specimen which occurred during the consolidation phase. In addition, the calibration factors of the axial force, deformation, torque, rotation, volume change and cell pressure transducers are given. Finally, the time between successive readings needs be specified before the test is started. Because of the large amount of data acquired and the memory limitations of the computer operating system, the data are stored into the computer's hard disk during the experiment using a multitasking procedure. After the experiment has been completed, the results are easily retrieved from the hard disk. The data files incorporate the measured and calculated values of stresses and strains used in this study. A flow chart of the program is shown in Fig 11.

CHAPTER 4

TESTING PROGRAM

4.1 General

A total of 46 stress-controlled laboratory experiments were performed as part of this research. The testing series included 42 monotonic and cyclic tests performed on hollow cylinders of glass beads and Ottawa sand and 4 cyclic (loading-unloading) hydrostatic compression experiments tested on a special apparatus to study the effect of membrane compliance on the results of the 42 tests. Of these 42 tests, 24 were cyclic and 18 monotonic. There were two mixtures of spherical glass beads and one type of sand having two values of void ratio, e ($e \cong 0.60$ and 0.68), while two methods of sample preparation were used. The first mixture (mixture 1) was composed of glass beads passing through sieve No. 30 (0.6 mm opening) while the second (mixture 2) was composed of glass beads passing through sieves No. 40 to 50 and No. 60 to 80 (0.25 mm to 0.18 mm) mixed with a ratio 1:2 in weight. The grain size distribution for mixture 2 appears in Fig. 12 and that of Ottawa sand in Fig. 13. The specimens were prepared either under dry undercompaction or dry pluviation. The membrane compliance tests were conducted on specialized equipment only for one value of void ratio ($e \cong .68$) using the second mixture of glass beads prepared by dry pluviation. All tests, except one, were performed under constant mean stress, $\sigma_m = \sigma_c$. Four values of mean stress were studied: σ_m=138, 180, 277 and 414 KPa. The complete list of experiments in this study appears in Tables 2, 3 and 4.

4.2 Monotonic tests

A series of monotonic tests was performed for each sand and glass bead specimen, void ratio and method of preparation used. In total, 18 monotonic tests were performed of which 12 were prepared by dry undercompaction and 6 by dry pluviation. Tests labeled "GBXX" were prepared by dry pluviation; all others were prepared by undercompaction (see tables 3, 4). All of these tests have been corrected for the errors introduced by membrane and torsional compliance. This correction was made either during or after the test. Of these tests:

- Thirteen (13) were performed under constant mean (σ_m=138 KPa) stress along proportional stress paths under three inclinations of principal stress (compression, extension, torsion) in order to study the material behavior under constant mean stress, determine the type of material symmetry (level of anisotropy) and define the initial yield loci.
    - Three (3) tests (ME12, MC14, MT18) were performed on glass beads (mixture 1) prepared by undercompaction. The void ratio was approximately equal to 0.58 ($0.58 < e < 0.59$). The behavior observed in these experiments exhibited strong anisotropy and instabilities during loading and after these 3 tests were completed, this material (mixture 1) was not further tested.
    - Four (4) experiments (MT21, ME22, MT25, MC23) were performed on mixture 2 prepared by undercompaction. The void ratio was approximately equal to 0.60.

These tests exhibited anisotropy in the direction of compaction during specimen preparation.

- Two (2) tests (MC32, MC33) prepared with mixture 2 and undercompaction ($e \cong .60$) were performed at higher values of mean stress (σ_m= 277 and 414 KPa). These tests were performed to investigate the material behavior at higher confining pressure and to define the failure envelope for all specimens having e=.60.
- Four (4) of these specimens (GB5, GB6, GB7, GB26) were prepared by dry pluviation using mixture 2 and were tested under constant mean stress. The value of void ratio, e, was approximately equal to 0.68 ($0.67 < e < 0.71$). The method of sample preparation changed at this point in an attempt to construct glass bead specimens exhibiting isotropic behavior.

- One (GB20) was a monotonic compression triaxial test in which the mean stress was allowed to vary (σ_m=138-200 KPa). This test was used to investigate the material behavior (mixture 2) under variable mean stress and to define the failure envelope for all tests with e=0.68.
- Two (GB32, MCT) were compression tests under constant mean stress (σ_m=138 KPa) up to a specified value of strain whereupon the compression loading test stopped and torsional shear was applied to failure. This type of non-proportional loading test was used to determine the specimen behavior during neutral loading and to extract parameters for constitutive modelling.
- One (MCE) was compression-extension (cyclic) test under constant mean stress (σ_m=138 KPa). One half cycle was performed.
- One (MC11) was a proportional compression test under constant mean stress (σ_m=138 KPa) on Ottawa sand. This test was used to compare the behavior of the idealized material composed of glass beads to that of a natural, yet uniform and rounded, sand.

4.3 Tests with stress reversal and probes defining yield surfaces

A total of 24 stress-controlled tests were performed in an attempt to define the shape of the subsequent yield surfaces of granular media. The shapes of the subsequent yield loci were determined along compression, extension and torsion for levels of prestrain ranging from γ_{oct}=0.25 to 0.8%. There were two series of tests, one for each method of sample preparation for samples made with mixture 2. All experiments were tested under constant mean stress at 138 KPa, except for one which was tested at 180 KPa. The exact procedure by which the points on the surface were obtained is described in detail in Chapter 7. Unfortunately, for a large number of tests, the errors introduced by membrane and torsional compliances were not corrected in real time and a correction could not be applied to the data obtained in these cyclic experiments. As a result, the data from most of these tests were either not used at all, or only the monotonic portion of the experiment could be corrected and used after the test. Finally, all of these tests were

computer controlled and a small percentage of them failed to succeed due to setup errors. Summarizing the experimental procedure:

- Four (4) experiments (D27, D29, D30, D31) were performed on mixture 2 ($e \cong 0.60$) prepared by undercompaction, at σ_m=138 KPa. The specimens exhibited strong anisotropy and the data were not corrected for the compliance effects during the test. As a result, only the monotonic portion of test D29 was corrected for membrane compliance and used as part of the monotonic proportional test database.
- Twenty (20) experiments (see Table 4) were performed on samples prepared by dry pluviation with mixture 2. The void ratio was $e \cong 0.68$. Unfortunately, while all tests were corrected for torsional compliance during the test, most of them were not corrected for membrane compliance. Only 6 of the 20 were corrected both for membrane and torsional compliance effects during the test.
    - Of the 18 experiments which were not corrected for membrane compliance in real time, one (GB19) was performed at σ_m=180 KPa to investigate the distortion of the yield surface at higher confining pressure. Only the monotonic portion of this test was used as part of the monotonic test database.
    - Of the six tests in which the compliance effects were corrected in real time, one (GB31) investigated the shape of the subsequent yield locus in strain space. The test was stress controlled, but the data were obtained in strain space. This was done to investigate the shape of a yield locus in strain space.
    - Of these six tests another experiment (GB28) was unloaded and reloaded due to a programming error. The data were used, but they may be of questionable value..

It can be seen that as a result of experimental problems only four of these tests could be actually used to define the shape of the subsequent yield loci of granular media. The rest of the tests were either partially used (their monotonic part) or not used at all.

4.4 Membrane compliance tests

A total of four tests were performed in a special apparatus to measure the effects of membrane compliance on the glass bead specimens prepared by dry pluviation using mixture 2. The void ratio was approximately equal to 0.68. It was found that the problem of membrane compliance was very important and had a significant influence on the macroscopic behavior. Moreover it was determined that the expression obtained from these special tests to correct for this effect was in excellent agreement with those proposed in the literature. Consequently, it was decided to correct the data obtained from specimens for which no special tests were performed (such as those composed of mixture 1) based on the values found in the literature.

CHAPTER 5

MEMBRANE COMPLIANCE TESTS

5.1 General

The phenomenon of membrane compliance (or membrane penetration) while usually associated with undrained triaxial tests of granular media, it also occurs in all triaxial-type tests where the lateral pressure is changing. This effect is caused by the compliance (or flexibility) of the rubber membrane used to enclose the soil specimen in a conventional triaxial test. During tests on granular media, the membrane penetrates into the peripheral voids of the specimen under the applied cell pressure, as shown in Fig. 14a at the end of isotropic consolidation. Figure 14b shows what happens when the cell pressure $\sigma_3 = \sigma_r$ is reduced by an amount $\Delta\sigma_3$, as would be the case of a compression test with constant mean stress, σ_m. This reduction in σ_3 reduces the existing membrane penetration into the peripheral voids, thus causing pore water migration to the lateral boundary. As a result, an artificial, non existent, dilation (negative volumetric strain) is measured which needs to be corrected for. Conversely, if σ_3 is increasing instead of decreasing, as in an extension test with constant σ_m, an artificial contraction (positive volumetric strain) is measured which must be corrected for. This membrane penetration correction is very important in our tests since the value of the volumetric strain is used to calculate the octahedral shear strain which is critical in controlling the experiment (see Fig. 11).

A variety of experimental solutions have been attempted to eliminate the membrane penetration effect during the test. In these attempts either: i) the membrane has been stiffened or modified to reduce the penetration effect, or ii) the variation of pore water volume due to a change in penetration has been compensated for by taking water in or out of the sample during the test (Kiekbush and Schuppener, 1977; Lade and Hernandez, 1977; Raju and Venkataramana, 1980).

An alternative way, instead of modifying the test, is to estimate the errors due to membrane penetration and to apply suitable corrections to the measured pore pressure or volumetric strains. The changes in volume associated with the variation in membrane penetration are generally measured using the Roscoe dummy rod method as modified and described by Raju and Sadasivan, (1974), and Martin et al., (1978). This is currently one of the most accurate correction methods available.

Simplified empirical expressions or charts for membrane penetration corrections, based on available dummy rod data, have been developed by Ramana and Raju, (1982) and Martin et al. (1978). These expressions provide simplified methods for predicting volume changes or pore pressure corrections for given membranes, densities and grain sizes. Experimental results from many researchers indicate that for a uniform sand and a given sample size, the membrane compliance effects are primarily a function of the particle size (as characterized by the mean grain size (d_{50}), and are reasonably independent of sample density. Experimental results on Ottawa sand (d_{50}=0.4mm) using membranes ranging in thickness from 0.5 to 0.05 mm (0.02 to 0.002 in.) have indicated that the membrane penetration characteristics are essentially independent of membrane thickness in this range.

Figure 15 presents the correlation proposed by Baldi and Nova (1984) between the normalized membrane penetration, S, and the mean grain size (d_{50}). This correlation was obtained by superimposing data on granular media obtained by many researchers. The normalized membrane penetration, S, is a function of the membrane penetration per unit area of membrane, v_m, and the lateral stress, σ_r:

$$S = \Delta v_m / \Delta \log| \bar{\sigma}_r | \qquad (5.1)$$

5.2 Description of Experimental Device for Membrane Compliance Tests

The chamber used is a triaxial cell which has been modified to accept coaxial, solid, rigid rods of different diameter so that the membrane area of the specimen is kept constant while the volume of the sand varies (Fig. 16). This configuration is slightly different from those presented in the literature, but the principle is the same and this device is simpler to use. The standard configurations proposed in the literature suggest that a flexible cap be used to achieve a uniform stress distribution within the specimen (Frydman et al. 1973). The cap used in this research is a regular steel cap, such as typically used in triaxial testing, but the internal rod does not touch the cap, and allows instead for a space full of granular medium which helps distribute the applied pressure more uniformly. This boundary condition is not equivalent to that supplied by the flexible cap and the fact that the rod does not extend to the same level as the membrane may cause an error in the correction. However, this type of device is widely used in soil mechanics practice, and has been found to give reliable results. There is strong evidence that a sufficiently thick sand "cushion" between the cap and the rod can prevent "arching" within the soil and help ensure an isotropic condition within the specimen. Finally, the fabrication of an elaborate device with flexible top would be expensive and complicated to design and use, while the present apparatus can be built by modifying an existing triaxial cell.

5.3 Description of Experimental Procedure

The specimens used were 10 cm in height and 5 cm in diameter. The rods were 8.1 cm tall and had a diameter, d = 1.9 or 3.18 cm (.75 or 1.25 in.). In addition to these two specimens, a specimen without a rod was tested to provide a third data point for the correction scheme. The space of sand between the top of the concentric rod and cap was 1.9 cm, which is believed to be sufficient to ensure a uniform stress distribution within the sample. The specimens were prepared under dry pluviation, as described in the preceding chapter. They were all subjected to an increasing isotropic confining pressure under *drained* conditions and then they were unloaded to the initial isotropic state. The principle of this particular experiment is to keep constant the volumetric changes associated with membrane penetration at a given confining pressure, σ_m, while reducing the volumetric changes due to the soil skeleton by increasing the rod size. The volumetric changes that would occur if there were no sand are extrapolated based on the fact that no membrane penetration should occur when the diameter of the rod is equal to that of the specimen (d=5.0 cm). This extrapolated volumetric change would then be the error in the experimental measurement due to membrane compliance. The corrected (true) volumetric strain

values are subsequently plotted as function of the lateral stress and a relationship is established between the error due to membrane compliance and change in lateral stress.

A total of four experiments were performed in this testing series as shown in Table 4: one with no internal rod, two with rod diameter d=1.9 cm and one with d=3.19 cm. The results are shown in Fig. 17, where the volumetric change is plotted versus the volume of the glass beads specimen. A zero volume of glass beads corresponds to a steel specimen (no membrane penetration). The data were initialized at 138 KPa, which is the value at which the constant mean stress triaxial hollow cylinder tests were started; σ_r either increased or decreased during these tests. The sign of the lateral stress change depends on the stress path followed; for example, during extension, σ_r increases, while during compression it decreases. The lateral stress does not change during a torsion test. Since a steel specimen would be unaffected by membrane penetration, the points of interception of the volumetric change axis by the linear equations fitted to these lines in Fig. 17 are the errors in volumetric change. It can be seen in the same figure that there is a significant volumetric change associated with membrane compliance. The lines were forced to pass from the data points obtained by the specimen without the rod, since these data points are believed to be more reliable than those obtained from the specimens with the rod, because of the boundary condition problems stated previously. Figure 18 presents the variation of the measured volumetric strain, as well as that caused by membrane compliance, with confining pressure. The true volumetric changes, normalized by the area of the membrane, were plotted versus the stress ratio, $\sigma_r(i)/\sigma_r(1)$, in Fig. 19. The following correction equation was obtained by fitting the data:

$$\varepsilon_v = 0.00001 - 0.00211\ A\ \log_{10}[\sigma_r(i)/\sigma_r(1)] \qquad (5.2)$$

where A is the area of the membrane of the specimen. In order to apply this equation and correct the volumetric strains in the hollow cylinder tests, which have a different area of membrane, A needs to be changed appropriately. In the case of a *typical* hollow cylinder used in the experiments of this study, the equation becomes:

$$\varepsilon_v = \varepsilon_v^m - 0.418 \log_{10}[\sigma_r(i)/\sigma_r(1)] \qquad (5.3)$$

where ε_v^m is the measured (not corrected) volumetric strain and $\sigma_r(1)$ the initial value of σ_r. In our case, for most of the experiments $\sigma_r(1) \equiv 138$ KPa.

The above equation was applied to the isotropic compression data obtained from i) a solid and ii) hollow cylinder tests. Fig. 20 is a plot of the confining pressure, σ_m, versus the volumetric strain for the above data and includes the variation of σ_m with $3\varepsilon_{zz}$ obtained from the solid specimens. Ideally all curves, including σ_m vs $3\varepsilon_{zz}$ should match, if the material were perfectly isotropic; the fact that they do not match perfectly may be attributed either to experimental scatter or to a small degree of anisotropy along the longitudinal direction of the material. The curves are very close which, given the anisotropy observed, suggests that the applied correction is very close to being true. Moreover, the value calculated for correction is in excellent agreement to that proposed by Baldi and Nova (1984). Therefore, the assumptions regarding the boundary conditions of the experimental configuration seem to be justified.

The error that can be introduced by not accounting for membrane penetration can be very significant, since it not only affects the magnitude of the strain, but the overall behavior of the material as well. Figs. 21 and 22 present a comparison of the stress-strain and volumetric-shear strain curves obtained with and without correcting for the effects of membrane compliance for monotonic compression test GB26. The test was performed under constant mean stress. While the octahedral shear stress-strain curve is not significantly altered by applying the appropriate correction, the difference observed in the volumetric-shear strain curve is dramatic. Not only the magnitude of the uncorrected volumetric strain is larger, but the trend shown is misleading. While at small strains the true (corrected) behavior is contractive, the measured (not corrected) behavior appears to be dilative from the beginning. Therefore, not correcting for membrane compliance can lead to serious errors.

5.4 Errors caused by Torsional Compliance Effect

The flexibility (or compliance) of the loading apparatus can also be a major source of experimental error. In the case of the RPI MTS axial torsional device, the torsional loading cell and rotational transducer are located at the top of the loading shaft (Fig. 23), while the torque is applied to the specimen at the other end. The shaft is connected to the specimen through a flexible connection to a steel rod 35 cm in length and 1.25 cm in diameter. This connection mechanism deforms during torsional testing and, as a result, the value of rotation measured at the top of the shaft is different from that experienced by the specimen. The value of the rotation is used to calculate the shear strain experienced by the specimen. Consequently, the error in measuring the rotation must be accounted and corrected for. This can be achieved by finding the contribution to the total rotation caused by the flexible rod and connection, and subtracting it from the measured value. The rotation of the flexible rod is given by:

$$\theta_{err} = T / K \qquad (5.4)$$

where T is the applied torque and K is the stiffness of the rod. In this case K = .323 KN-m. Then, the error in strain is:

$$\gamma_{err} = R_e \, \theta_{err} / H \qquad (5.5)$$

where R_e is the equivalent radius of the hollow cylinder and H is the height of the specimen. The correct strain, γ, is computed by subtracting the error in strain from the measured value of strain, γ_m:

$$\gamma = \gamma_m - \gamma_{err} \qquad (5.6)$$

In the case of the monotonic, proportional tests, this can be achieved easily after the test, even though both R_e and H are changing during the test. This is not the case with the cyclic tests where the precise value of octahedral shear strain is needed to control the test (see Fig. 11 and discussion in section 7.4). Therefore, in these experiments, the correction must be applied in real time through the control algorithm in the computer. Failure to do so, renders the data

obtained in the cyclic portion of the test useless. All tests prepared by dry pluviation were corrected in real time.

The error introduced by not correcting for torsional compliance can be significant since it affects the magnitude of the shear strain. Figs 24 and 25 present a comparison of the stress-strain and volumetric-shear strain curves obtained with and without correcting for the effects of torsional compliance for torsion test MT18. No correction for membrane compliance needs to be applied to a torsional test because the lateral stress does not change throughout the test. Both the octahedral stress-strain and volumetric strain-shear strain curves are different before and after the correction has been applied. Nevertheless, the trend in both curves is the same. Consequently, correcting for torsional compliance is very important, but it does not lead to erroneous conclusions about the material behavior, as is the case when the effect of membrane compliance is not accounted for.

5.5 Conclusion

It has been demonstrated that the error caused by the membrane and torsional compliances can significantly influence not only the magnitude of the measured values, but the macroscopic behavior of a granular medium as well. However, these errors are particularly significant in this testing program. The values affected by this error include the volumetric and shear strains used in turn to calculate the value of octahedral shear strain that is the controlling parameter in these computer controlled tests. Consequently, an erroneous value of octahedral shear strain would result in the wrong stress path. In the case in which a test was performed along a monotonic, proportional stress path, the correction can be applied after the test. If the test included stress reversals along non-proportional paths or along paths, with simultaneous application of axial and shear stresses, the task becomes impossible and the cyclic part of this experiment can not be used at all.

CHAPTER 6

MECHANICAL BEHAVIOR OF A GRANULAR MEDIUM UNDER MONOTONIC LOADING

6.1 General

A total of 14 stress-controlled monotonic drained tests were performed on hollow cylindrical specimens made out of glass beads and one (1) was performed on Ottawa F125 sand. Of these tests, 10 (including that in Ottawa sand) were conducted on specimens prepared by undercompaction while the other 5 were prepared by dry pluviation. Of the 9 glass bead specimens prepared by undercompaction, 3 had one size of glass beads, (those passing sieve no. 30 with an opening of 0.600 mm); while the other 6 were composed of two ranges of sizes of glass beads. All specimens prepared by dry pluviation were composed of a mixture of particles having two ranges of diameters. These specimens consisted of beads passing through sieves No. 40 and 50 (0.430 mm to 0.300 mm) and between sieves No. 60 and 80 (0.250 mm to 0.180 mm) mixed with a weight ratio of 1:2. The specimen preparation technique is described in detail in Chapter 4. There were two values of void ratio, e, for the specimens prepared by undercompaction: those which were composed of one particle size had $0.58<e<0.59$, while those consisting of two particle diameters had $0.59<e<0.60$. The specimens prepared by dry pluviation had $0.67<e<0.71$. The properties of all tests appear in Tables 3 and 4.

Each specimen was isotropically consolidated to the desired confining pressure, σ_m, before it was sheared along the predetermined stress paths. For all tests, except one, the normal mean stress, $\sigma_m=(\sigma_{zz}+\sigma_{rr}+\sigma_{\theta\theta})/3$, was kept constant throughout the shearing stage by changing in appropriate manner the vertical stress and cell pressure simultaneously. Therefore, each experiment corresponds to a single π-plane defined by this σ_m.

6.2 Stress and Strain Parameters

The π-plane, which is also termed "octahedral plane", is expressed by $\sigma_1+\sigma_2+\sigma_3=$const. Normal to that plane is the isotropic stress line defined by: $\sigma_1 = \sigma_2 = \sigma_3$ which is also called "space diagonal" (Fig. 26). The three dimensional state of stress can be expressed by the normal and tangential components of the stress acting on the octahedral plane. The normal component is usually called "effective mean normal stress" and is given by:

$$\sigma_m=(\sigma_1+\sigma_2+\sigma_3)/3 \qquad (6.1)$$

while the tangential component termed as "octahedral shear stress" is expressed by:

$$\tau_{oct}=(1/3)[(\sigma_1-\sigma_2)^2 + (\sigma_2-\sigma_3)^2 + (\sigma_3-\sigma_1)^2]^{0.5} \qquad (6.2)$$

It should be noted that σ_m is related to the length of the space diagonal from the origin to octahedral plane, OO', and τ_{oct} is related to the magnitude of the shear stress on the octahedral plane, O'P. They are expressed as:

$$\overline{O}\ \overline{O'} = 3\sigma_m \qquad (6.3)$$

$$\overline{O'}\ \overline{P} = 3\tau_{oct} \qquad (6.4)$$

In order to specify the three dimensional stress condition, another variable, θ, must be introduced, called "angle of shear direction", which determines the direction of shear stress on the octahedral plane shown in Fig. 26. This variable can also be expressed as a function of the principal stresses as follows:

$$\tan\theta = \sqrt{3}(\sigma_2 - \sigma_3) / (2\sigma_1 - \sigma_2 - \sigma_3) \qquad (6.5)$$

The relative magnitude of the intermediate principal stress between the major and minor principal stresses is expressed by the coefficient, b, given by:

$$b = (\sigma_2 - \sigma_1) / (\sigma_2 - \sigma_1) \qquad (6.6)$$

This coefficient has been adopted since it is a non-dimensional parameter ranging between zero and unity and can be set to any value between theses limits for drained and undrained tests et al. 1985. Many researchers, (Bishop, 1966; Ergun, 1981; Lewin et al., 1982) investigated the effects of the intermediate principal stress σ_2 on the behavior of soils in terms of the parameter b. The parameter b has also been used in studying anisotropy of granular media at different relative values of the intermediate principal stress, (Haruyama, 1981). In this earlier work, the investigation of σ_2 was limited to the case of principal stress directions that are fixed during shear. However, these investigations were later extended to the case of varying principal stress directions provided that σ_2 is not rotated. In the same manner, the strain conditions are characterized by the volumetric strain given by:

$$\varepsilon_v = (\varepsilon_1 + \varepsilon_2 + \varepsilon_3) \qquad (6.7)$$

the engineering distortion strain, γ_{oct}, expressed as:

$$\gamma_{oct} = (2/3)[(\varepsilon_1 - \varepsilon_2)^2 + (\varepsilon_2 - \varepsilon_3)^2 + (\varepsilon_3 - \varepsilon_1)^2]^{0.5} \qquad (6.8)$$

and the direction angle of distortion strain defined as follows:

$$\tan\delta = \sqrt{3}(\varepsilon_2 - \varepsilon_3) / (2\varepsilon_1 - \varepsilon_2 - \varepsilon_3) \qquad (6.9)$$

Tables 3 and 4 summarize all monotonic tests performed and the values of the stress and strain parameters characterizing each test.

6.3 Behavior of an assembly of identical spherical particles prepared by undercompaction under monotonic loading

This section describes the results of experiments performed on specimens of equally sized spheres prepared by undercompaction. The diameter of the spheres was approximately 0.6mm (sieve No. 30). The void ratio of these specimens was approximately 0.58. The densest possible packing of equal spheres corresponds to a void ratio of 0.35, while the loosest stable possible structure to a void ratio of 0.92 (Lambe and Whitman, 1969). The relative density was $D_r = 60\%$ and as a result this material could be characterized as medium dense (Lambe and Whitman, 1969).

Table 3 lists the specimen properties and test conditions. Each specimen was initially consolidated under the isotropic pressure shown in Table 3, and then was sheared under drained conditions along a constant ω until failure, where ω is the angle between the direction of the maximum principal stress and the vertical direction, which in this case coincides with the direction of deposition. These tests had three different values of ω, equal to 0°, 45° and 90°, and their corresponding stress paths in q - p space are shown in Fig. 27. Using standard soil mechanics notation, $p = (\sigma_1 + \sigma_3) / 2$, while q is the maximum shear stress $q = (\sigma_1 - \sigma_3) / 2$. The intermediate principal stress, σ_2, varies in each of the tests: $\sigma_2=\sigma_\pi$ decreases for $\omega = 0°$, is constant for $\omega = 45°$ and increases for $\omega = 90°$. This variation of the intermediate principal stress can also be expressed by the values of the parameter b, (b = 0, 0.5, 1.0 for ω = 0°, 45°, 90°, respectively).

In each test the mean stress is kept constant during the shearing stage. This type of test is termed "radial shear test" and all data points of that test lie on one octahedral plane π-plane. The angle of shearing direction, θ, as it was defined in the previous section, is 0°, 30° and 60° for ω= 0°, 45° and 90°, respectively. In all tests, the circumferential strain, $\varepsilon_{\theta\theta}$, and the radial strain, ε_π, were calculated from the measured volume change, ε_v, and axial strain, ε_{zz}:

$$\varepsilon_{\theta\theta} = \varepsilon_\pi = (\varepsilon_v - \varepsilon_{zz}) / 2 \qquad (6.10)$$

The assumption that the radial and circumferential strains are equal in an anisotropic material is reasonable since it is supported by results from isotropic compression tests performed on cubical specimens consisting of glass beads by Haruyama (1981). Figure 28a (from Haruyama, 1981) shows the measured values, obtained from isotropic compression tests, of the principal strains ε_x, ε_y, ε_z, and volumetric strain, V_s, plotted versus the hydrostatic pressure, $p=\sigma_m$. The strains ε_x, ε_y, and V_s, versus ε_z, are shown in Fig. 28b. It can be seen that the values of the two horizontal strains, ε_x, ε_y, are the same.

The stress-strain curves on the octahedral plane obtained from the above experiments are shown in Fig. 29, where the octahedral shear stress, τ_{oct}, is plotted vs the octahedral shear strain, γ_{oct}. It can be seen that the material behavior exhibits strong anisotropy since there are three distinct curves for each inclination of principal stress, ω. The compression test, which was loaded in the

direction in which tamping occurred during undercompaction, has the highest values of strength and stiffness, while the extension test has the lowest. Moreover, the data reveal the existence of "discontinuities" in the stress-strain curve which appear as sudden jumps. This phenomenon, which occurs more often as the strain increases, appears for the first time at a value of octahedral shear strain to 0.25-0.3% for all tests. As the strain increases, the discontinuities become increasingly more pronounced until failure.

The volumetric strains versus the octahedral strains for the same three tests are shown in Fig. 30. The volumetric behavior is different for each experiment. The specimen sheared along $\theta=0^\circ$ ($\omega=0^\circ$; compression) was dilative, whereas the specimen sheared along $\theta=30^\circ$ ($\omega=90^\circ$; extension) was initially contractive and then started to dilate. Finally, the third specimen, sheared in torsion along $\theta=60^\circ$ ($\omega=45^\circ$) was contractive until failure. This difference in volumetric behavior demonstrates the inherent anisotropy present in these samples which was also observed in the stress-strain curves.

The differences in the volumetric behavior of the three monotonic radial shear tests on the specimens of identical spheres can also be seen in Fig. 31, where the octahedral shear stress is plotted versus volumetric strain. The volumetric strains start to deviate from zero approximately at τ_{oct} = 30 KPa for the torsion test, at τ_{oct} = 40 KPa for the extension test, and at τ_{oct} = 65 KPa for the compression test. Since the samples sheared in torsion, extension and compression fail at approximately τ_{oct} = 40, 60 and 90 KPa respectively, this implies that the volumetric strains take place near failure. A closer look at Figs 29, 30 and 31 reveals that the volumetric strains occur when the first discontinuity appears on the stress-strain curve at τ_{oct} = 30, 40 and 70 KPa for the torsion, extension and compression experiments, respectively.

It is believed that the inherent anisotropy of this essentially monodispersed granular material is the result of the method of sample preparation combined with the crystallization which takes place when the material is compacted in the axial direction during undercompaction. The discontinuities are also attributed to the above phenomena and, as a result, the monodispersed samples were not used again in the remainder of this work, and a new mixture composed of beads passing through sieves No. 40-50 and 60-80 mixed 1:2 in weight was chosen instead. A discussion on the inherent anisotropy, crystallization and discontinuities of the material behavior appear in section 6.7.

6.4 Behavior of an assembly of spherical particles of different sizes prepared by undercompaction under monotonic loading

This section presents the behavior under shear loading of specimens prepared by undercompaction that were composed of glass beads having different diameters. The particle diameters ranged from 0.18 mm to 0.43 mm; this was the result of mixing particles of 0.43 to 0.3mm in diameter (sieves No. 40 and 50) with particles of 0.25 mm to 0.18 mm in diameter (sieves No. 60 and 80), with a ratio of 1 to 2 by weight; this material has been named "mixture 2". The grain size distribution of mixture 2 is shown in Fig. 12. A mixture of several sizes of spherical particles was used for constructing the specimens in order to obstruct the regular packings and crystalline regions present in specimens of identical spheres, which were

responsible for the observed anisotropy and discontinuities in the stress-strain curve, discussed in the previous section and in Section 6.7. The mixture used has a minimum void ratio, e_{min}, equal to 0.517 and a maximum void ratio, e_{max}, equal to 0.680 (Chen, 1986). The specimen properties appear in Table 3.

Seven drained monotonic radial shear tests were performed on specimens made out of this mixture of different sizes of glass beads. In five of those tests, the specimens were isotropically consolidated at $\sigma_m \equiv 138$ KPa (20 psi), while the remaining two were consolidated at 275.9 KPa (40 psi), and 413.8 KPa (60 psi). The test conditions and the stresses parameters of each test are also summarized in Table 3.

Two of the five radial shear tests, conducted on the specimens consolidated at the lower confining pressure, consisted of shear along $\omega = 0°$ (compression), two along $\omega = 45°$ (torsion) and one along $\omega = 90°$ (extension). In all tests the mean stress was kept constant. Therefore, the test results for all tests lie on a single octahedral plane (π-plane) at approximately 138 KPa.

Figure 32 depicts the experimentally obtained stress-strain curves for mixture 2. There is strong anisotropy present in the axial direction as can be seen by the differences in strength and stiffness between the specimens sheared along $\omega = 0°$ (MC23 and D29) and along the other directions (MT21, MT25, ME22). The test results from the two torsion and the extension test are in very good agreement. The "discontinuities" observed in the stress-strain behavior of the assemblies of identical spheres, are not present any more in the stress-strain curves of specimens sheared along $\omega = 0°$; i.e. in the case in which the principal stress direction coincides with the direction of compaction during specimen preparation. On the other hand, samples tested under the same test conditions, but at $\omega = 45°$ and $90°$ experienced "strain-jumps" in their stress-strain curves. By comparing the observed "discontinuities" in the behavior of the mixture of glass beads with those observed in the behavior of the identical spheres, we see that this time the slips are not as pronounced and they occur at much larger strains, close to failure.

Figure 33 presents the relationship between volumetric and octahedral shear strain obtained from the same tests discussed above. While there is a small difference in the magnitude of volumetric strain measured along each stress path, the overall trend is the same, with all specimens dilating with increasing strain. All tests, with the exception of compression test MC23, contracted at very small strains and dilated thereafter. The volumetric strains in the torsional, extension and compression test D29 are near zero at small strains ($\gamma_{oct} < .025\%$). The volumetric strains in these tests also take place at large values of octahedral shear stress, near failure. This can be seen in Figure 34, where the octahedral shear stress is plotted versus the volumetric strain. Consequently, significant dilation in medium dense assemblies of equal and unequal spheres take place near failure.

Figure 35 presents the octahedral stress-strain curves obtained from three compression tests, performed at three different values of mean stress, $\sigma_m = 138$, 276 and 414 KPa. The volumetric strain versus octahedral strain curves appear in Fig. 36, and the octahedral shear stress plotted versus the volumetric strain appears in Fig. 37. It can be seen that the strength and volumetric behavior of the material are a function of the confining pressure. The strength increases with

confining pressure, and specimens consolidated at higher pressures exhibit contractive behavior over a larger strain range than specimens consolidated at lower values of σ_m. Significant volumetric strains occur at large values of octahedral shear stress, near failure.

The p-q stress paths for all of the above seven experiments appears in Fig. 38. The end points of the "stress paths", which correspond to the peak points of the stress-strain curves are defined as failure points. The line passing through these points line is known as the "K_f - line" in the soil mechanics literature (Lambe and Whitman 1969). The value of K_f is related to the angle of internal friction of the material, ϕ, where $\sin\phi$ is equal to q/p at failure. Based on this data, it appears that either this K_f line is not a line but a curve, or the strength obtained from compression test MC23 and torsional test MT21 is inconsistent to that obtained from the other tests. The stress path, plotted now as the octahedral stress versus the mean stress, appears in Fig. 39 together with the failure envelope for this material in stress space. It can be assumed that the trace of the failure envelope on this plane is a straight line with angle, ϕ, approximately equal to 28°.

Finally, the behavior of the two mixtures of glass beads prepared by undercompaction is compared. The octahedral stress-strain curve obtained from compression test MC14 (one particle size) appears in Fig. 40 together with the curve obtained from compression test MC23 (many particle diameters). The volumetric strain is plotted versus the octahedral shear strain for both mixtures in Fig. 41. It can be seen that the behavior of both granular media is very similar. The only difference is the presence of discontinuities (or slips) on the stress-strain and volumetric-shear strain curves of the material composed of particles with a narrow range of diameters. Mixture 2 has higher strength than mixture 1; this was expected since mixture 2 is composed of particles with a wide range of diameters.

6.5 Behavior of an assembly of spherical particles of different sizes prepared by dry pluviation under monotonic loading

In an attempt to avoid the anisotropy present along the longitudinal axis of the specimen, which is believed to be the result of the compaction taking place in the same direction during specimen preparation, the method of specimen preparation was changed. It was decided to prepare the specimen without compacting it, but by pluviating glass beads in the presence of gravity. Although no sample prepared in gravity will ever be truly anisotropic, it was anticipated that the absence of compaction would make the sample less anisotropic in the longitudinal direction.

Six monotonic proportional tests were performed using specimens prepared by undercompaction using mixture 2. Four of these were proportional experiments performed under constant mean stress σ_m = 138 KPa. Two of them were compression tests, one was a shear test and the fourth was an extension test. The first compression test (GB5) had a low B-parameter and lower void ratio than the others and was repeated in test GB26. The fifth experiment was a triaxial compression test in which the mean stress was allowed to vary, while the sixth was a special test along a non-proportional path to investigate the behavior of the material under neutral loading. The details of these experiments appear in Table 4.

The stress paths in the octahedral shear stress - mean stress plane from all six experiments appear in Fig. 42. The octahedral shear stress-strain curves from the monotonic proportional experiments under constant mean stress appear in Fig. 43, and the volumetric strain-octahedral shear strain curves are included in Fig. 44. All data from tests, except for those obtained from the extension test (GB6) are very close and those of GB6 are within a narrow band. The data from the compression test (GB26), in contrast to those obtained from compression on the specimens prepared by undercompaction, do not plot higher than the data obtained from the compression and extension tests. The volumetric strains (Fig. 44) in these tests are very close to zero at small strains (except for experimental noise) and then the material dilates regardless of the stress path. Figure 45 depicts the variation of volumetric strain with octahedral shear stress for the three monotonic experiments. It can be seen, that similar to the data obtained from the specimens prepared by undercompaction, significant volumetric strains occur only at large values of octahedral shear stress, near failure. In all figures, the data points from all experiments plot within a narrow band and as a result, the behavior of this material can be approximated as isotropic.

As discussed in Chapter 5, a large number of tests with stress reversal did not produce meaningful results because of the error introduced by membrane penetration. In an attempt to salvage a part of this valuable information, the data files were post processed and corrected for membrane compliance. However, as discussed in chapter 5, this was possible only for the monotonic portion of those tests, which extended to values of octahedral shear strain of approximately 0.25%. There were 14 tests which were post processed; they included 7 compression tests, 1 extension, 4 torsion and 2 combined compression/torsion tests. The stress-strain curves of these tests appear in Fig. 46 and the volumetric strain-shear strain behavior in Fig. 47. It can be seen that all data in both figures, regardless of stress path, plot within a narrow range. The agreement between data is excellent and the material can be approximated to be isotropic, thus justifying the change in the method of sample preparation.

The results obtained from the triaxial compression test GB20 appear in Figs 48, 49 and, 50. In this test, the lateral stress, σ_r was kept constant and as a result, the mean stress increased throughout the test. Figure 48 presents the octahedral stress-strain curve, while Figs. 49 and 50 present the variation of volumetric strain with octahedral shear strain and shear stress, respectively. The strength and stiffness for this experiment are higher than in the tests performed under constant mean stress, because in this case the mean stress increased during compression. The volumetric strains are also higher (compare Figs. 49 and 47) with the material behavior being initially contractive and then becoming dilative. The same phenomenon can be observed in Fig. 50, where significant volumetric strains take place at very low values of octahedral shear stress, in contrast to the data obtained from experiments under constant mean stress where volumetric strains occurred only near failure. This difference in volumetric behavior is attributed to the mean stress which induces elastic volumetric strains as it increases during compression.

6.6 Behavior of Ottawa sand under monotonic compression

A compression test under constant mean stress at 138 KPa was performed on F-125 Ottawa sand. The specimen was prepared with undercompaction to a void ratio of 0.68 which

corresponds to a value of relative density, D_r = 40%. The purpose of this test was to compare the behavior of a uniform, rounded sand to the results obtained from specimens on both mixtures of glass beads prepared either by undercompaction or pluviation. The octahedral stress-strain curve obtained from the compression of Ottawa sand appears in Fig. 51 together with the stress-strain curve obtained from compression test MC23 (mixture 2 of glass beads: undercompaction), MC14 (mixture 1: undercompaction) and GB20 (mixture 2: pluviation). The corresponding plot of volumetric strain versus octahedral shear strain appears in Fig. 52. It can be seen that even though MC23 and MC14 have a different value of void ratio ($e \equiv 0.60$) the behavior of the sand in both plots is very similar to that of the glass beads. Experiment GB26 had a void ratio of 0.68, which is the same as that of Ottawa sand. The method of sample preparation appears to make a difference: by reducing the anisotropy along the longitudinal axis, the strength of test GB26 is much lower than that of the other tests. However, given the good qualitative agreement between all tests, it can be concluded that using glass beads to model granular media presents a good approximation to reality, while at the same time allowing more control of the physical and geometric properties of the material during the experiment.

6.7 Anisotropy, discontinuities and strain "jumps" in the materials used

All specimens tested exhibited higher strength and stiffness when compressed along the direction in which they had been compacted during specimen preparation. The effect was most pronounced in the case of the glass bead specimens composed of one particle diameter prepared by undercompaction (Figs. 29 and 30). The stress-strain curves obtained from specimens fabricated with mixture 2 by undercompaction were very similar between the shear and extension paths which in turn were different from that obtained in compression (Figs. 32 and 33). Consequently, specimens composed of mixture 2 were anisotropic along the vertical direction, though less anisotropic than specimens fabricated with one size of glass beads. Samples prepared by pluviation exhibited some form of anisotropy along the longitudinal direction, but overall the behavior could be assumed to be isotropic (Figs. 43 and 44). Therefore, preparing specimens by pluviation causes less fabric (structural) anisotropy than undercompaction, and the decision to change the method of sample preparation has been fully justified. Fabricating a truly isotropic material in the presence of gravity is almost impossible since the interparticle contacts along the vertical direction will always experience at least more load than contacts in other directions. In addition, undercompaction creates a strong anisotropic fabric which is most evident when equal spheres are used to create a sample. In this case, the tendency of the equal spheres to crystallize is further amplified by the compaction in one direction.

The above conclusion is in agreement with observations made by Kallstenius and Bergau (1961), who conducted tests on glass beads and concluded that the number of spheres within a vertical cross-sectional unit area for the random packing of equal spheres was greater than that within a horizontal cross-sectional unit area. Also, Borowicka (1973) showed that for a loose coarse sand, before shearing the number of points of contact was greater in the vertical direction than along other directions. It is clear from these studies that the difference in arrangements of spheres between vertical and horizontal directions causes the specimen to show an inherent anisotropy.

The discontinuities or strain jumps observed during the monotonic loading would be very important if they could be attributed to the material properties and not to the setup of the experimental apparatus. A close look at the stress-strain curves of all four materials tested (Figs 29, 32, 43 and 51) at σ_m=138 KPa reveals that these discontinuities are most pronounced for the material having one particle diameter and that they become less visible as the variability in particle diameter increases (Figs. 29 and 32). Moreover, as the variability of the particle size increases, the phenomenon occurs at larger strains (Fig. 32) and, in the case of Ottawa sand, one can assume that it occurs at failure. Consequently, one factor which appears to be affecting the observed "discontinuities" is the distribution of the particle diameters, which is one of the parameters controlling the fabric of the material. Observing the compression experiments performed on mixture 2 prepared by undercompaction at σ_m=138, 276 and 414 KPa, it can be seen that the "jumps" on the stress strain curve appear once more (Fig. 35). On the other hand, there is little evidence of discontinuities in the stress-strain curves of samples prepared with pluviation (Fig. 43). Therefore, it appears that the combination of sample preparation technique and distribution of particle sizes, is responsible for the observed behavior, by creating a fabric that has the potential of being locally unstable. In order to gain an insight on the micromechanical processes possible for this behavior, a small number of numerical simulations on random packings of elastic rough spheres were performed to confirm and interpret the experimental findings. The results of these numerical simulations appear in the following section.

6.8 Micromechanical Observations

In order to gain insight into the micromechanical phenomena taking place at the particle level and influencing the macroscopic response, a number of numerical simulations were performed on a 2-D random array of 531 elastic, rough spheres. This array was composed of particles of two radii, R_1 and R_2 with $R_1 / R_2 = 1.5$. Another set of numerical simulations were conducted on an array of 477 particles of equal diameter, to investigate the influence of the distribution of particle diameters on the macromechanical response. The numerical experiments were performed using program CONBAL-2 (Petrakis et al. 1988, Ng 1989) which is based on the Discrete Element Method (Cundall and Strack 1979), and has been modified to take into account the nonlinear force-displacement relationship at the interparticle contacts by applying a numerical solution to problem of the contact between two spheres subjected to an oblique force (Dobry et al. 1991). In this version of program CONBAL-2, the particles are not allowed to rotate and the friction angle of the material was reduced to f=0.35 to account for this. This was done in order to use the full nonlinear Mindlin solution at the contact which does not allow for rotation. The numerical simulations were performed along the same stress paths as the laboratory experiments. The results of two of the numerical simulations are shown in Figs. 53 to 57.

Figure 53 shows the stress strain curve obtained from compressing the 531 particle array under a constant mean stress of 130 KPa, and Fig. 54 shows the variation of total number of contacts with octahedral shear strain during loading for the same simulation. It can be seen that slips are present in the stress strain curve and, as a result, the stress fluctuates with increasing strain. At the same time, while globally of the number of contacts is decreasing from 900 to 790 contacts, locally the number of contacts is fluctuating considerably. It can also be seen that this

fluctuation of the number of contacts is in *phase* with the stress-strain response; thus it can be assumed that it directly influences the macroscopic stress-strain response. Figure 55 shows the following micromechanical statistics of this numerical simulation at the end of the isotropic consolidation:

1. Distribution of Contact Angle
2. Distribution of Mobilized Angle
3. Distribution of Contacts per Particle, and
4. Distribution of Contact Force.

Figure 56 displays the same information at the end of the compression phase of the simulation. While at the beginning of loading the contact distribution is uniform throughout the sample (Fig. 55), at the end of the loading simulation the contacts have formed along the direction of the major applied principal stress and have been essentially eliminated in other directions (Fig. 56). This is in good agreement with findings in polycrystalline aggregates, where during plastic deformation, slips in the monocrystals also occur in the same direction.

The stress strain curve obtained by compression under constant mean stress on the array of 477 equal elastic rough spheres is shown in Fig. 57. The shape of the stress strain curve is different from that obtained by compressing the 531 sphere array, but is also similar in that at large strains the stress-strain curve fluctuates with increasing strain.

The above numerical simulations and the laboratory experiments suggest that these slips are associated with local instabilities in the material microstructure. Similar to a polycrystalline aggregate, a granular medium is overconstrained and is composed of dense (stiff and strong) and loose (less stiff and weak) regions. A stiff region may be either actually stiff by having a large number of contacts per particle or they may appear stiff by being oriented in such a direction that its slip systems are perpendicular to the direction of the applied principal stress. During loading, the dense regions support an increasingly larger load compared to the weak regions, which may even unload and transfer the stresses to stiffer packings. Throughout the loading process, the material is shedding its constraints and the global number of contacts is decreasing, while fluctuating locally while decreasing. At some point during loading the stiff regions cannot support additional load and they collapse, strength is lost, and a sudden drop in macroscopic strength is observed. When the break down of the stiff regions occurs, there is a rapid reorganization of the fabric, loose regions become dense and start supporting the load. This manifests itself macroscopically by an increase in the shear strength. Then, these newly formed microstructures collapse as well, and the overall strength drops once more. New structures emerge, which by having a lower coordination number are less constrained and as a result their stiffness is lower than that of the packings of the previous step. Consequently, the macroscopic stress-strain curve exhibits a yielding behavior. The same procedure is repeated all over again, while the number of contacts per particle drops and tends to become uniformly distributed throughout the sample. At the limit, the coordination number becomes 3 which is the value at which a statically determinate fabric emerges. This was the case with the numerical experiment with 531 particles, where the total number of contacts dropped from 900 to 790; the corresponding coordination number dropped from 3.4 to 3.0 at failure.

This process is more clear and pronounced in granular media composed of particles of equal diameters because of the crystallization, which divides the medium into distinct dense and loose packings. This is in agreement with both the laboratory and numerical simulation findings. The phenomenon described is similar to that of shearing a simple cubic array of spheres (Fig. 58) which had been consolidated under isotropic compression. In the beginning, the load increases until the array fails (a); at this point a new packing is formed which has more contacts per particle, and more load can be sustained (b). Then, this packing fails as well, and a new simple cubic array is formed (c) with fewer contacts. Since there is no adjacent structure to take the load, the phenomenon repeats itself ad infinitum. The resulting stress strain curve is similar to that of the 477 particle array (Fig. 57) which fluctuated periodically with increasing strain.

Concluding, the same phenomena are observed in the experiments, numerical simulations and in the simple cubic array: i) the fluctuations in the number of contacts is in phase with the macroscopic fluctuations in strength, and ii) new contacts are formed in the direction of applied principal stress, while contacts are lost in the other directions. This process can be continued until the number of contacts decreases to yield a coordination number of approximately 3 where the sample acquires a statically determinate fabric. At this point a global geometric instability may occur and the whole sample may collapse. Specifically, at very large strains ($\gamma_{oct} > 10\%$) hollow cylinder specimens subjected to compression buckled and collapsed.

CHAPTER 7

BEHAVIOR OF A GRANULAR MEDIUM UNDER REVERSIBLE LOADING

7.1 General

This chapter presents the results of experiments using hollow cylindrical specimens composed of mixture 2 of glass beads. In this mixture, the particle diameters ranged from 0.180mm to 0.430mm and were mixed with a ratio 1:2 in weight. The specimens were loaded along specific stress paths to determine their initial and subsequent yield loci. All specimens were prepared by the dry pluviation technique as described in Section 3.3 and were consolidated under isotropic confining pressure. A total of five such successful tests are presented.

The purpose of these tests was to determine the initial yield surfaces and the motion, expansion, and distortion of the subsequent yield surfaces of specimens composed of glass beads. In all tests the mean stress, σ_m, was kept constant and equal to the confining pressure during shear, so that all experimental data from the tests were on one octahedral plane π-plane. In all experiments presented in this chapter, σ_m = 138 KPa.

7.2 Yielding in Soils

Granular media exhibit nonlinear inelastic stress-strain behavior even at very small strains. Thus, cohesionless aggregates do not have a clear "elastic region" followed by an initial yield surface. Therefore, contrary to metals and other materials with clearly defined elastic and plastic behavior, each initial yield surface can not be defined as the locus of all points beyond which plastic deformation occurs.

In contrast to metals, there are two distinct deformation mechanisms which take place during loading of a granular medium. At very small strains there are no particles sliding and all macroscopic nonlinearity is the result of nonlinearities at the intergranular contacts. The normal component of the deformation at the contact is nonlinear elastic, while the tangential component is nonlinear inelastic as a result of the slip at the edges of the contact annulus between two spheres (Mindlin and Deresiewicz 1953). In soils, hysteretic behavior is observed during low level shear strain cycling in the resonant column device, but no permanent volumetric changes or pore pressure buildup accumulates. At larger strains, there is *sliding* between the particles, which move and rearrange themselves and as a result the fabric changes. This change of fabric manifests itself by irreversible volumetric changes if the loading takes place under drained conditions or by irreversible pore pressure, if the loading occurs under undrained conditions. The strain level at which this occurs has been experimentally determined (Dobry et al. 1982) to be on the order of 10^{-4} for the level of mean stress used in soil testing (40-270 KPa) and it is called the *threshold strain*, γ_t. This sliding of particles is directly analogous to "slip" in the micromechanics of crystals. The macroscopic strain caused by the slip at the contact annulus is an order of magnitude smaller than the strain caused by sliding, and it can be considered to be a second order effect. There is no term analogous to "slip" in granular media in the micromechanics of polycrystalline aggregates. Therefore, one possible definition of yielding, in

a manner directly analogous to yielding in metals, is the point in stress space at which the fabric of the material changes, that is when the first granules *slide*. Since this is very difficult to monitor in the laboratory, yielding could be defined as the locus of all points in stress space at which the value of the octahedral shear strain is less than 10^{-4}.

Another possible definition of a yield surface is to assume a mathematical model of the type proposed by Mroz (1967) or Prevost (1978), which describes the nonlinear behavior of materials by a number of nested yield surfaces associated with a constant tangent elastoplastic modulus. However, this is very difficult to achieve in the laboratory. This approach has been attempted in this testing program, but a sophisticated algorithm was needed to smooth the data in real time so that the tangent modulus could be accurately defined. Unfortunately, this was beyond the capabilities of the computer used to control the experiments. Simple smoothing techniques did not work well enough, and the scheme was abandoned.

As a result of the inability to use the tangent modulus approach, the yield surface was defined as the locus of all points in stress space [$\tau_{z\theta}$, (σ_{zz} - σ_{rr})/2] that had the same value of total (elastic plus plastic) octahedral shear strain, $\gamma^{t}_{oct} = \gamma^{e}_{oct} + \gamma^{p}_{oct}$. The value of γ^{e}_{oct} should be as close to the threshold value as possible, given the restrictions posed by the experimental device, so that γ^{p}_{oct} would be close to zero. While a criterion of an octahedral shear strain of 10^{-4} does not necessarily imply that only one sphere has slipped, it is assumed that a small percentage of particles have slid and that the yield loci obtained using this approach are *homothetic* to the true yield surfaces. Throughout this experimental research it has been attempted to approach the above "yield" criterion, but it has been determined that, given the accuracy of the measuring devices, the smallest value of γ^{e}_{oct} which can give meaningful results is $\gamma^{e}_{oct} = 3X10^{-4} = 0.03\%$. Consequently, this value of octahedral shear strain was used as the yield criterion in the yield surface tests of this experimental work.

7.3 Initial Yield Loci

The initial yield locus of this granular medium was defined based on the monotonic tests on the same material presented in the previous chapter, including the monotonic portion of cyclic tests. Four stress paths were used on one π-plane (138 KPa): compression (θ=0°) , torsion (θ=30°), compression/torsion (θ=15°) and extension (θ=60°). The stress values at $\gamma^{e}_{oct} = 3X10^{-4}$, measured from the origin, were recorded and a smooth curve was fitted through the points in the [$\tau_{z\theta}$, (σ_{zz} - σ_{rr})/2] stress space.

Figure 59 sketches an initial yield locus (surface) obtained from such experiments. Each point on the yield surface satisfying the criterion $\gamma^{e}_{oct} = 3X10^{-4}$ is obtained from drained proportional monotonic radial shear tests conducted on undisturbed specimens. Once this monotonic test series was completed and the shape and locations of the initial yield locus were determined, a series of cyclic tests (tests with stress reversal) followed. The purpose of these tests was to determine the location and shape of yield locus after prestraining (subsequent yield locus).

7.4 Subsequent Yield Loci

The subsequent yield loci of a granular medium were defined based on a new series of experiments along specific stress paths presented in this section. The subsequent yield surface is the yield surface after prestraining. The goal is to identify any differences in material symmetry that would occur as a result of a new texture created during prestraining and the hardening mechanism of the material. A sketch of the stress paths followed to determine the subsequent yield surface (locus) are presented in Fig 59. In this sketch, each isotropically consolidated specimen was first subjected to a monotonically increasing axial or torsional load to a point in stress space corresponding to a value of octahedral shear strain, γ_{oct}, much larger (approximately one order of magnitude) than γ^e_{oct}. This prestraining point (point 1 in the axial direction in Fig. 59) is by definition on the yield locus. Based on this, the location of a second point on the surface was sought. The loading was reversed from point 1 along the same direction as loading (in this case along the $(\sigma_{zz} - \sigma_{rr})/2$ axis) to point 2 (Fig. 59) so that the octahedral of the shear strain difference between points 1 and 2 was equal to twice the value of the octahedral shear strain, γ^e_{oct}, used as yield criterion. At point 2 the load was reversed until point O' was reached at a strain equal to that used as the yield criterion measured from point 2. Point O' was assumed to be the center of this subsequent yield locus and was kept fixed in stress space. To obtain the other points on the surface, the same procedure was repeated with O' as the origin: the load would increase until an octahedral difference in shear strain between O' and the new point equal to the criterion was observed. This is illustrated in Fig. 60, where points O' and A are on the octahedral π-plane, **O'A** is the prestraining to point A on this octahedral strain plane, O' is the center, and **O'A** is the radius of the yield locus; in our case $|\mathbf{O'A}| = \gamma^e_{oct} = 0.03\%$. $|\mathbf{O'A}|$ is the octahedral of the difference between strains **OO'** and **OA**. Analytically, the expression for defining the octahedral strain difference used as criterion at point A on the yield locus is:

$$\Delta\gamma^e_{oct} = (2/3)\{[(\varepsilon_{1A}-\varepsilon_{1O'})-(\varepsilon_{2A}-\varepsilon_{2O'})]^2+[(\varepsilon_{2A}-\varepsilon_{2O'})-(\varepsilon_{3A}-\varepsilon_{3O'})]^2+[(\varepsilon_{3A}-\varepsilon_{3O'})-(\varepsilon_{1A}-\varepsilon_{1O'})]^2\} \qquad (7.1)$$

There is no specific order of the sequence in which the points are followed; special care has been taken to ensure that all points on one side of the yield locus are never recorded in a sequence so as to avoid accumulated experimental error. In all cases, however, the load reverses along the direction of prior loading to correct for the plastic strain which would have accumulated by overshooting the yield locus due to numerical control errors.

A typical sequence used for obtaining the data points during a test is illustrated if the numbers in Fig. 59 are followed in ascending order either along the compressive or torsional prestress paths. After prestraining to 1 and determining point 2, the stress returns to point O' in stress space and then increases to point 3. Equation 7.1 is continuously applied and once $\Delta\gamma^e_{oct}$ reaches the prescribed value for yielding, the loading stops, the coordinates of point 3 in stress *and* strain space are recorded and the stress reverses in the opposite direction to point 4. On the way to point 4, the location of point O' in stress space is checked to see if and how much it has moved. If the movement is excessive, the error due to accumulated plastic deformation is serious and the experiment stops. To determine the location of point 4, the same procedure as in point 3 is followed. Equation 7.1 is computed continuously and compared to the yielding value in real time. Then, from point 4, the stress returns to O' and once its location is verified, a stress

trajectory to point 5 is followed. To determine point 5, the same procedure followed for establishing points 3 and 4 is used. During a typical test 4, 8 or 12 points are obtained per surface. While in principle more points on the surface could be defined, the subsequent yield locus shape is accurately described by 8 or 12 points, while 4 points give a good indication of the distortion of the surface during prestraining. In addition, given the criterion being used (γ_{oct} = 0.03%) the accumulated error due to plastic strain usually becomes important after that many points at large prestrains (γ_{oct} > .5 %) and these points may have to be discarded. As a result of this, in a typical experiment the number of points defining a surface has been dropped to four for large prestrains. Another reason for reducing the number of points probes is that these experiments are very time consuming, and by taking fewer points per surface considerable time is saved.

7.3 Experimentally Obtained Yield Loci

A total of five tests with stress reversal were performed on hollow cylindrical specimens made out of glass beads using mixture 2. In all tests the mean stress σ_m was kept constant and equal to the initial confining pressure which was approximately equal to 138 KPa. Therefore, all experimentally determined yield surfaces lie on this octahedral plane. In this testing series, specimens were prestrained in compression, extension and torsion so that the effect of prestraining on the yield surface would be identified and compared in three directions. No yield surfaces were obtained after prestraining along a non-proportional path.

The initial yield surface was defined by all radial monotonic experiments as described in detail in sections 6.5 and 7.1 (Figs 43 and 46). The yield surface obtained appears in Fig. 61; its shape is circular since the behavior of the material can be assumed in first approximation to be isotropic. The radius of the initial locus is approximately 17 KPa.

Figure 62 depicts the octahedral shear stress-strain curve obtained during the first prestraining experiment in compression (GB27). In this and all subsequent experiments defining the yield locus, the loading sequence performed was identical to that described in the previous section. The specimens were prestrained first to $\gamma_{oct} \cong 0.24\%$, were unloaded 0.06% to point 2 and then they were reloaded by $\Delta\gamma_{oct} = 0.03\%$ to point O'. Thus O' was defined as the reference point from which the subsequent yield surface passing through points 1 and 2 was determined. There were 5 investigations for the subsequent yield surfaces in this experiment performed after prestraining to γ_{oct}= 0.24, 0.38, 0.5, 0.657 and 0.77 %. There were four probes per yield locus investigated. It can be seen from the stress-strain curve in Fig. 62 that there is little accumulated plastic strain throughout the cyclic loading which is the result of using as amplitude of cyclic loading a strain value close to the threshold strain. The volumetric strain - shear strain curve which appears in Fig. 63 indicates that there are significant volumetric strains taking place when the loading is reversed. The material dilates with increasing strain and its behavior is similar to that obtained from the monotonic tests, but any time the loading is reversed it is accompanied by significant contractive volumetric strains. Given that the material fabric has changed because of prestraining and that a new anisotropic texture with coupled shear and normal components has essentially developed, it is believed that the observed volumetric strains are mostly elastic since they dissipate when the loading reverses. The yield loci obtained appear in Fig. 64 plotted in

stress space. Although only four points per locus were obtained, it can be seen that all subsequent yield loci have developed an apex in the direction of prestraining, while they have become flatter in the opposite direction. Their dimension in the direction of prestraining has shortened compared to the initial locus, whereas in the direction perpendicular to prestraining, the width of the yield locus has remained the same. The apex and the flattening become more pronounced with increasing strain.

Figure 65 presents the yield surfaces obtained after prestraining a specimen in torsion (GB28) to γ_{oct}= 0.36, 0.507 and 0.65%. The first subsequent surface was defined by 12 points, the second by 8 and the third by four. Unfortunately, there was a problem during setup which caused an error in the control algorithm which caused unloading and then loading along the intermediate strain range and the results of this test may be not be reliable.

Figure 66 presents the yield surfaces obtained after prestraining a specimen in torsion (GB29) to γ_{oct}= 0.263, 0.352, 0.506 and 0.738%. All subsequent loci were defined by 8 probes, except for the last which was defined by four. The yield loci obtained in this experiment have developed an apex in the direction of prestraining, and have flattened in the opposite direction with both effects becoming more pronounced with increasing prestrain. The width of the surface has shrunk both in the direction of loading and perpendicular to it. Distortions occur only in the direction of loading. The octahedral shear stress-shear strain from this experiment appears in Fig. 67 and the volumetric strain vs octahedral shear strain curve in Fig. 68. The volumetric strain, although globally dilative, exhibits significant fluctuations during small strain probing, as in all tests in this series.

Figure 69 presents the yield loci obtained after prestraining in compression to γ_{oct}= 0.255, 0.39, 0.498 and 0.706%. All subsequent loci were defined by 8 points, except for the third which was defined by four. The yield surface size decreases in all sizes, but the distortions take place only in the direction of prestraining. Both the apex and the flattening of the surface become more pronounced with increasing prestrain. The stress-strain and the volumetric strain versus shear strain curves appear in Figs. 70 and 71. Figure 71 also contains the volumetric versus shear strain curves from compression probe test (GB27) and monotonic compression test GB26. It can be seen that the behavior of the monotonic and cyclic tests is dilative and that the volumetric curves of both cyclic tests coincide. The large volumetric strains which occur during the probes on the onset of load reversal, appear to be mostly elastic since they are cancelled when the incremental loading is stopped. Once the yield locus has been determined and the cyclic loading stops the volumetric strain experienced during probing returns to the "backbone" volumetric strain curve, which is in good agreement with the curve from the monotonic experiment. If the difference in volumetric strains between the monotonic and cyclic experiments during prestraining to γ_{oct}=0.25% is considered to be the result of specimen variability, the total accumulated volumetric strain is less than 0.005%, which is at the limit of the resolution of the measuring devices. Consequently, these sudden increases in volumetric strain appear to be largely elastic and they are the result of the anisotropy in the fabric of the material developed during prestraining. The material has developed a texture in the direction of prestraining, and as long as the glass beads specimen is strained in this direction, the behavior continues to be similar to that observed in the monotonic experiments. Once the loading is reversed, even the smallest

decrement reveals the anisotropy present. This anisotropy is manifested by large elastic volumetric strains which are the result of coupling between shear and normal terms in the textured material properties.

The yield loci obtained after prestraining the material in extension appear in Fig. 72. In this case specimen GB33 was prestrained to γ_{oct}= 0.271, 0.370, 0.521 and 0.838%. All loci were defined by 4 points except for the first which was defined by 8. The shape of the subsequent yield surfaces is very similar to that obtained after prestraining along compression and torsion. The size of the surface decreases with straining in all directions, while the distortions take place only in the direction of prestraining. The stress-strain and volumetric-shear strain curves appear in Figs. 73 and 74, where it can be seen that the volumetric behavior is dilative as in the monotonic tests, but, as in all other cyclic experiments, significant volumetric strains occur during the small amplitude cycling performed to investigate the subsequent yield locus.

Finally Fig. 75 is a composite plot presenting the initial yield locus with the subsequent loci that were obtained after prestraining in compression, torsion and extension. Figure 76 presents the same information, this time only for the first subsequent yield surface obtained after prestraining to $\gamma_{oct} \equiv 0.25\%$. In both figures the yield surfaces obtained after prestraining along different stress paths are very similar, although the loci obtained after prestraining in compression are somewhat smoother than those obtained after prestraining in the other directions. This may be the result of inherent anisotropy due to gravity. Nevertheless, these experiments demonstrate that after prestraining, the material develops an anisotropic texture in the direction of loading which manifests itself by a distortion of the yield surface. In order to understand and interpret the micromechanical phenomena present in this distortion a series of numerical simulations was performed on two and three dimensional assemblies of rough, elastic quartz spheres using program CONBAL. These numerical simulations along the same stress paths as this experimental study are presented in Volume III of this investigation.

CHAPTER 8

DISCUSSION AND CONCLUSIONS

The object of this experimental project has been to investigate the behavior of granular media and to determine the necessary parameters for a micromechanically based constitutive law for these materials. This investigation consisted of experiments on long, thin, hollow cylindrical specimens on glass beads, conducted on an MTS servolydraulic device by applying a combination of axial and torsional stresses. Since the properties of the grain packings within the assembly of spherical particles are pressure dependent, each test was performed under a constant mean stress.

A key issue of this research has been the determination of the initial and subsequent yield surfaces (loci) of a granular medium. The yield surfaces were defined as the set of all points in stress space which have a constant value of octahedral strain, defined low enough so as not to cause plastic deformation. This definition of the yield surface in granular media was adopted because of the nonlinear inelastic stress-strain behavior exhibited by granular materials, even at very low strain levels, which is caused by the slip taking place at the intergranular contact annulus. This definition of the initial yield surface is similar to that used by Sture and his coworkers (Sture et al. 1987) for studying the yielding characteristics of sand. In contrast to similar studies in sands, the present study uses only one specimen which is first presheared and then loaded and unloaded in a number of directions. This procedure is analogous to that developed by Phillips and now widely used in experimental plasticity studies of metals, and is also very similar to that used by Dvorak et al (1988) for metal matrix composites. It has been determined that the plastic strains accumulated using this procedure in the experiments presented in this volume are not significant.

The experimental results obtained indicate that the subsequent yield surfaces distort in the direction of loading by forming an apex along the prestrain direction, while becoming flatter in the opposite direction. The size of the surface decreases with prestrain in all directions, although distortions take place only in the prestraining direction. This distortion of the yield surface, which has also been found in metals, is the result of sliding mechanisms which occur at the micromechanical level during loading. Specifically, during loading, the interparticle contacts form in the direction of the applied major principal stress and they are eliminated along the minor principal stress. On the average, the number of contacts drops with increasing strain. This process of contact formation and elimination creates an anisotropic fabric in the material by aligning the sliding mechanisms in one direction. These sliding planes define parallel yield planes, the envelope of which defines the yield surface. During loading, sliding occurs in these sliding planes which causes macroscopic plastic deformations. After sliding has occurred, each surface of the macroscopic yield surface expands and shifts differently. These slip directions are more or less parallel to the direction of the plane of the maximum shear stress acting on the aggregate, and as the load is increased more slip planes are activated and increasingly more yield planes pass through the loading point on the macroscopic yield surface. These yield planes of different orientations intersect at this point on the surface and form a smooth vertex, similar to that observed in the experiments. Other sliding mechanisms stop at dense (stiff) packings in the material and the resulting strain gradient causes an elevation of the yield point and the apex. In

the opposite direction, once loading is reversed, the sliding of the particles occurs along the same sliding mechanisms activated during loading, but now in the opposite direction. There is no strain gradient, the yield point drops and the yield surface flattens in this direction. Along directions perpendicular to prestraining, the material has not developed a strong texture, its behavior is similar to that of the initial undisturbed medium, and the yield locus does not deform significantly in this direction. Therefore, the macroscopic behavior of a granular medium is controlled by micromechanical phenomena at the interparticle contact level, without which the macroscopic behavior can not be fully interpreted.

Besides these yield surface findings that are central to plasticity theory typically used to model experimental data, a number of other important aspects of the behavior of granular medium have been observed. These include the importance of correction for errors caused by membrane compliance in experiments where the lateral stress is changing, the existence of local instabilities in a granular medium composed of equal spherical particles, and the significant volumetric changes that occur during small strain unloading after preshearing.

The errors due to membrane compliance are of great importance to both undrained and drained testing. The macroscopic volumetric behavior is affected by these errors, which, if not corrected, can lead to the wrong conclusions and measurements. Correcting for these effects is very simple and does not require any specialized equipment.

The discontinuities observed in the monotonic stress-strain curves of specimens composed of equally sized particles are the result of instabilities of the microstructure. The phenomenon is most pronounced in packings of regular spheres, and is the result of crystallization that takes place in such packings. These regular regions collapse and form during loading and these sudden changes in the microstructure are reflected by the discontinuities or jumps in the macroscopic measurements.

REFERENCES

Alawi, M.M., Sture, S., and Ko H.–Y. (1988), "True Triaxial and Directional Shear Cell Experiments on Dry Sand," U.S. Army Waterways Experiment Station Report.

Arthur, J.R.F., Cutler, F., Dunstan, T., Ford, J. Leavell, D. A., Peters, J. F. and Pulsford, J. R. (1988), "Design Development and Operation of an Advanced Directional Shear Cell", U. S. Army WES Report.

Baldi, G., and Nova, R. (1984), "Membrane Penetration Effects in Triaxial Testing," ASCE, JGED 110(3), March.

Baladi, G.Y. and Rohani, B. (1979), "Elastic–plastic Model for Saturated Sand," Journal of the Geotechnical Engineering Division, ASCE, Vol. 105, No. GT4, April, pp. 465–480.

Baziar, M.H., (1987), "Influence of the Testing Technique on the Steady State Lines of a Sand," M.S. Thesis submitted to RPI, Troy, N.Y.

Bishop, A.W., (1966), "The Strength of Soils as Engineering Materials," Geotechnique, Vol. 16, No. 1, pp. 89–130

Borowicka, H. (1973), "Rearrangements of Grains by Shear Test with Sand," Proc., 8th ICSMFE, Vol. 1, pp. 71–77.

Budiansky, B. and Wu, T. (1962), "Theoretical Predictions of Plastic Strains of Polycrystals," Proc., 4th U.S. Nat. Congr. Appl. Mech., pp 1175–1185.

Broms, B.B. and Casbarian, A.O. (1965), "Effect of Rotation of Principal Stress Axes and the Intermediate Stress on Shear Strength," Proc. 6th Inter. Conf. on Soil Mech. and Found. Eng., Montreal, Vol. 1, pp. 179–183.

Broms, B.B. and Jamal, A.K. (1965), "Analysis of the Triaxial Test–Cohesionless Soil," Proc. 6th Inter. Conf. on Soil Mech. and Found. Eng., Montreal, Vol. 1, pp. 184–188.

Broms, B.B. and Ratnam, M.V. (1963), "Shear Strength of an Anisotropically Consolidated Clay", Journal of Soil Mechanics and Foundation Engineering Division, ASCE, Vol. 89, No. SM6, pp. 1–26.

Canova, G.R., Kocks, U.F., Tome, C.N., Jonas, J.J. (1985), "The Yield Surface of Textured Polycrystals," J. Mech. Phys. Solids, Vol. 33, No. 4, pp. 371–397.

Chen, W.F. (1975), Limit Analysis and Soil PLasticity, Elsevier Scientific Publishing Co., Amsterdam, The Netherlands.

Chen, Y., (1986), "Experimental Determination of Fabric for Granular Materials," Ph.D. Thesis presented to the Faculty of the Graduate School of Cornell University, Ithaca, N.Y.

Cooling, L.F. and Smith, D.B. (1936), "The Shearing Resistance of Soils," Proc. Institution of Civil Engineers, London 3, pp. 333–343,

Cundall, P. A. and Strack, O. D. (1979), "A Discrete Numerical Model for Granular Assemblies," Geotechnique, 29, No. 1, pp. 47–65.

Dafalias, Y.F. and Popov, E. (1976), "Plastic Internal Variables Formalism of Cyclic Plasticity," Inter. Symp. on Soils under Cyclic Plasticity, Journal of Applied Mechanics, Dec., pp. 645–651.

Dafalias Y. (1979), "Anisotropic Hardening of Initially Orthotropic Materials, " ZAMM, 59, pp. 437–416.

Dafalias Y.F., and Hermann, L.R. (1982), "Bounding Surface Formulation of Soil Plasticity," Intl. Symp. on Soils under Cyclic and Transient Loading", G. Pande and O.C. Zienkiewicz, eds., Wiley, London, U.K., pp. 253–282.

Dafalias, Y.F. (1982), "Bounding Surface Plasticity. I: Mathematical Foundation and Hypoplasticity, " J. Eng. Mechanics, Vol. 112, No. 9, pp. 966–987.

DiMaggio, F.L. and Sandler, I.S. (1976), "Materials Models for Granular Soils," J. Eng. Mechanics, Vol. 97, No. EM3, June, pp. 935–950

DeNatale, J.S. and Vrymoed, J.L. (1981), "Analysis and Stress Distribution in Torsional Shear Testing," First Conference on Recent Advances on Geotechnical Earthquake Engineering, Univ. Missuri–Rolla, St Louis, Vol. 1, pp. 145–148.

Dobry, R., Ladd, R., Yokel, F.Y., Chung, R.M., Powell, D. (1982), "Prediction of Pore Water Pressure Buildup and Liquefaction of Sands During Earthquakes by the Cyclic Strain Method," Building Science Series 138, National Bureau of Standards.

Dobry, R., Ng., T., Petrakis, E., Seridi, A. (1989), "An Incremental Elastic–Plastic Model for the Force–displacement Relation at the Contact Between Two Spheres," submitted for publication to the Journal of Engineering Mechanics, ASCE.

Drnevich, V.P. (1972), "Undrained Cyclic Shear of Saturated Sands," Journal of Mechanics and Foundation Division, ASCE, Vol. 98, No. SM8, August, pp. 807–825.

Drucker, D.C., and Palgen, L. (1981), "On Stress–Strain Relations Suitable for Cyclic and Other Loading," J. Appl. Mechanics, September, pp. 479–485.

Dvorak, G.J. (1987), "plasticity of Fibrous Composites," Report to U.S. ARO, Dept. Civil Engineering, Rensselaer Polytechnic Institute, Troy N.Y.

Dvorak, G.J. Bahei–El–Din, Y.A., Macheret, Y., and Liu, C.H. (1988), "An Experimental Study of Elastic–Plastic Behavior of a Fibrous Boron Aluminum Composite," Report to ONR, dept. Civil Engineering, Rensselaer Polytechnic Institute, Troy, N.Y.

Eisenberg, M.A. and Yen, C.F. (1981), "A Theory of Multiaxial Anisotropic Viscoplasticity," J. Appl. Mechanics, Vol. 48, June, pp. 276–284.

Eisenberg, M.A. and Yen, C.F. (1984), "The Anisotropic Deformation of Yield Surfaces," J. Engineering Materials and Technology, Vol. 106, Oct., pp. 355–360.

Ergun, M.U., (1981), "Evaluation of the Three–Dimensional Shear Testing, " Proc. 10th Int. Conf. Soil Mech. and Found. Engng, Stockholm, Vol. 1, pp. 593–596.

Ersig, M.I. and Bembem, S.M. (1965), "Discussion on Soil Properties–Shear Strength and Consolidation," Proc. 6th Inter. Conf. on Soil Mechanics and Foundation Engineering, Montreal, Vol. 3, pp. 321–323.

Frydman, S., Zeitlen, J. G., and Alpan, I. (1973), "The Membrane Effect in Triaxial Testing of Granular Soils," J. Testing and Evaluation, 1(1):37-41, January.

Goode, C.D. and Helmy, M.A. (1967), "The Strength of Concrete under Combined Tensile and Compressive Stress," Magazine of Conc. res. 19, pp. 105–112.

Hardin, B.O. (1978), "Plasticity Theory for Soil Stress–Strain Behavior," Journal of the Engineering Mechanics Division, ASCE, Vol. 104,No. EM5, pp. 1177–1194.

Haruyama, M. (1981), "ANisotropic Deformation–Strength Characteristics of an Assembly of Spherical Particles under Three Dimensional Stresses," Soil and Foundations, Vol. 21, No. 4, Dec., pp. 41–55.

Helling, D.E., Miller, A.K., and Stout, M.G. (1986), "An Experimental Investigation of the Yield Loci of 1100–0 Aluminum, 70:30 Brass and an Overaged 2024 Aluminum Alloy After Various Prestrains," J. of Engineering Materials and Technology, Vol. 108, pp. 313–320.

Hight, D.W., Gens, A., and Symes, M.J. (1983),"The Development of a New Hollow Cylinder Apparatus for Investigating the Effect of Principal Stress Rotation in Soils," Geotechnique, Vol. 33, No. 4, pp. 355–383.

Hight, D.W., Gens, A., and Symes, M.J. (1985), "The development of a New Hollow Cylinder Apparatus for Investigating the Effects of Principal Stress Rotation in Soils, and Undrained Anisotropy and Principal Stress Rotation in Saturated Sand," Discussion, Geotechnique, Vol. 35, No. 1, March, pp. 78–85.

Hersey, A.V. (1954), "The Plasticity of an Isotropic Aggregate of Anisotropic Face–Centered Cubic Crystals," J. Appl. Mechanics, Sept., pp. 241–249.

Hill, R. (1950), The Mathematical Theory of Plasticity, Oxford University Press, London, U.K.

Hill, R. (1967), "The Essential Structure of Constitutive Laws for Metal Composites and Polycrystals," J. Mech. Phys. Solids, Vol. 15, pp. 79–95.

Ishibashi, I. and Sherif, M.A. (1974), "Soil Liquefaction by Torsional Shear Device," Journal of Geotechnical Engineering Division, ASCE, Vol. 100, No. GT8, Aug., pp. 871–888.

Iwan, W.D. (1976), "On a Class of Models for the Yielding Behavior of Continuous and Composite Systems," Journal of Applied Mechanics, Vol. 34, pp. 612–617.

Jenkins and Satake, editors (1983), Mechanics of Granular Materials: New Models and Constitutive Relations, Proceedings of US–Japan Seminar, Ithaca, New York.

Kallstenius, T. and Bergau, W. (1961), "Research on the Texture of Granular Masses," Proc. 5th Int. Conf. on Soil Mechanics and Foundation Engineering, Vol. 1, pp. 165–170.

Keikbusch, M., and Schuppener, B. (1977), "Membrane Penetration and Its Effect on Pore Pressures," ASCE, JGED 103(GT11):1267-1279, November.

Kelley, E.W., and W.F. Hosford (1968), "The Deformation Characteristics of Textured Magnesium," Transactions of the Metallurgical Society of AIME, Vol. 242, April, pp. 654–660.

Kirkpatrick, W.M. (1957), "The Conditions of Failure for Sands," Proc. 4th Int. Conf. on Soil Mechanics and Foundation Engineering, London, Vol. 1, pp. 172–178.

Klisinski, M., Sture, S., Runesson, K., and Ko, H.K. (1988), "Incremental Constitutive for Cohesionless Granular Materials Based on Fuzzy Sets," Proceedings, 7th ASCE–EMD Specialty Conference, Blacksburg, VA, pp. 150.

Knox, D.P., Stokoe, K.H., and Kopperman, S.E. (1982), "Effects of State of Stress on Velocity of Low Amplitude Shear Waves Propagating Along Principal Stress Directions in Dry Sand," Geotechnical Engineering Report, GR82–22, University of Texas, TX.

Kondner, R.L. (1963), "Hyperbolic Stress–Strain Response: Cohesive Soils," Journal of Soil Mechanics and Foundation Division, ASCE, Vol. 89, No. SM1, pp. 883–897.

Konishi, J. (1978), "Microscopic Model Studies on the Mechanical Behavior of Granular Materials," Proceedings US–Japan Seminar on Continuum Mechanical and Statistical Approaches in the Mechanics of Granular Materials, Cowin and Satake, editors, pp. 26–46.

Koppermann, S.E., Stokoe, K.H., and Knox, D.P. (1982), "Effect of State of Stress on Velocity of Low Amplitude Compression Waves Propagating Along Principal Stress Directions in Sand," Geotechnical Engineering Report, GR82–22, University of Texas, Austin, Texas.

Ladd, R.S. (1978), "Preparing Test Specimens Using Undercompaction," Geotechnical Testing Journal, Vol. 1, No. 1, March, pp. 16–23.

Ladd, R.S. and Silver, M.L. (1975) "Discussion of Soil Liquefaction by Torsional Simple Shear Device," Journal of Geotechnical Engineering Division, ASCE, Vol. 101, No. GT8, Aug., pp. 827–829.

Lade, P.V. (1977), "Elastoplastic Stress–Strain Theory for Cohesionless Soil with Curved Yield Surfaces," Int. J. Solids Structures, Vol. 13, pp. 1019–1035.

Lade, P.V. and Duncan, J.M. (1975), "Elastoplastic Stress–Strain Theory for Cohesionless Soil,"Journal of Geotechnical Engineering Division, ASCE, Vol. 101, No. GT10, pp. 1177–1194.

Lade, P. V., and Hernandez, S. B. (1977), "Membrane Penetration Effects in Undrained Tests," ASCE, JGED 103(GT2):109-125, February.

Lambe, T. and Whitman, R. (1969), Soil Mechanics, John Wiley and Sons, NY.

Lewin, P.I., Yamada, Y., and Ishihara, K. (1982), "Correlating Drained and Undrained 3D Tests on Loose Sand," Proc. IUTAM Conf. Deformation and Failure of Granular Materials, Delft., pp. 419–429.

Lin, T.H. and Ito, M. (1965), "Theoretical Plastic Distortion of Polycrystalline Aggregate under Combined and Reversed Stresses," J. Mech. Phys. Solids, Vol. 13, pp. 103–115.

Lin, T.H. and Ito, M. (1966), "Theoretical Plastic Stress–Strain Relationship of a Polycrystal and the Comparison with the Von Mises and the Tresca Plasticity Theories," Intl. J. Eng. Sci. 4:543–561.

Martin, G. R., Finn, W. D. L., and Seed, H. B. (1978), "Effects of System Compliance on Liquefaction Tests," ASCE, JGED 104(GT4):463-479, April.

Mroz, Z. (1967), "On the Description of Anisotropic Workhardening," J. Mech. Phys. Solids, Vol. 15, pp. 163–175.

Naghdi, P.M., Essenburg, F., and Knoff, W. (1958), "An Experimental Study of Initial and Subsequent Yield Surfaces in Plasticity," J. Appl. Mech., June, pp. 201–209.

Ng, T.T. (1989), "Numerical Simulations of Granular Soil under Monotonic and Cyclic Loading: A Particulate Mechanics Approach". Dissertation submitted to the graduate School at Rensselaer Polytechnic Institute as a partial fulfillment of the requirement for the degree of Doctor of Rhilosophy. Rensselaer Polytechnic Institute, Troy, NY.

Oda, M., Konishi, J, and Nemat–Nasser, S. (1983), "Experimental Micromechanical Evaluation of the Strength of Granular Materials; Effects of Particle Rolling," Mechanics of Granular Materials: New Models and Constitutive Relations, Jenkins and Satake,editors, pp. 21–30.

Peters, J.F. (1988), "Kinematic Hardening under Jump Rotations," Proceedings 7th Engineering Mechanics Conference, Blacksburg, VA, pp. 207.

Petrakis, E., and Dobry, R. (1986), "A Self Consistent Estimate of the Elastic Constants of a Random Array of Equal Spheres with Application to Granular Soil under Isotropic Conditions," Report CE–86–04, Dept. Civil Engineering, Rensselaer Polytechnic Institute, Troy, NY.

Petrakis, E., and Dobry, R. (1987a), "A Two–Dimensional Numerical Micromechanical Model for a Granular Soil at Small Strains," Report CE–87–01, Rensselaer Polytechnic Institute, Troy, NY.

Petrakis, E., and Dobry, R. (1987b), "Micromechanical Modeling of Granular Soil at Small Strain by Arrays of Elastic Spheres," Report CE–87–02, Dept. Civil Engineering, Rensselaer Polytechnic Institute, Troy, NY.

Petrakis, E., Dobry, R., and Ng, T. (1988), "Small Strain Response of Random Arrays of Elastic Spheres Using a Nonlinear Distinct Element Procedure," Report CE–88–02, Dept. Civil Engineering, Rensselaer Polytechnic Institute, Troy, NY.

Petrakis, E. and Dobry, R. (1989), "Micromechanical behavior and Modeling of Granular Soils,"Report to Airforce, Dept. Civil Engineering, Rensselaer Polytechnic Institute, Troy, N.Y.

Phillips, A. (1968), "Yield Surfaces of Pure Aluminum at Elevated Temperatures," IUTAM–Symposium on Thermoinelasticity, pp. 241–258.

Phillips, A., Liu, C.S., and Justusson, J.W. (1970), "An Experimental Investigation of Yield Surfaces at Elevated Temperatures," Acta Mechanica, Vol. 14, pp. 119–146.

Phillips, A. and Tang, J.L. (1972), "The Effect of Loading Path on the Yield Surface at Elevated Temperatures," Int. J. Solids and Structures, Vol. 8, pp. 463–474.

Phillips, A. and Weng, G.J. (1975), "An Analytical Study of an Experimentally Verified Hardening Law," J. Appl. Mech., June, pp. 375–378.

Prager, N. (1955), "The Theory of Plasticity: A Survey of Recent Achievement," Proceedings Inst. Mech. Eng., Vol. 169, pp. 41–57, London, U.K.

Prevost, J.H. (1978), "Plasticity Theory for Soil Stress–Strain Behavior," Journal of the Engineering Mechanics Division, ASCE, Vol. 104, No. em5, pp. 1177–1194.

Raju, V. S., and Sadasivan, S. K. (1974), "Membrane Penetration in Triaxial Tests on Sands," ASCE, JGED 100(GT4):482-489, April.

Raju, V. S., and Venkataramana, K. (1990), "Undrained Triaxial Tests to Assess liquefaction Potential of Sands Effect of Membrane Penetration," Intl. Symp. Soils under Cyclic and Transient Loading, Swansea, 7-11 January, pp. 483-489.

Ramana, K. V., and Raju, V. S. (1982), "Membrane Penetration in Triaxial Tests," ASCE, JGED 108(GT2):305-310, February.

Roscoe, K.H. (1970), "The Influence of Strains in Soil Mechanics," Geotechnique, Vol. 20, pp. 129–170.

Rowe, P.W. (1962), "The Stress–Dilatancy Relation for Static Equilibrium of an Assembly of Particles in Contact," Proc. Roy. Soc., A269, pp. 500–527.

Saada, A.S. (1987), "International Workshop on Constitutive Equations for Granular Non–Cohesive Soils," Case Western Reserve University, Cleveland, OH., July.

Saada, A.S. and Baah, A.K. (1967), "Deformation and Failure of a Cross–Anisotropic Clay under Combined Stresses," Proc. 3rd Panamerican Conf. on Soil Mechanics and Foundation Engineering, Caracas, Vol. 1, pp. 67–88.

Saada, A.S. and Townsend, F.H. (1981), "Strength Laboratory Testing Of Soils – A State–of–the–Art," Proc. ASTM Sumb. Laboratory Shear Strength of Soil, Philadelphia STP 740, pp. 7–77.

Scott, G.D. (1960), Packing of Equal Spheres, Nature, Vol. 188, pp. 908–909.

Scott, R. and Ko, H. (1969), "Stress–Deformation and Strength Characteristics," State–of–the–Art Report, Proceedings 7th Int. Conf. on Soil Mechanics and Foundation Engineering, Mexico City, pp. 1–47.

Shiratori, E., Ikegami, K., Yoshida, Kaneko, K., Koike, S. (1976), "the Subsequent Yield Surfaces after Preloading under Combined Axial Load and Torsion," Bulletin of the LSME, Vol. 19, No. 134, August, pp. 877–883

Stout, M.G., Martin, P.L., Helling, D.E., and Canova, G.R. (1985), "Multiaxial Yield Behavior of 1100 Aluminum Following Various Magnitudes of Prestrain," Int. J. of Plasticity, Vol. 1, pp.163–174.

Sture, S., Alawi, M.M., and Ko, H.–Y. (1987), "True Triaxial and Directional Shear Cell Experiments on Dry Sand," Report to US Army Engng Waterways Experiment Station, Dep. of Civil, Environmental, and Architectural Engng, University of Colorado, Boulder, Colorado.

Suklje, A.S. and Baah, A.K. (1965), "Investigation of the Tensile Deformability of Soils using Hollow Cylinders," Proc. 6th Int. Conf. on Soil Mechanics and Foundation Engineering, MOntreal, Vol. 1, pp. 368–372.

Taylor, G.I. and Quinney, H. (1931), "The Plastic Distortion of Metals," Philosophical Transactions of the Royal Society of London, Series A, No. 230, pp. 323–362.

Voyiadjis, G. Z., and Fooroozesh, M. (1990), "Anisotropic Distortional Yield Model," J. Appl. Mechanics, ASME, Vol. 57, pp. 537-547.

Whitman, R.V. and Luscher, U. (1962), "Basic Experiment into Soil–Structure Interaction," Journal of Soil Mechanics and Foundation Engineering Division, ASCE, Vol. 88, No. SM6, pp. 135–167.

Wright, R.V., Gilbert, P.A., and Saada, A.S. (1978),"Shear Devices for Determining Dynamic Soil Properties," Proc. of the Earthquake engineering and Soil Dynamics Conference, Geotechnical Engineering Division, ASCE, Pasadena, June, pp. 19–21.

Yamada, Y. and Ishihara, K. (1979), "Anisotropic Deformation Characteristics under Three Dimensional Stress Condition," Soils and Foundations, Vol. 16, No. 2, pp. 1–18.

Yen, C.F. and Eisenberg, M.A. (1987), "The Role of a Loading Surface in Viscoplasticity Theory," Acta Mechanica, 69, pp. 77–96.

Yoshimi, Y. and Oh–Oka, H. (1973), "A Ring Torsion Apparatus for Simple Shear Tests," Proc. 8th Int. Conf. on Soil Mechanics and Foundation Engineering, Vol. 1, Part 2, Moscow, pp. 501–506.

Table 2

Tests on glass beads prepared with dry pluviation

Membrane compliance tests on a mixture of Glass Beads

Test ID	Stress path	Mean Stress	Rod diameter	Void Ratio	B-parameter	Material properties	Notes
MEMC1	Hydrostatic (cyclic)	37.2 - 344.0 KPa	1.90 cm	0.680	0.960	Glass Beads (40-50 and 60-80)	
MEMC2	Hydrostatic (cyclic)	35.7 - 311.8 KPa	3.19 cm	0.680	0.960	Glass Beads (40-50 and 60-80)	
MEMC3	Hydrostatic (cyclic)	33.6 - 309.6 KPa	NO ROD	0.680	0.960	Glass Beads (40-50 and 60-80)	
MEMC4	Hydrostatic (cyclic)	37.6 - 311.7 KPa	1.90 cm	0.680	0.960	Glass Beads (40-50 and 60-80)	

Table 3

Tests on glass beads prepared with dry undercompaction

Monotonic Tests on Glass Beads (1-diameter), Glass Beads (mixture) and Ottawa F125 Sand:

Test ID	Path	Mean Stress	Material	e	B-parameter	Material properties	Notes
MC11	Compression	138.6 KPa	Ottawa Sand	0.680	0.980	F-125	1
ME12	Extension	134.3 KPa	Glass Beads	0.590	0.994	Sieve No. 30 (0.6mm)	1
MC14	Compression	137.6 KPa	Glass Beads	0.580	0.968	Sieve No. 30 (0.6mm)	1
MT18	Torsion	142.1 KPa	Glass Beads	0.580	0.987	Sieve No. 30 (0.6mm)	1
MT21	Torsion	141.2 KPa	Glass Beads (mixt.)	0.603	0.963	Mixture: sieves No. 40-50 and 60-80	1
ME22	Extension	140.0 KPa	Glass Beads (mixt.)	0.602	0.985	Mixture: sieves No. 40-50 and 60-80	1
MT25	Torsion	138.0 KPa	Glass Beads (mixt.)	0.600	0.960	Mixture: sieves No. 40-50 and 60-80	1
MC23	Compression	136.8 KPa	Glass Beads (mixt.)	0.593	0.954	Mixture: sieves No. 40-50 and 60-80	1
MC32	Compression	277.0 KPa	Glass Beads (mixt.)	0.605	0.965	Mixture: sieves No. 40-50 and 60-80	1
MC33	Compression	414.1 KPa	Glass Beads (mixt.)	0.603	0.955	Mixture: sieves No. 40-50 and 60-80	1
MCT	Compression/Torsion	138.0 KPa	Glass Beads (mixt.)	0.600	0.960	Mixture: sieves No. 40-50 and 60-80	1,2
MCE	Compression/Extension	138.0 KPa	Glass Beads (mixt.)	0.600	0.960	Mixture: sieves No. 40-50 and 60-80	1,2

Tests with stress reversal and probes defining Yield Surfaces:

Test ID	Prestrain	Mean Stress	Material	e	B-parameter	Yield Criterion	Special (3)	No. cycles	Notes
D27	Torsion	138 KPa	Glass Beads (mixt.)	0.598	0.950	go=0.05%	Precycling	500	3,4
D29	Compression	138 KPa	Glass Beads (mixt.)	0.595	0.987	go=0.10%	N/A	N/A	1,5
D30	Torsion	138 KPa	Glass Beads (mixt.)	0.604	0.978	go=0.10%	Precycling	500	3,4
D34	Compression	138 KPa	Glass Beads (mixt.)	0.597	0.954	go=0.05%	N/A	N/A	4

Notes:

1) Data were corrected for membrane and torsional compliance after test
2) Non-proportional test
3) Precycling 500 cycles in low amplitude (0.05%) torsion to stiffen the specimen in the transverse direction
4) Due to difficulty in correcting for compliance errors after the test, data were not used
5) Due to difficulty in correcting for compliance errors after the test, only monotonic portion was used

Table 4

Tests on Glass Beads prepared under dry pluviation

Monotonic proportional and non-proportional tests

Test ID	Path	Mean Stress	Material	Void Ratio	B-parameter	Material properties	Notes
GB5	Compression	138 KPa	Glass Beads (mixt.)	0.633	0.872	Sieves No. 40-50 and 60-80	1,4,7a
GB6	Extension	138 KPa	Glass Beads (mixt.)	0.669	0.940	Sieves No. 40-50 and 60-80	4,7a
GB7	Torsion	138 KPa	Glass Beads (mixt.)	0.681	0.950	Sieves No. 40-50 and 60-80	2,4
GB20	Compression	138-200KPa	Glass Beads (mixt.)	0.680	0.970	Sieves No. 40-50 and 60-80	Triaxial
GB26	Compression	138 KPa	Glass Beads (mixt.)	0.672	0.950	Sieves No. 40-50 and 60-80	7a
GB32	Compression+Torsion	138 KPa	Glass Beads (mixt.)	0.673	0.970	Sieves No. 40-50 and 60-80	3,8,12

Tests with stress reversal and probes defining Yield Surfaces:

Test ID	Prestrain Direction	Mean Stress	Material	Void Ratio	B-parameter	Prestrain level	Yield Criterion	Notes
GB8	Compression	138 KPa	Glass Beads (mixt.)	0.695	0.925	γ_o=0.50%	γ_o=0.05%	3,6,7a,9
GB9	Compression	138 KPa	Glass Beads (mixt.)	0.674	0.960	γ_o=0.40%	γ_o=0.04%	3,6,7a,9
GB10	Compression	138 KPa	Glass Beads (mixt.)	0.682	0.950	γ_o=0.20%	γ_o=0.03%	3,6,7a,9
GB11	Compression/Torsion (+)	138 KPa	Glass Beads (mixt.)	0.668	0.950	γ_o=0.20%	γ_o=0.03%	3,6,7a,8,9
GB12	Compression	138 KPa	Glass Beads (mixt.)	0.667	0.930	γ_o=0.26%	γ_o=0.03%	3,6,7a,9
GB13	Compression	138 KPa	Glass Beads (mixt.)	0.670	0.940	γ_o=0.25%	γ_o=0.03%	5,7a,9
GB16	Extension	138 KPa	Glass Beads (mixt.)	0.680	0.970	γ_o=0.25%	γ_o=0.03%	5,7a,9
GB18	Torsion (+)	138 KPa	Glass Beads (mixt.)	0.710	0.950	γ_o=0.25%	γ_o=0.03%	5,7a,8,9
GB19	Compression	180 KPa	Glass Beads (mixt.)	0.693	0.944	γ_o=0.25%	γ_o=0.03%	7a,9
GB21	Compression/Torsion (+)	138 KPa	Glass Beads (mixt.)	0.671	0.970	γ_o=0.25%	γ_o=0.03%	7a,8,9
GB22	Compression + Torsion (+)	138 KPa	Glass Beads (mixt.)	0.683	0.970	γ_o=0.097%	γ_o=0.03%	7a,8,9
GB23	Compression	138 KPa	Glass Beads (mixt.)	0.673	0.970	γ_o=0.097%	γ_o=0.03%	7a,9
GB24	Compression	138 KPa	Glass Beads (mixt.)	0.683	0.960	γ_o=0.25%	γ_o=0.03%	7a,9
GB25	Torsion (+)	138 KPa	Glass Beads (mixt.)	0.674	0.930	γ_o=0.25%	γ_o=0.03%	7a,8,9
GB27	Compression	138 KPa	Glass Beads (mixt.)	0.683	0.970	γ_o=0.24–0.8%	γ_o=0.03%	3,7b
GB28	Torsion (+)	138 KPa	Glass Beads (mixt.)	0.683	0.970	γ_o=0.56–0.8%	γ_o=0.03%	7b,8,10
GB29	Torsion (+)	138 KPa	Glass Beads (mixt.)	0.684	0.960	γ_o=0.26–0.7%	γ_o=0.03%	3,7b,8
GB30	Compression	138 KPa	Glass Beads (mixt.)	0.672	0.954	γ_o=0.25%	γ_o=0.03%	3,7b
GB31	Compression	138 KPa	Glass Beads (mixt.)	0.660	0.960	γ_o=0.25%	γ_o=0.03%	3,7b, 11
GB33	Extension	138 KPa	Glass Beads (mixt.)	0.660	0.960	γ_o=0.25–0.8%	γ_o=0.03%	3,7b

Notes:

Tests GB1-GB4 had setup problems; data not used

1) Due to a bug in the data acquisition program, the specimen was initially pre-loaded with a vertical stress; initial condition not isotropic
2) The raw experimental data were post-processed with the program "RODTWIST" to correct for torsional compliance
3) The specimen exhibited creep-like behavior.
4) The specimen did not exhibit creep-like behavior.
5) The specimen was examined for creep-like behavior and none was observed.
6) Due to excessive creep, the probe portion of this test is of questionable value.
7) Correction applied for membrane compliance after test, (b) during test
8) Correction applied for torsional compliance during test
9) Because of the difficulty in correcting for membrane compliance after the probes, only the monotonic portion of the test was used
10) Specimen was loaded to 0.25% and then unloaded to zero stress; than it was reloaded; probes of questionable quality
11) Point O' was defined in strain space
12) Compression with constant mean stress (138 KPa) up to 0.25%; then tosrion (+) to failure (neutral loading)

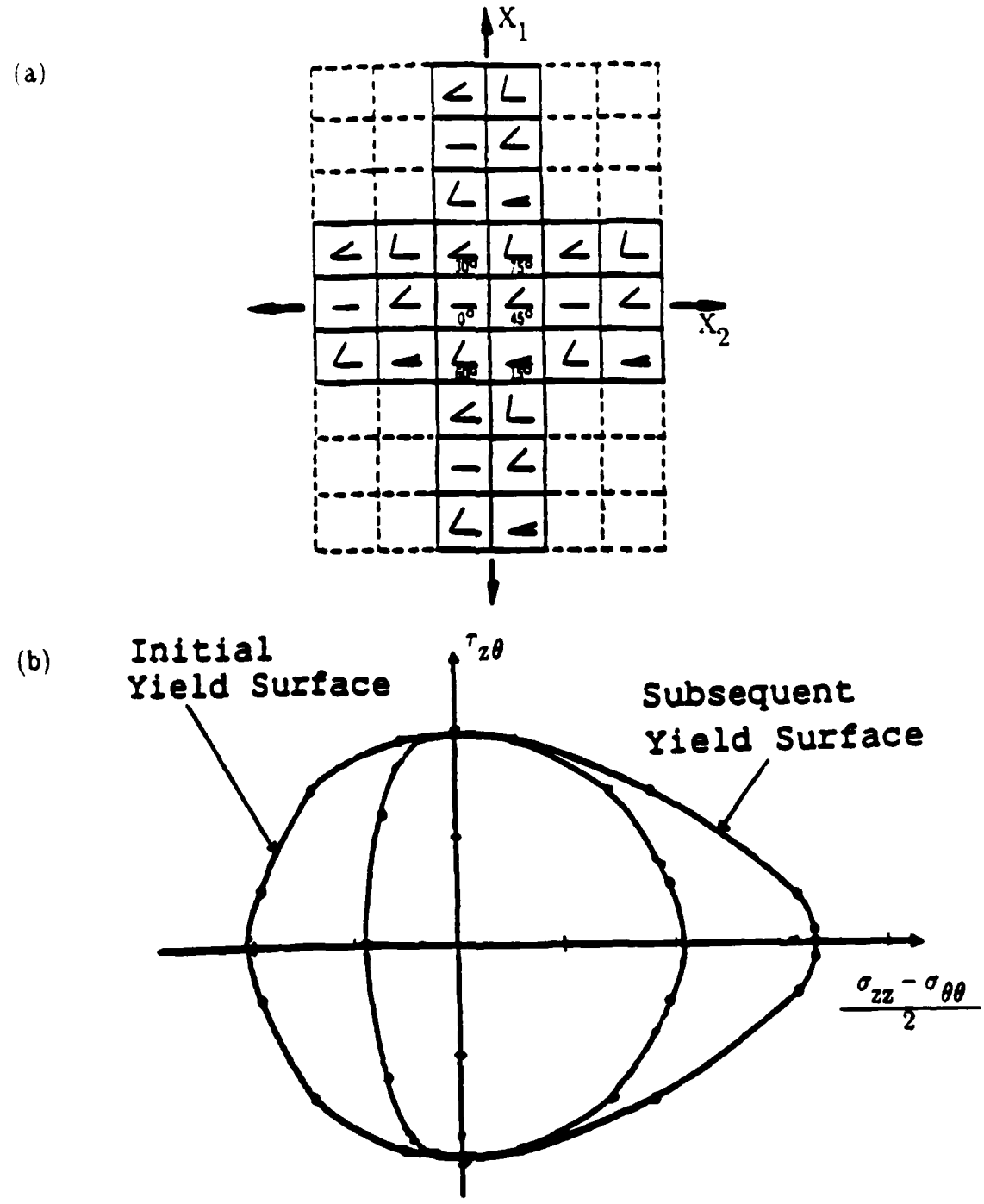

Figure 1 The repeating six crystal aggregate in the infinite plane (angle of slip shown in each crystal) (a), yield loci of the aggregate at different stages of tensile loading with an observed vertex (b), (after Lin and Ito, 1965).

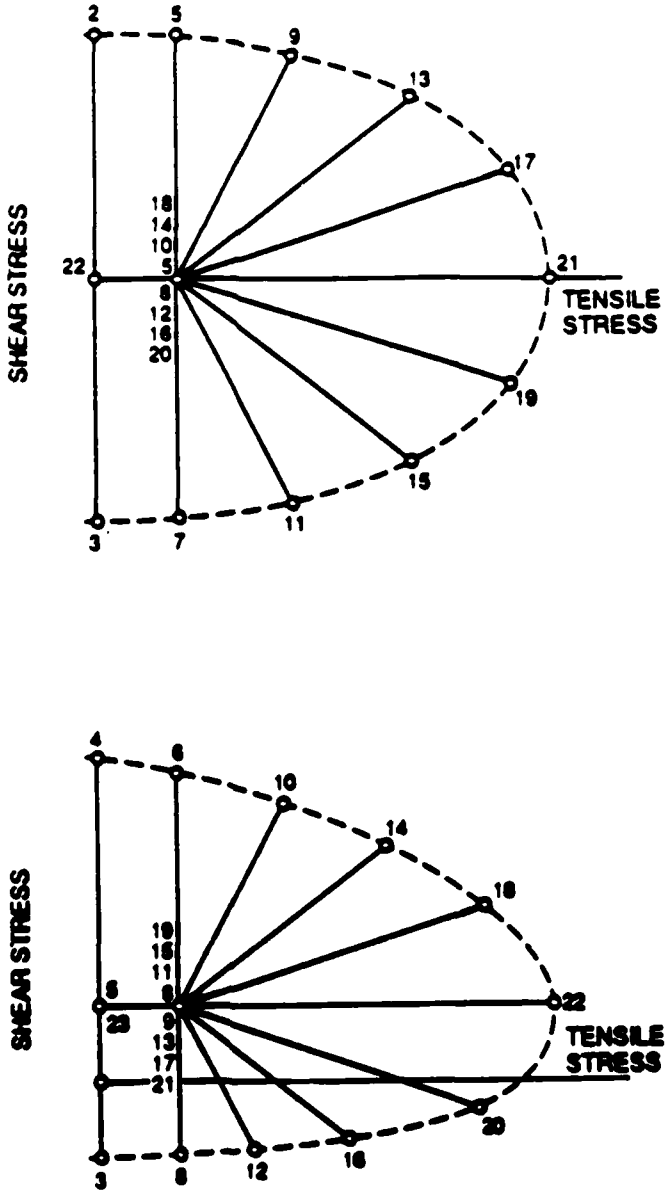

Figure 2 Loading paths for (a) initial, and (b) subsequent yield surfaces, (after Phillips, 1968)

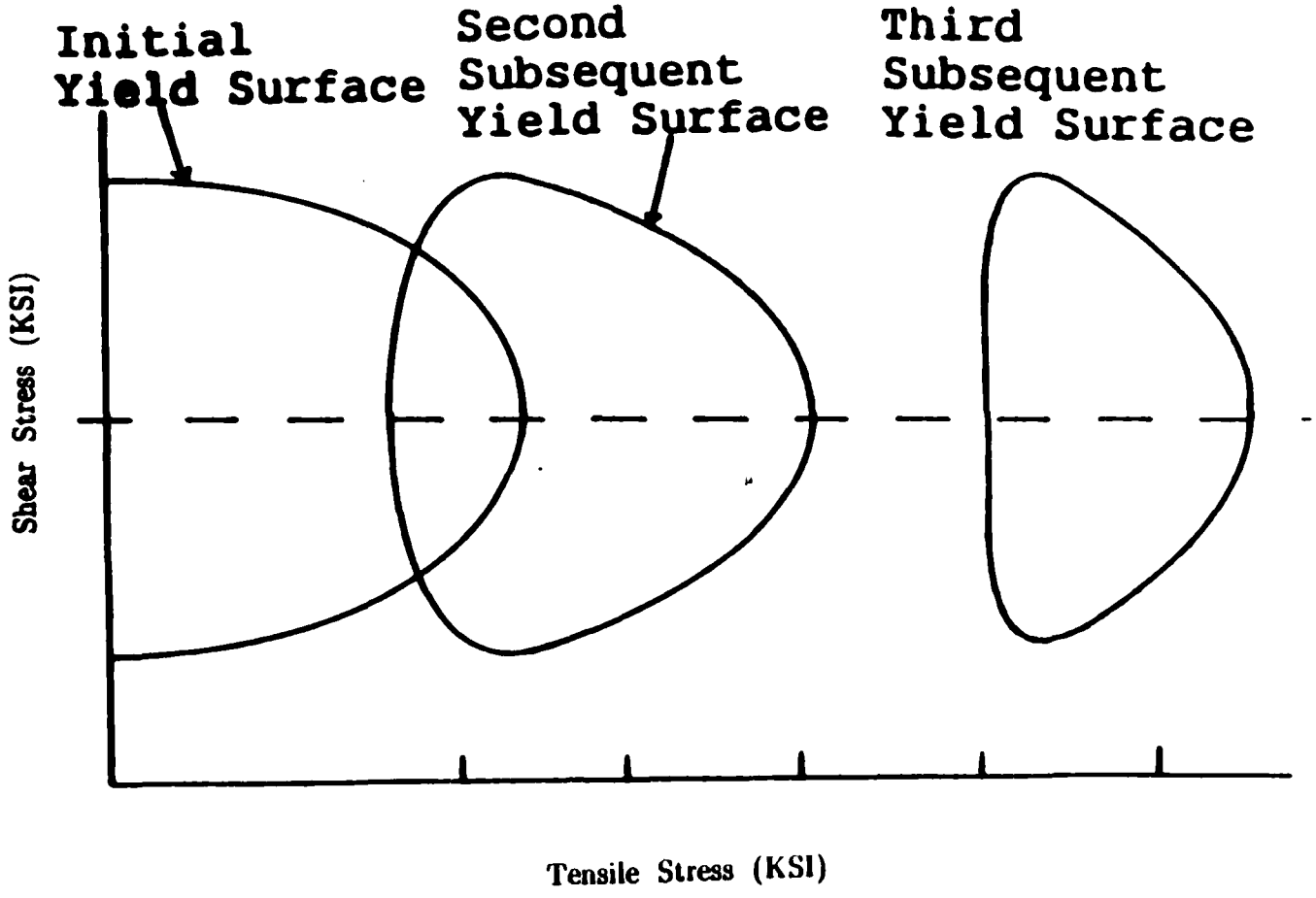

Figure 3 Experimentally obtained initial and subsequent yield surfaces for aluminum at 70^{o} F temperature, (after Phillips and Tang, 1972).

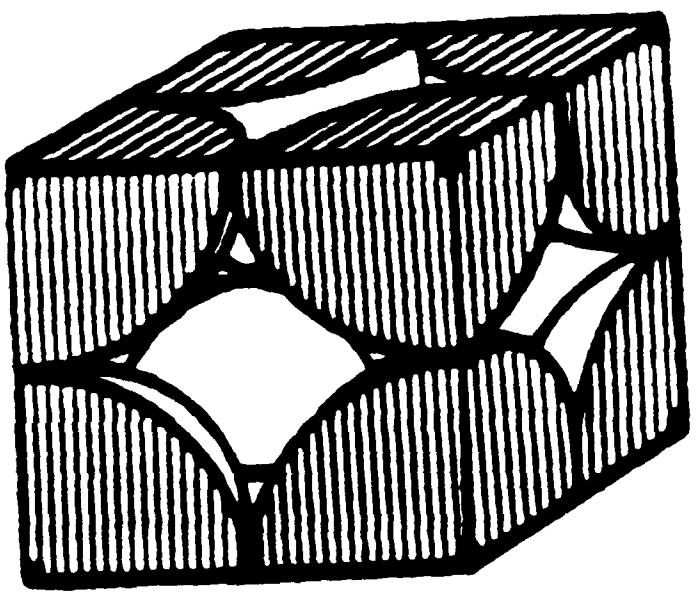

Figure 4 Simple cubic array of spheres.

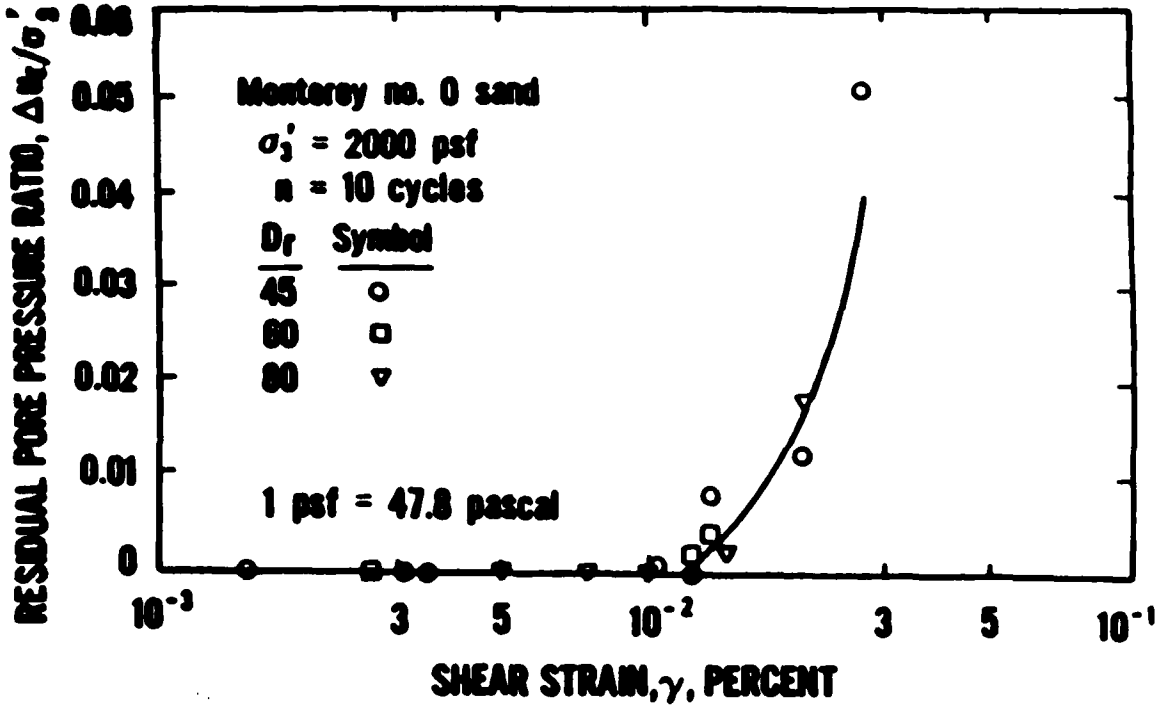

Figure 5 Experimental verification of the existence of the threshold strain in granular soil
(after Dobry, et al., 1982)

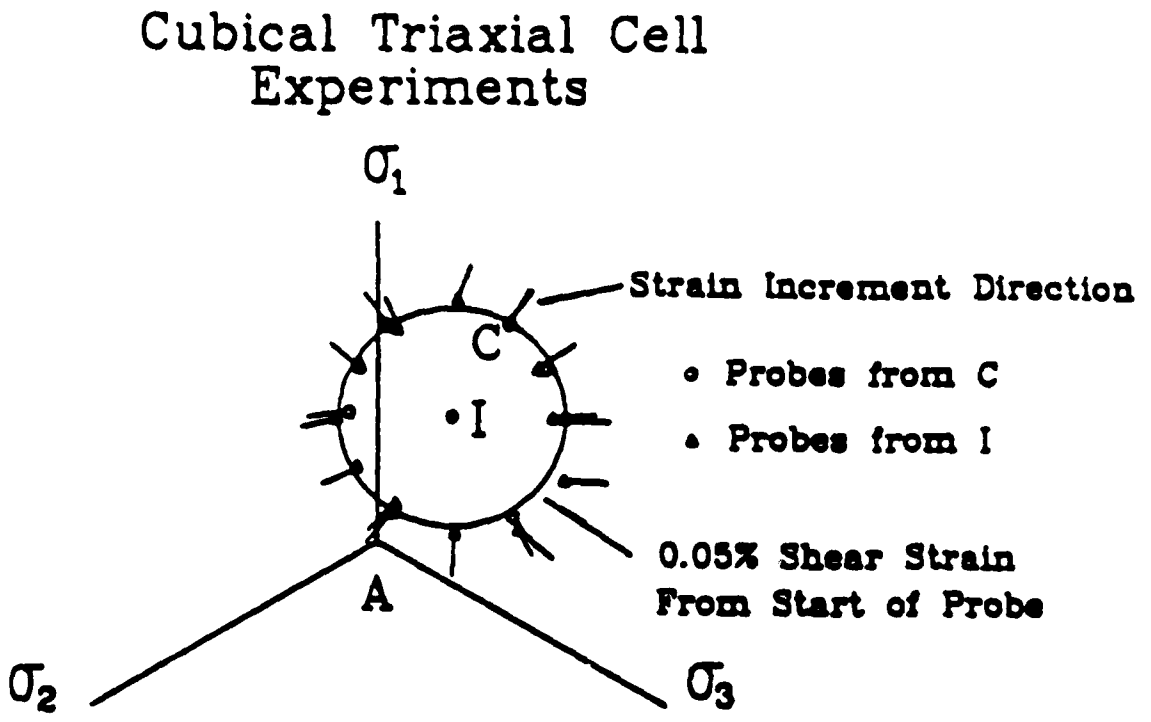

Figure 6 Experimentally obtained yield surface of sand from cubical triaxial experiments, (after Peters, 1988)

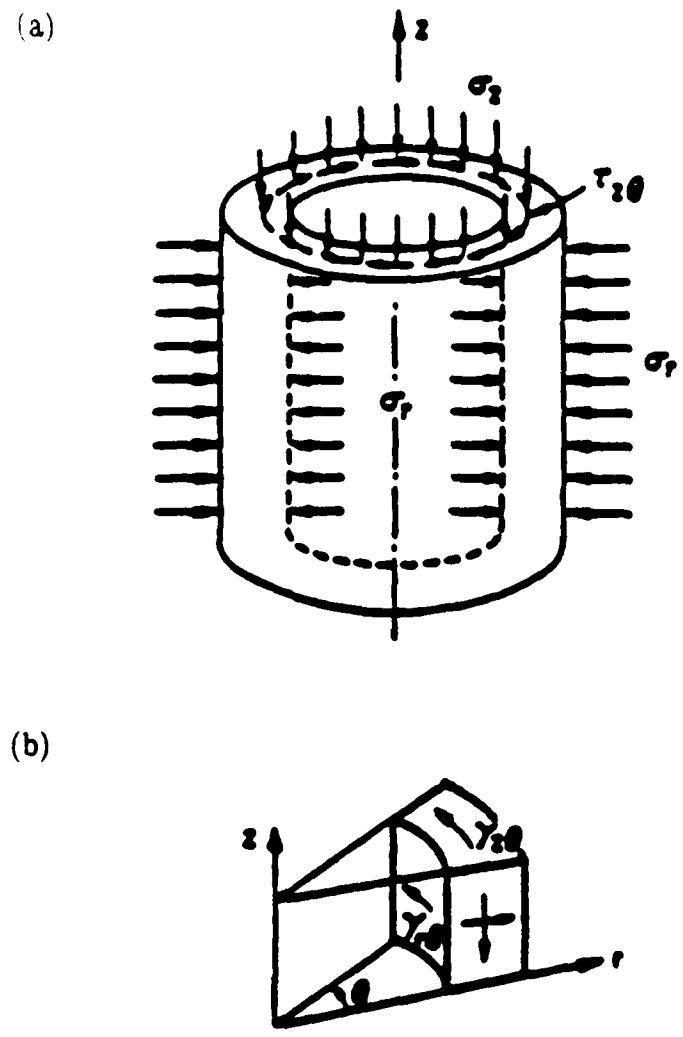

Figure 7 Stresses (a) and Strains (b) on a hollow cylindrical specimen.

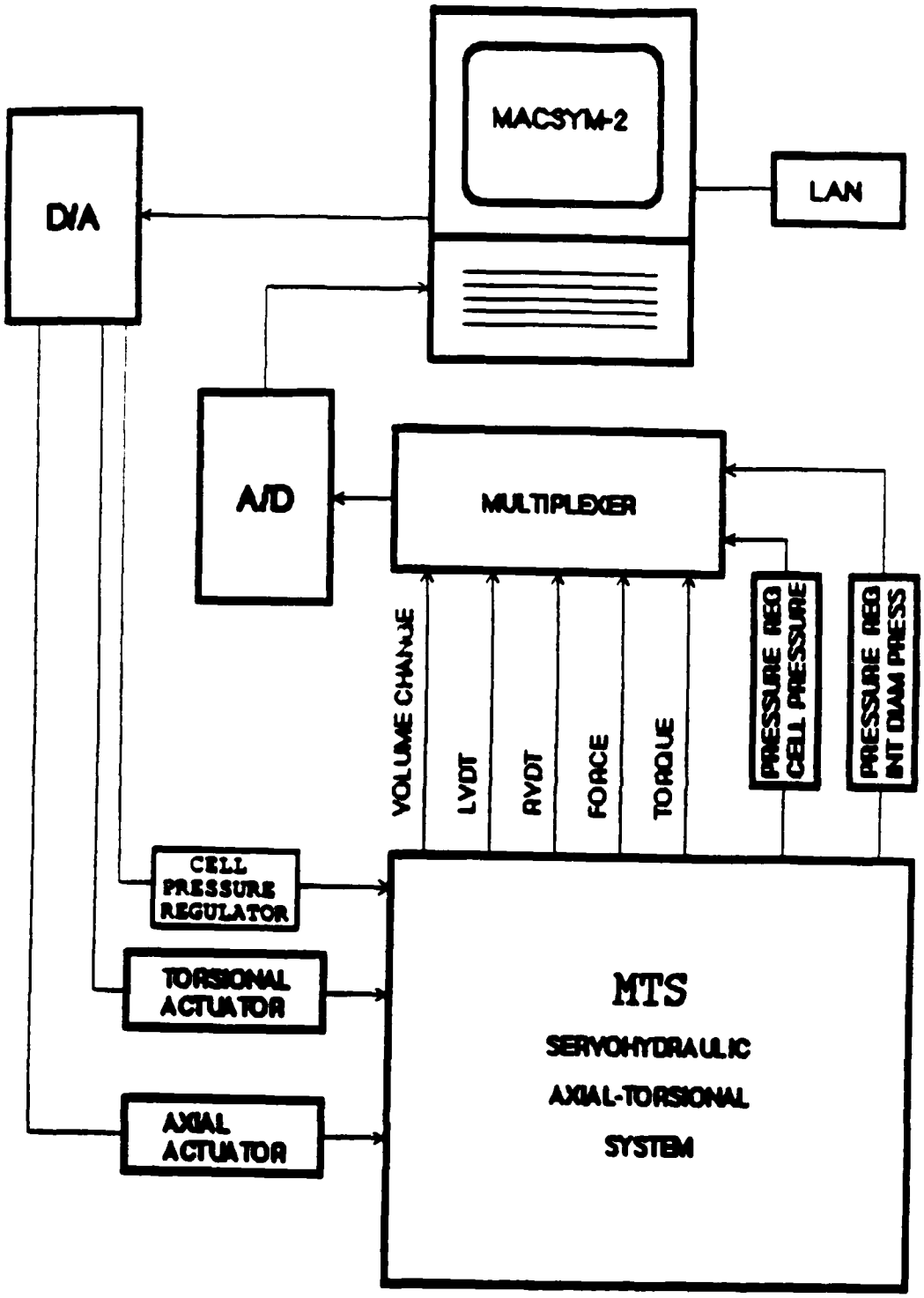

Figure 8 The RPI Soil Mechanics Laboratory MTS servohydraulic axial/torsional and computer control system configuration.

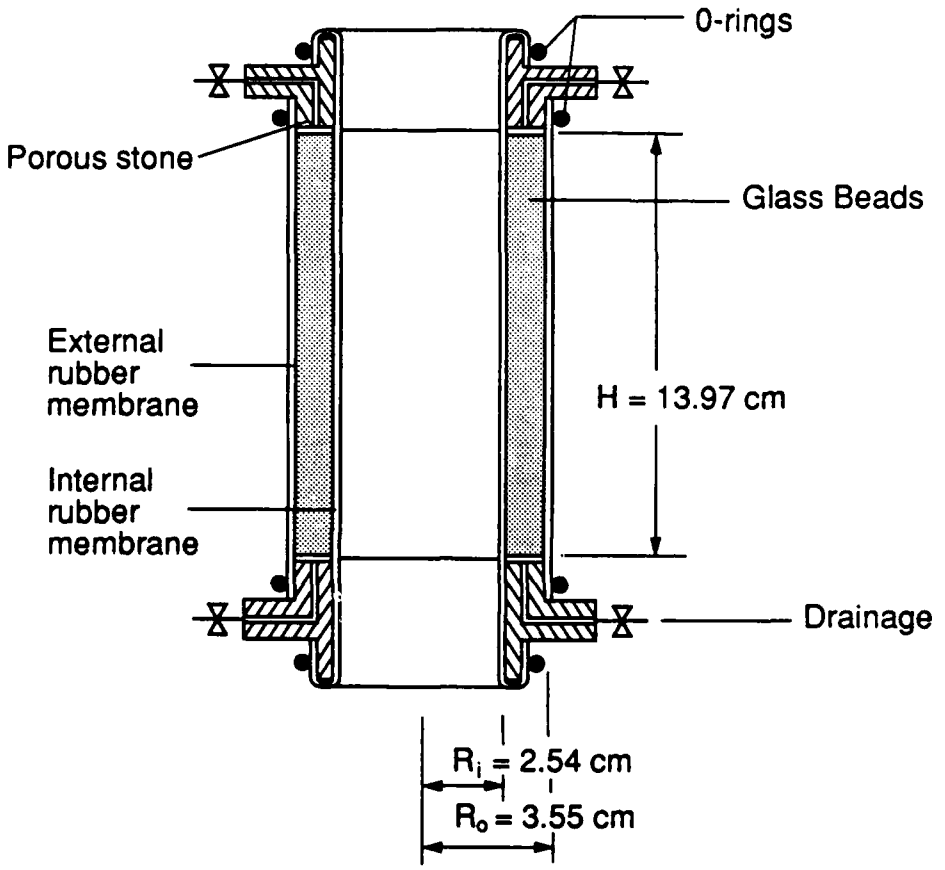

Fig. 9. Sketch of hollow cylinder specimen used in this study

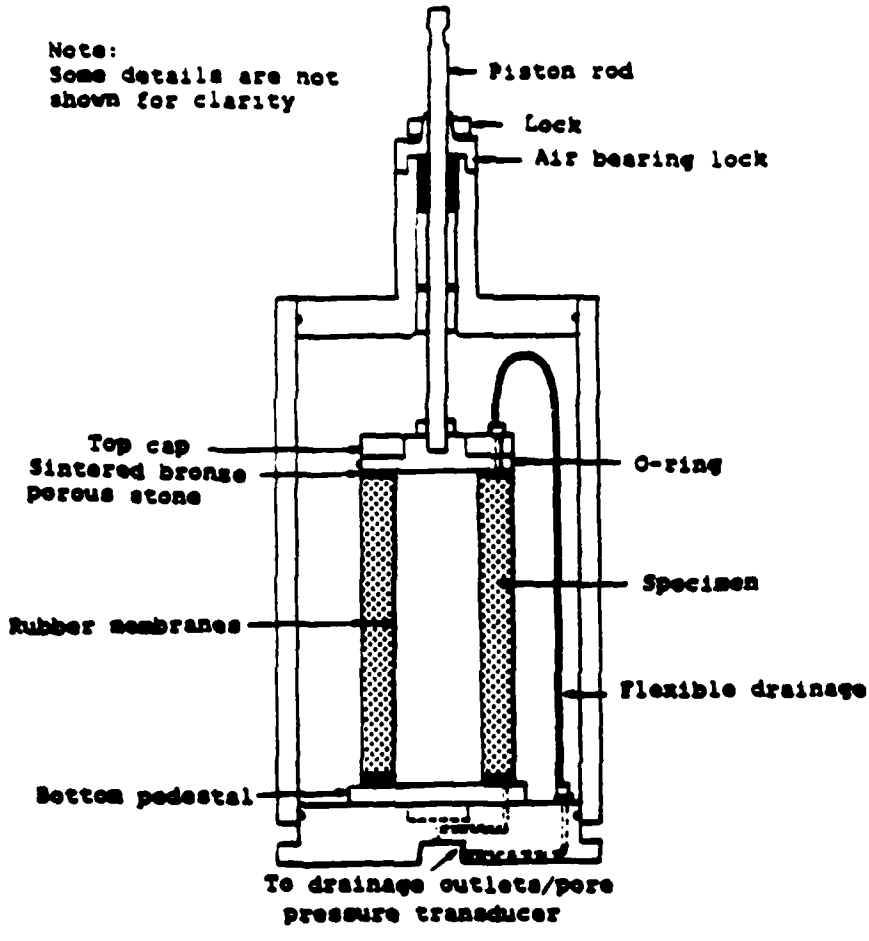

Figure 10 Sketch of triaxial cell and hollow cylindrical specimen.

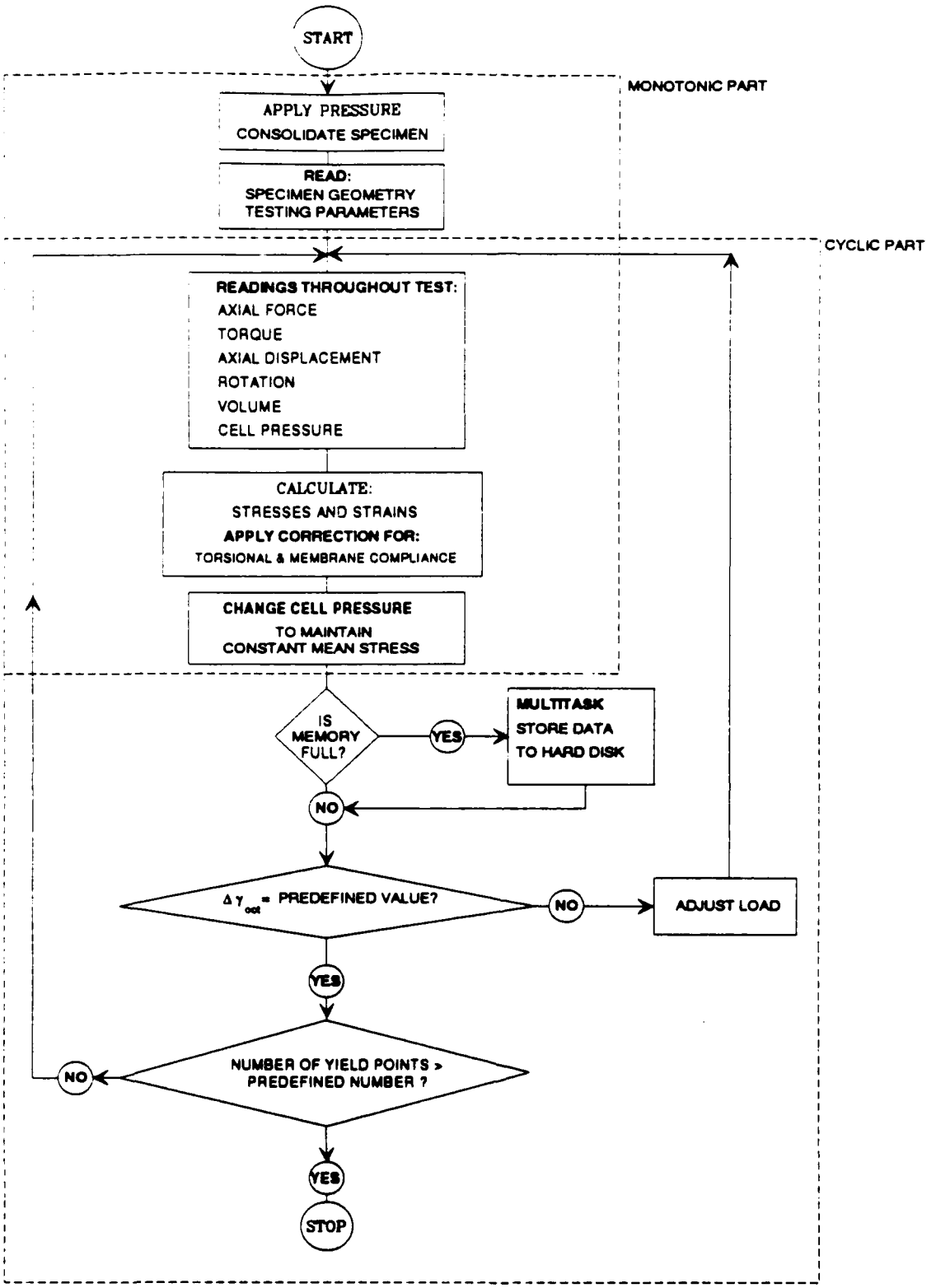

Fig. 11. Flowchart of the program controlling the hollow cylinder experiments

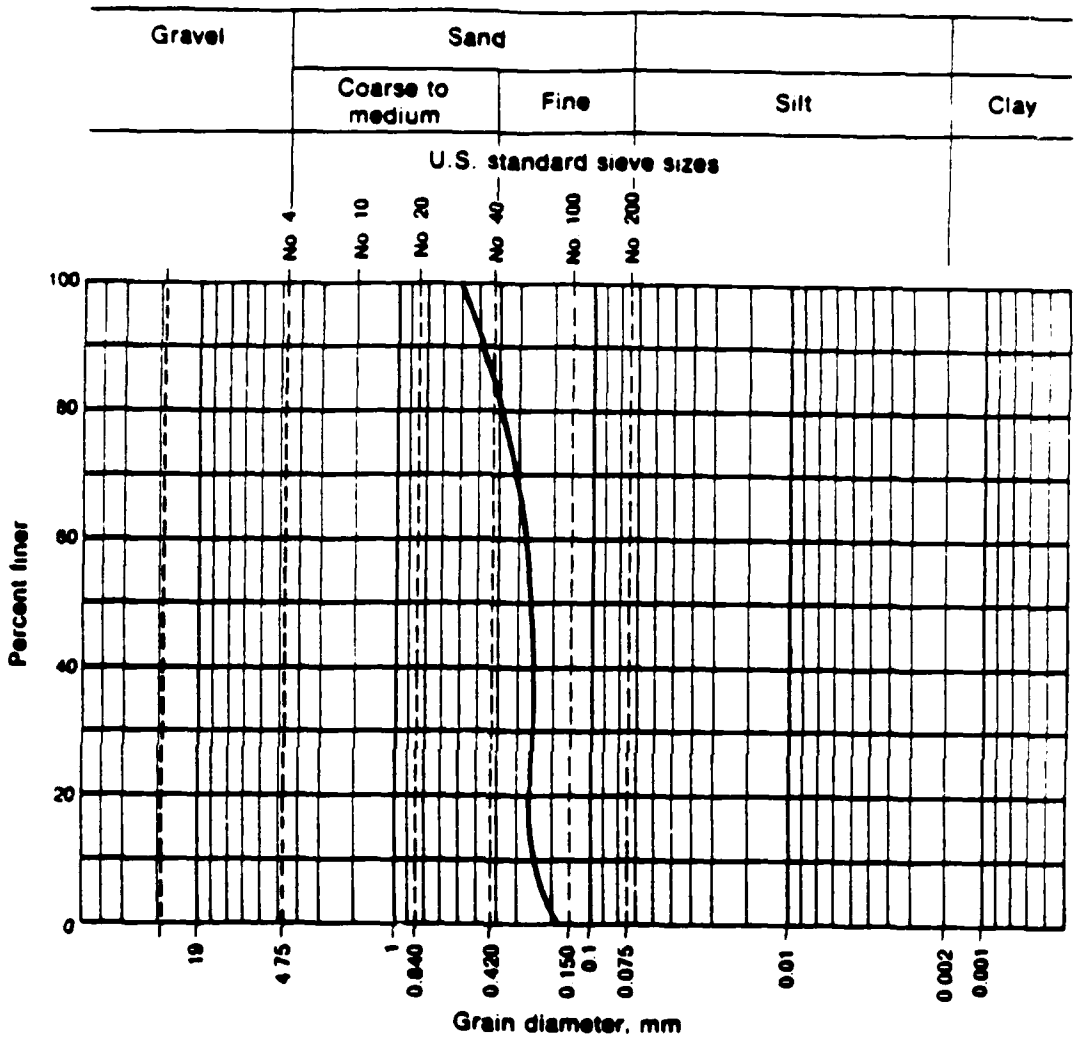

Figure 12 Grain size distribution curve for mixture of glass beads used in this study

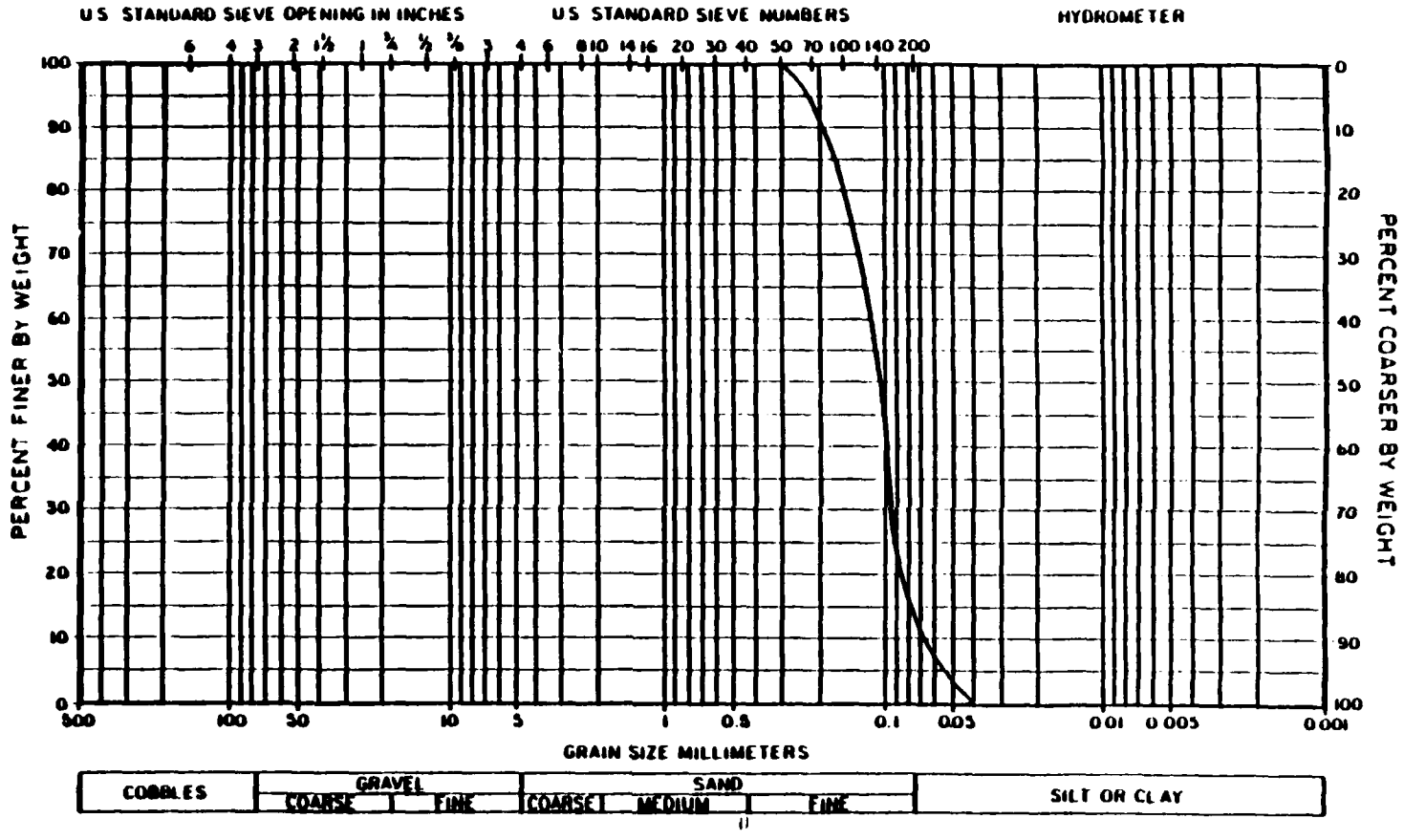

Figure 13 Grain size distribution curve for F 125 Ottawa sand

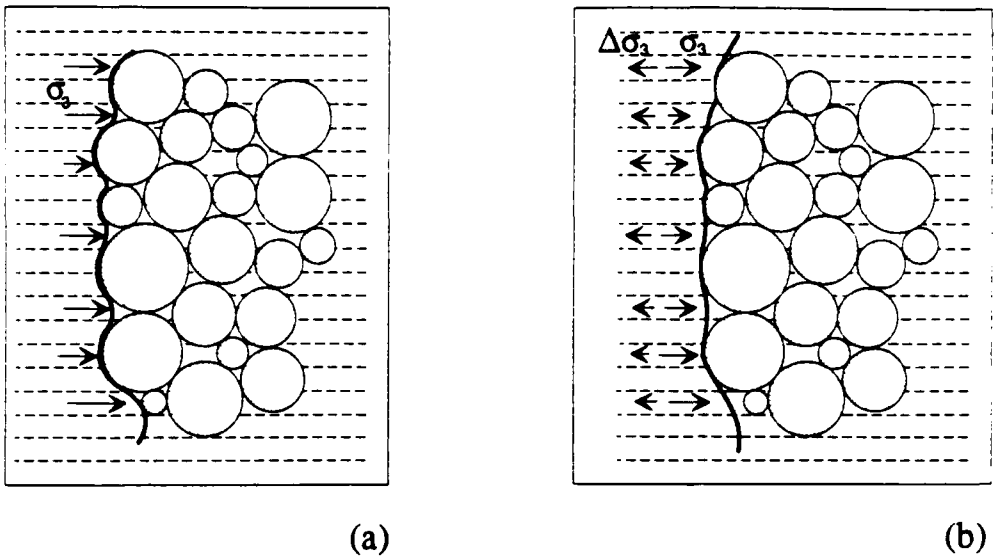

Fig. 14. Sketch of the membrane penetration phenomenon in a drained test of sand in which the cell pressure is changing: (a) immediately after consolidation, and (b) during loading under constant mean stress.

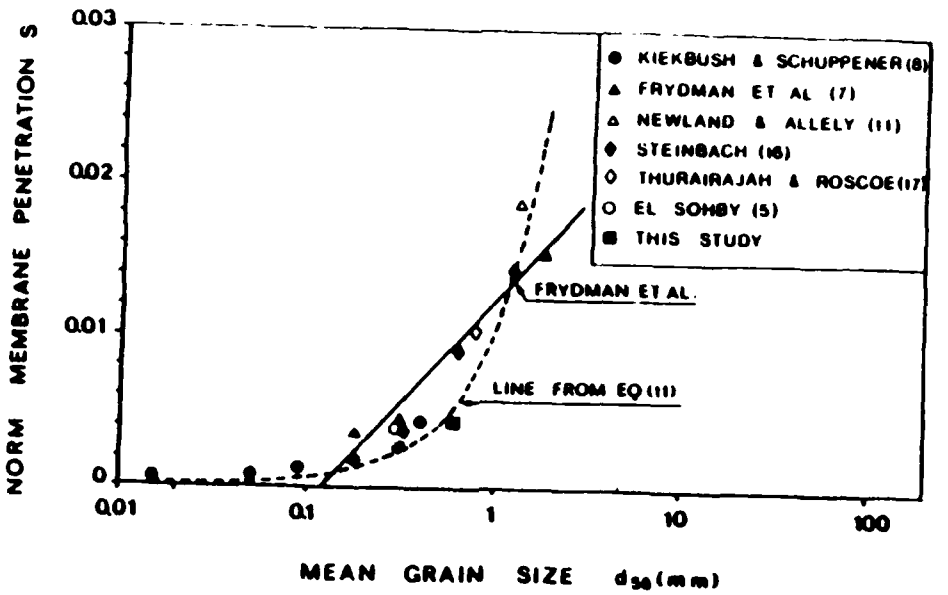

Fig. 15. Comparison of Relationships for Normalized Membrane Penetration versus Mean Grain Size d_{50} (after Baldi and Nova, 1984).

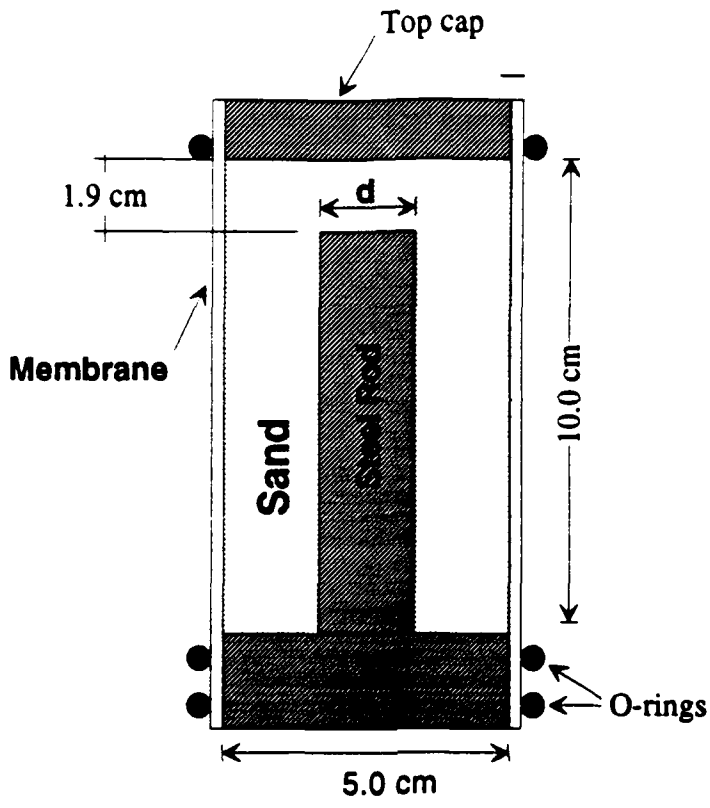

Fig. 16. Configuration of specimen used in membrane compliance tests.

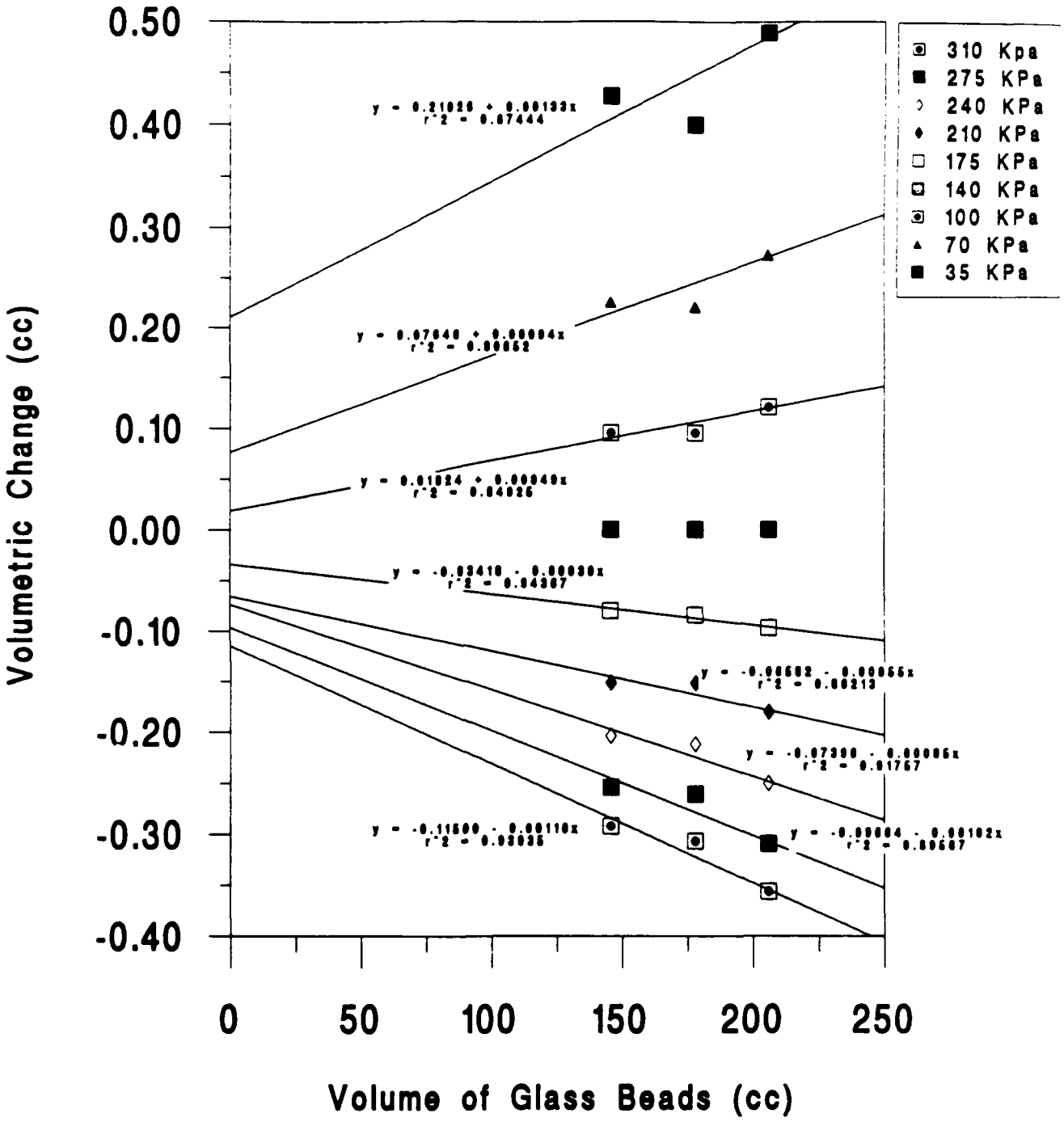

Fig. 17. Volumetric strain versus volume of glass beads obtained from hydrostatic compression experiment for membrane compliance correction.

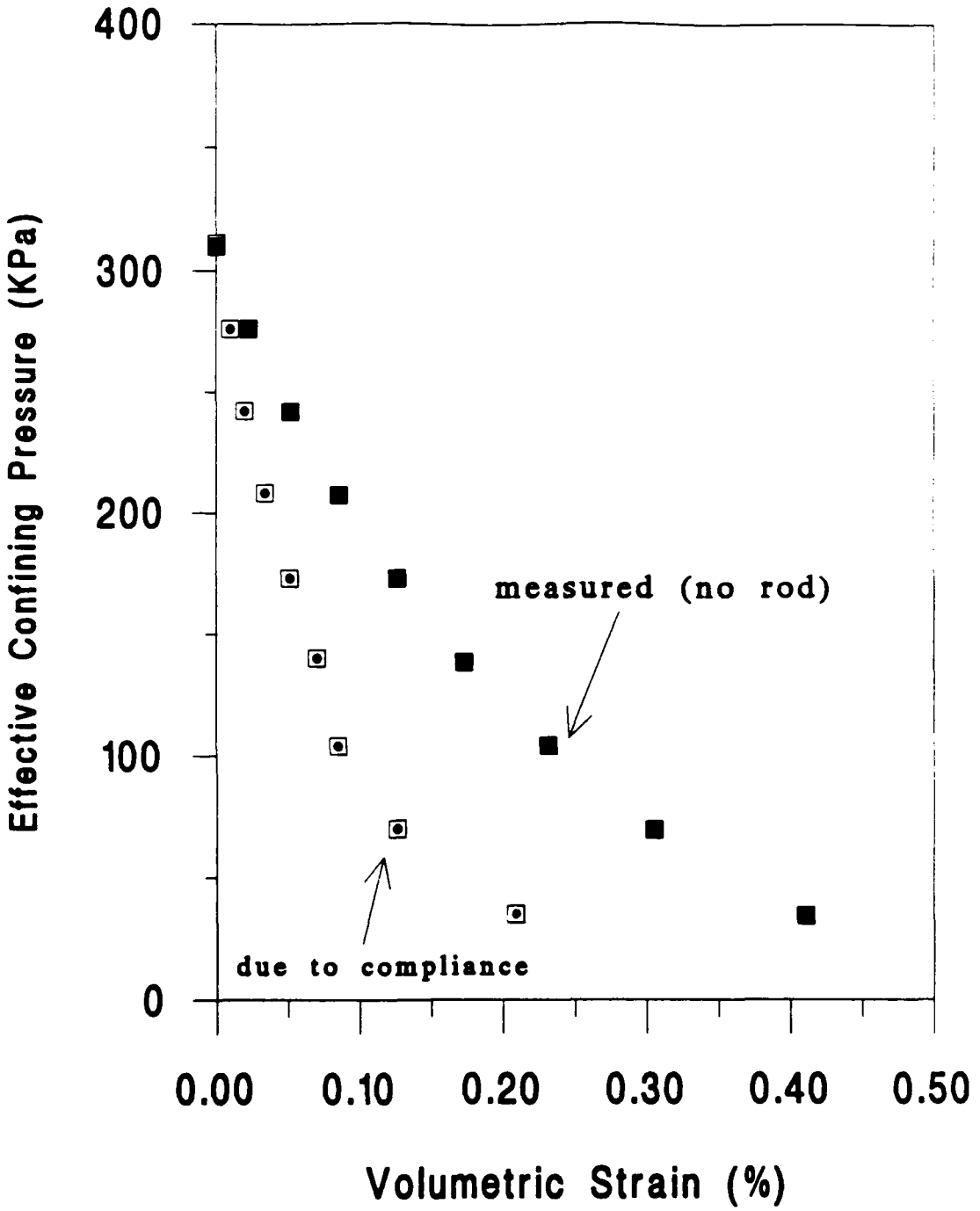

Fig. 18. Membrane compliance data obtained during unloading

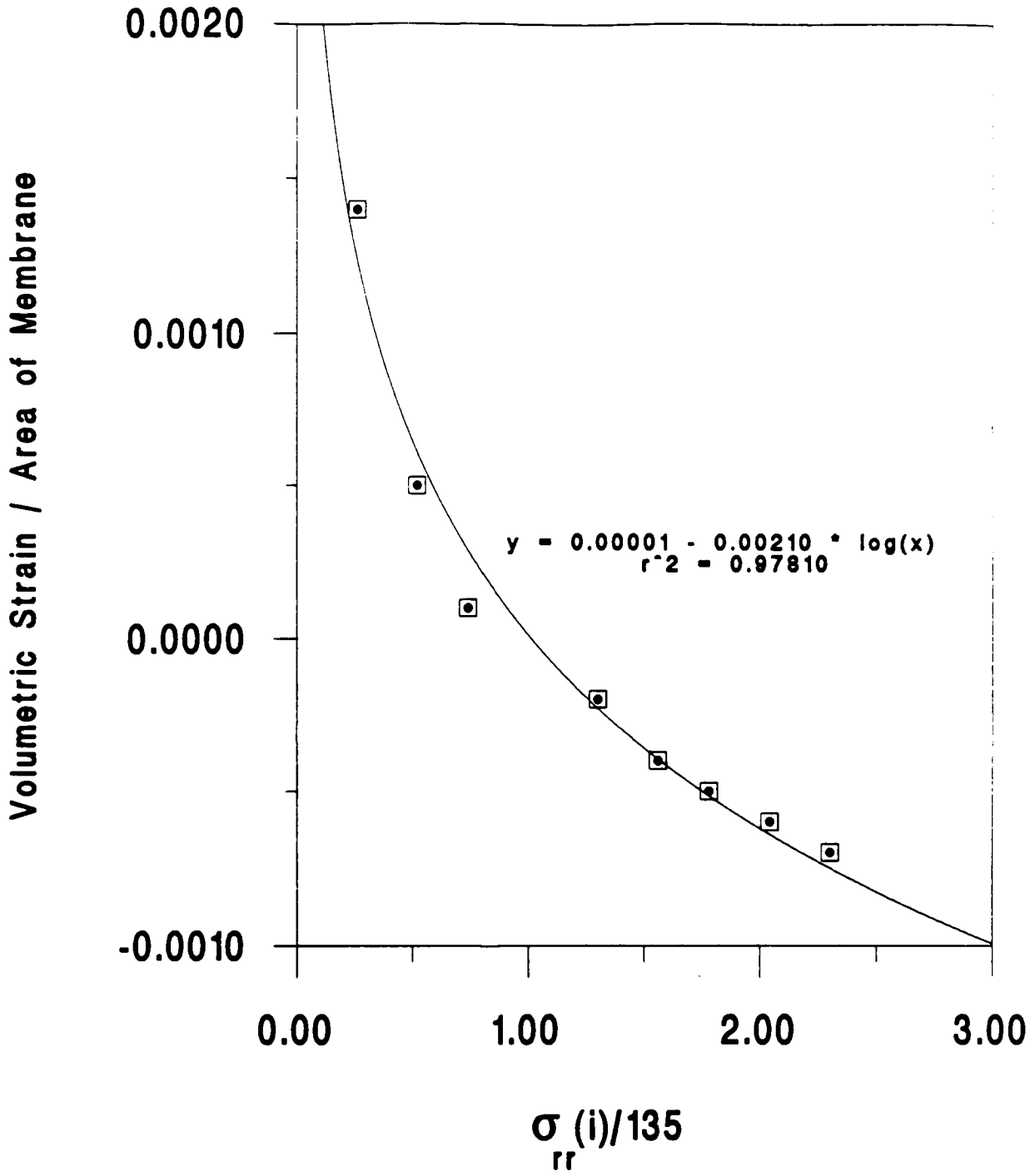

Fig. 19. Membrane correction factor used in membrane correction equation

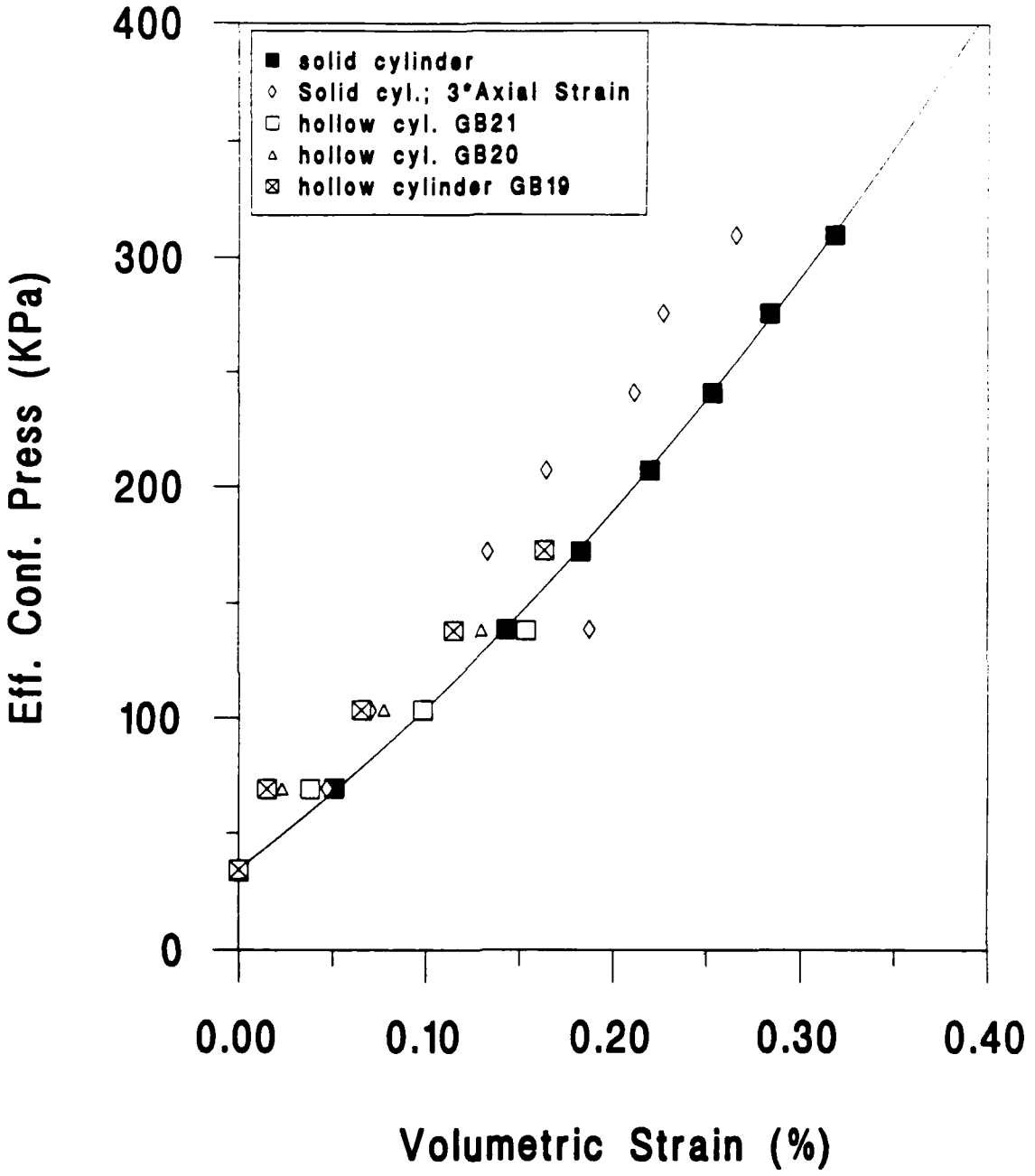

Fig. 20. Comparison between volumetric strain obtianed under isotropic compression in solid and hollow cylindrical specimens. Data have been corrected for membrane compliance.

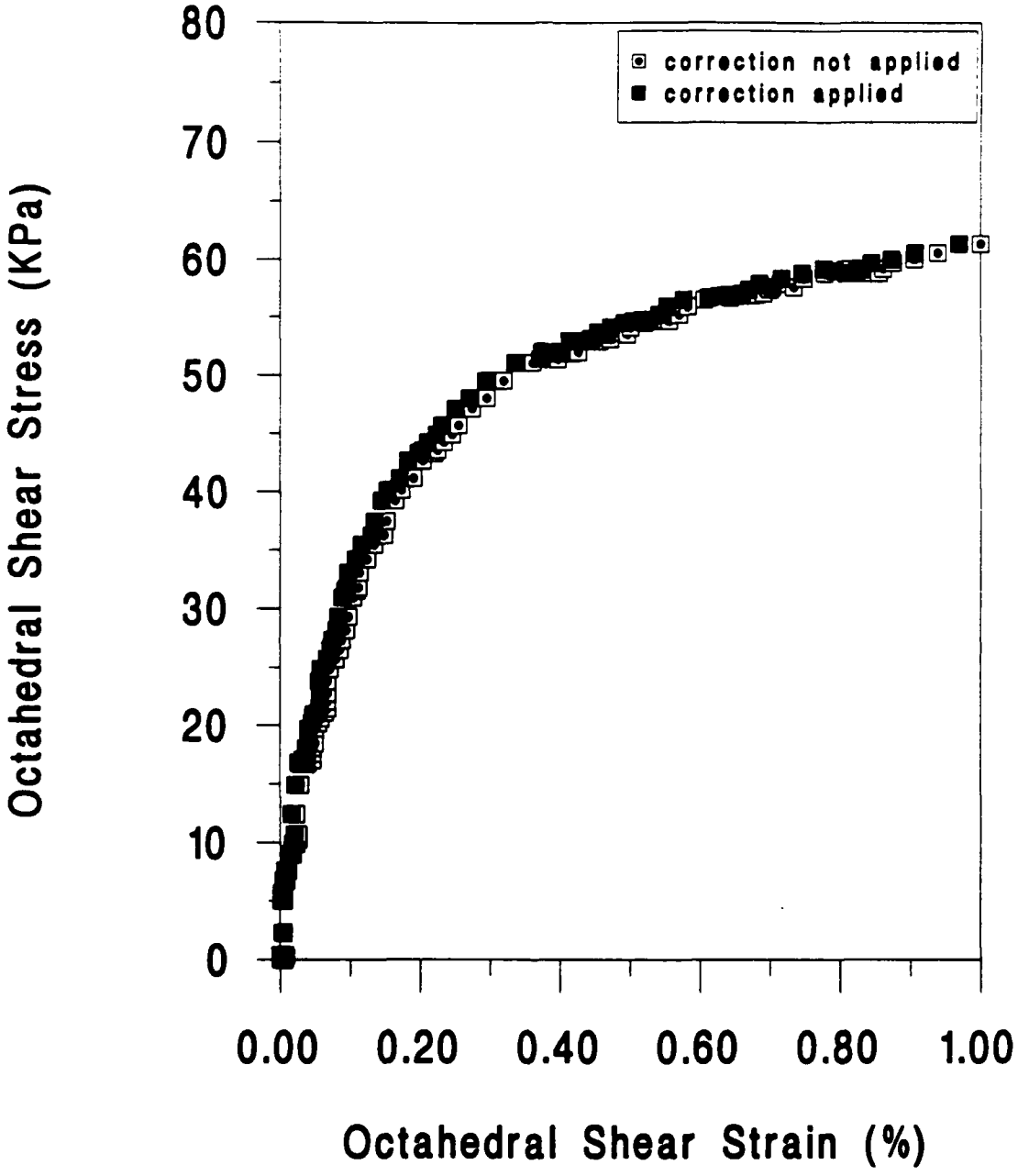

Fig. 21. Comparison between stress strain curves obtained in compression test GB26 with and without correction for membrane compliance. Test performed on specimen composed of mixture 2 prepared with dry pluviation.

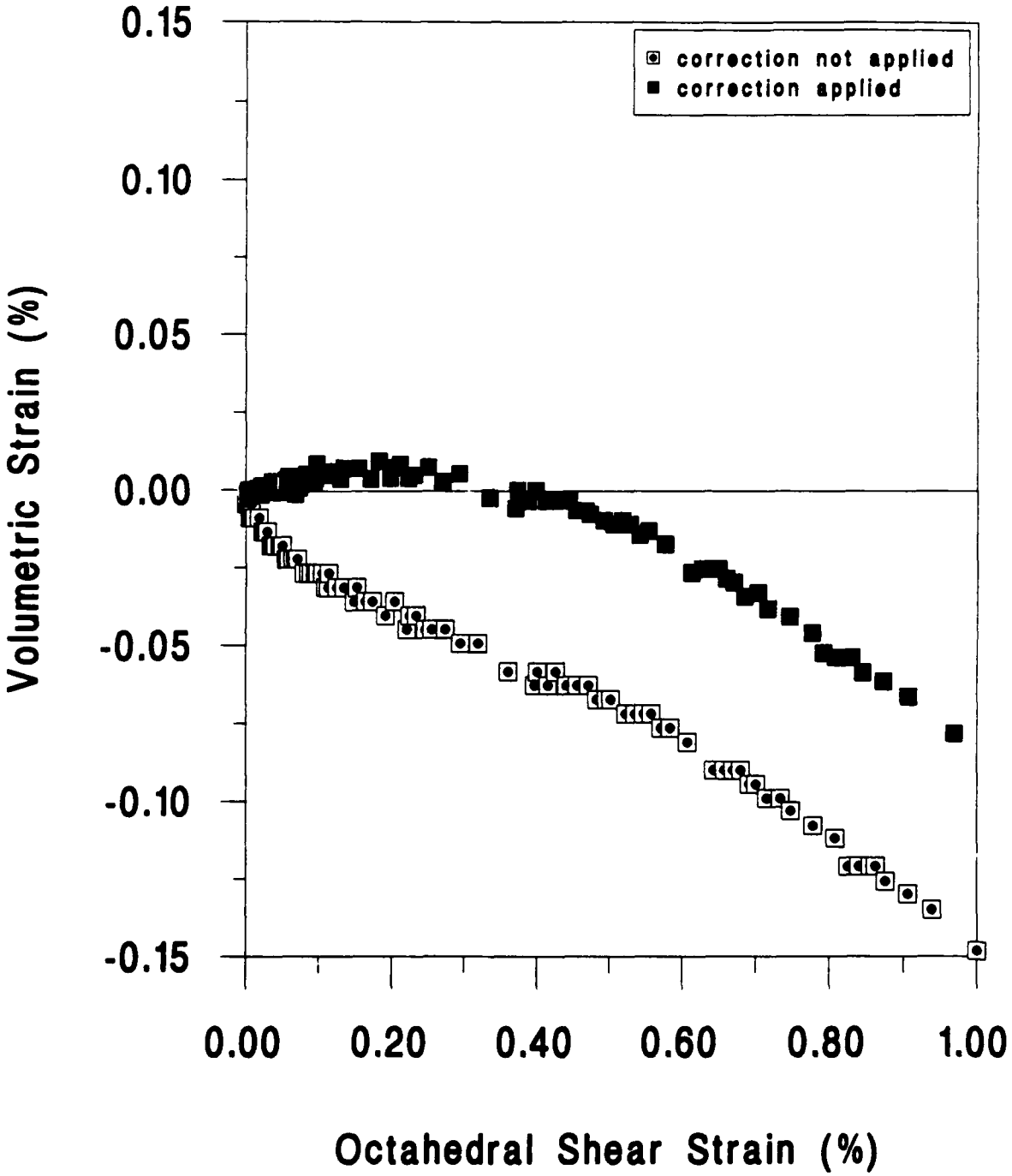

Fig. 22. Comparison between volumetric-shear strain curves with and without correction for membrane compliance obtained in compression test GB26.

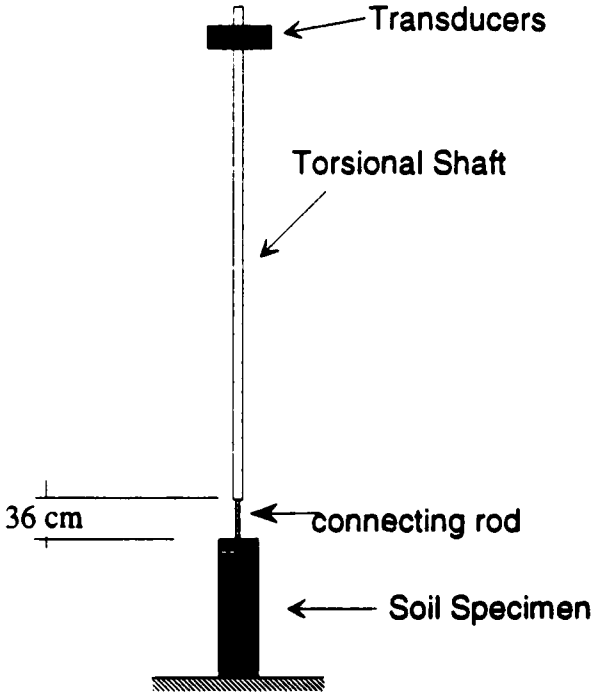

Fig. 23. Sketch of the loading apparatus and the flexible connection

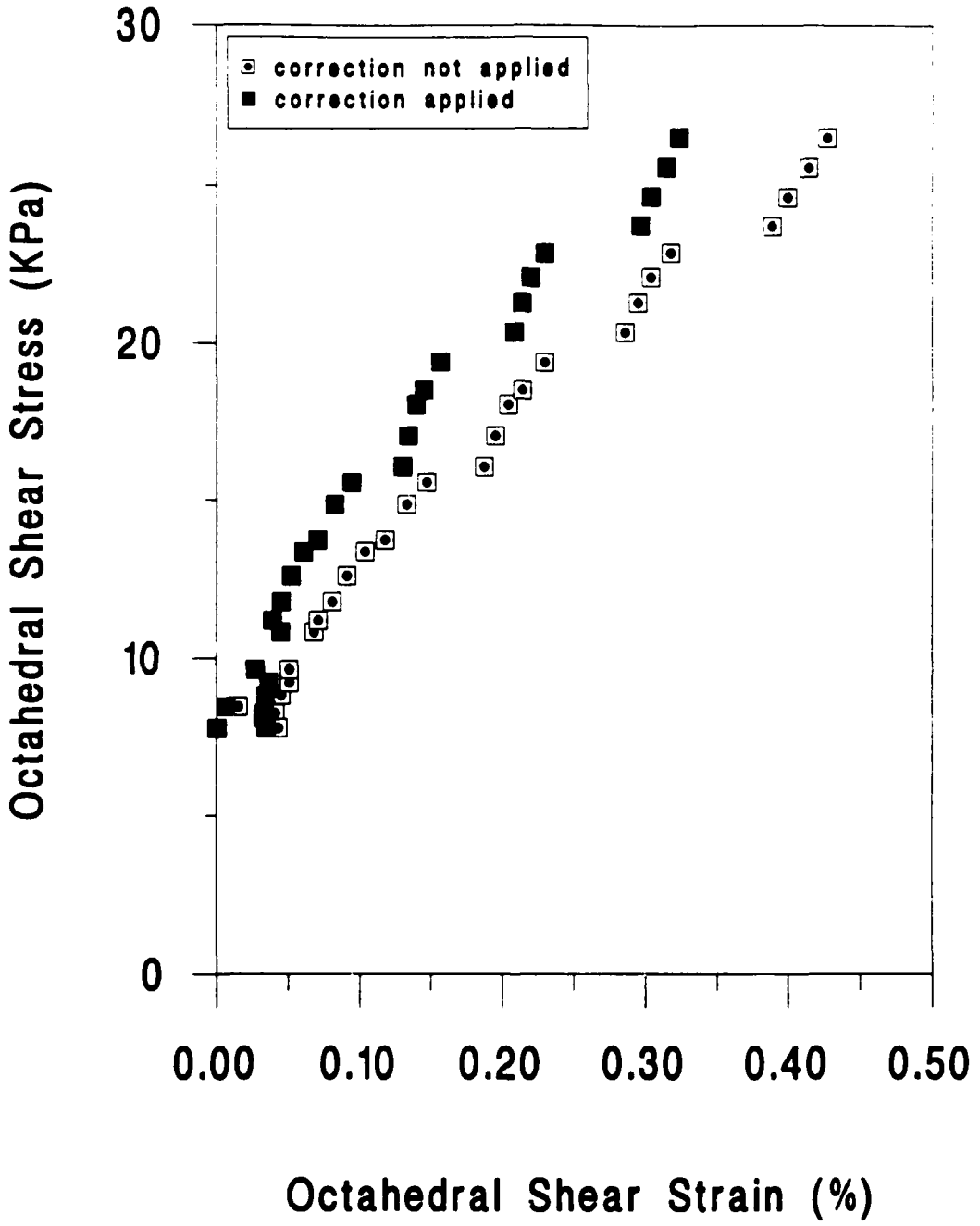

Fig. 24. Comparison between stress strain curves obtained with and without correction for torsional compliance from torsional test MT18.

mt18vtcc

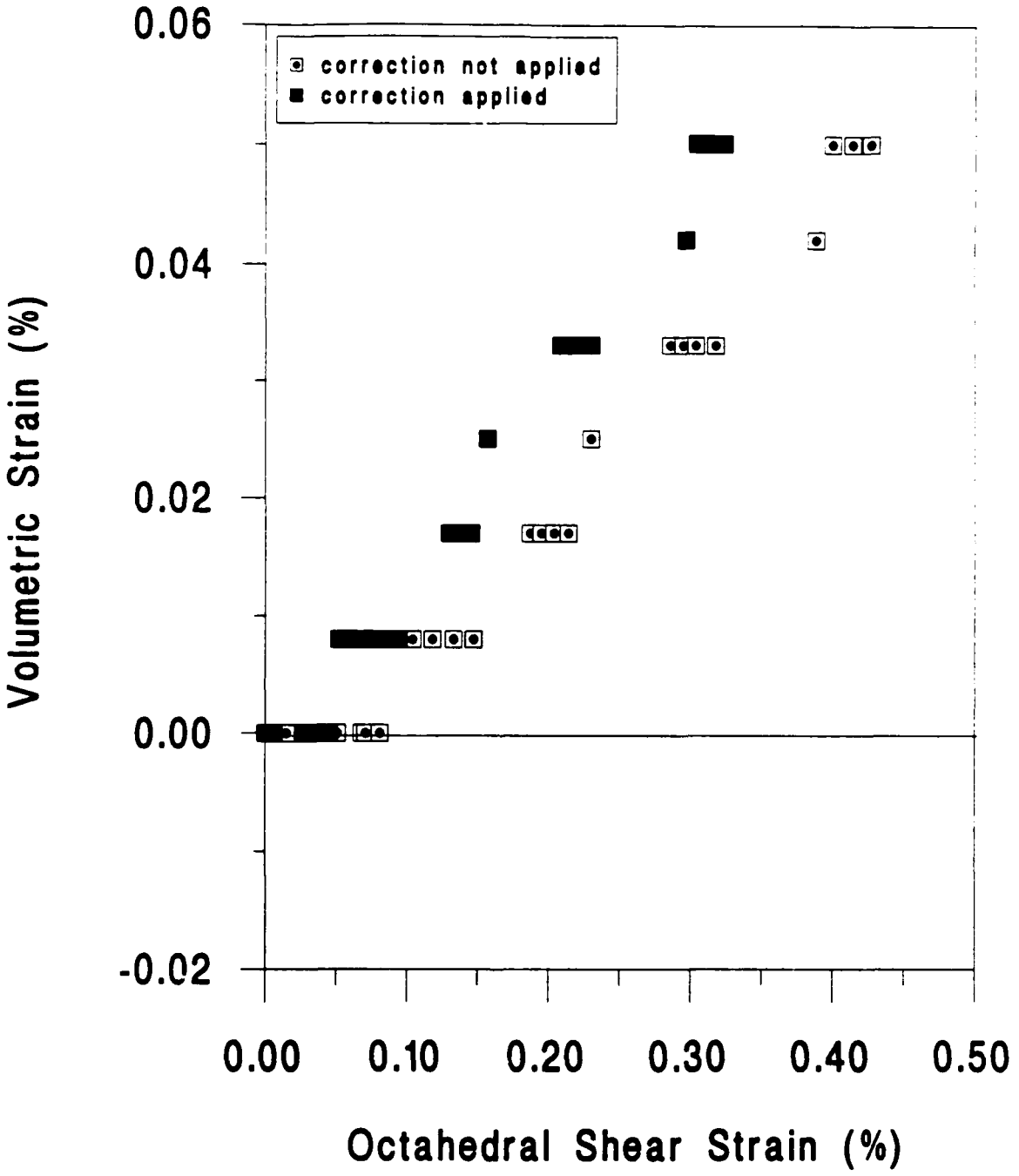

Fig. 25. Comparison between volumetric-shear strain curves with and without torsional compliance correction obtained in torsion test MT18.

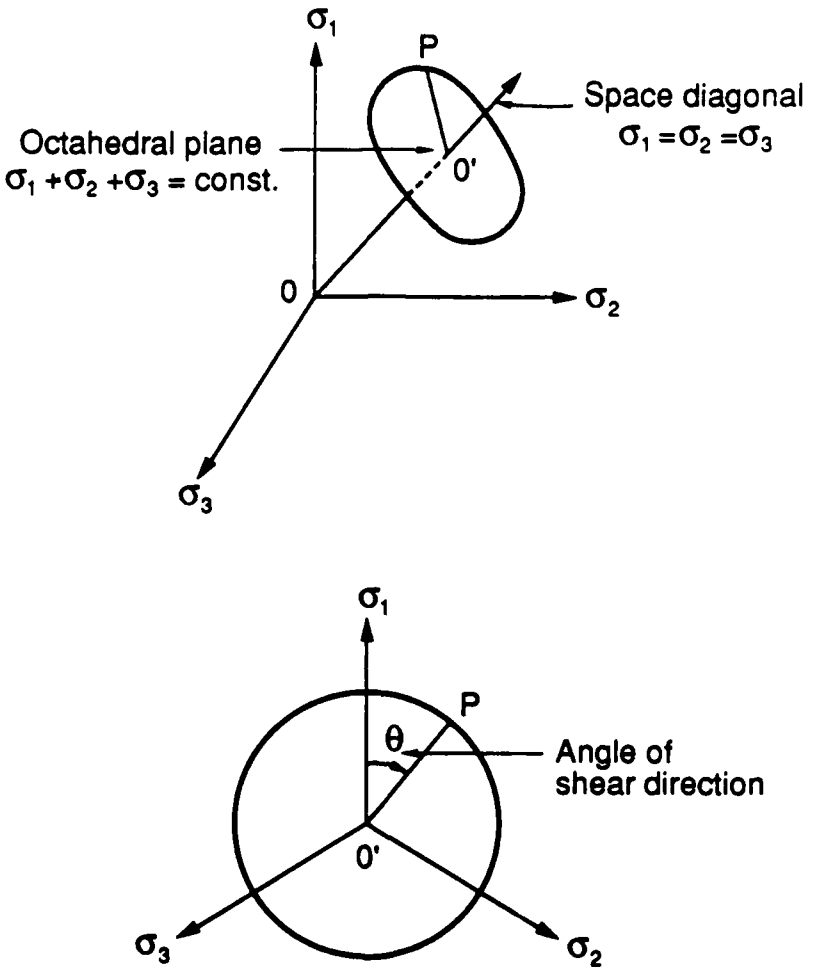

Fig. 26. Representation of stress conditions on the octahedral plane (π-plane)

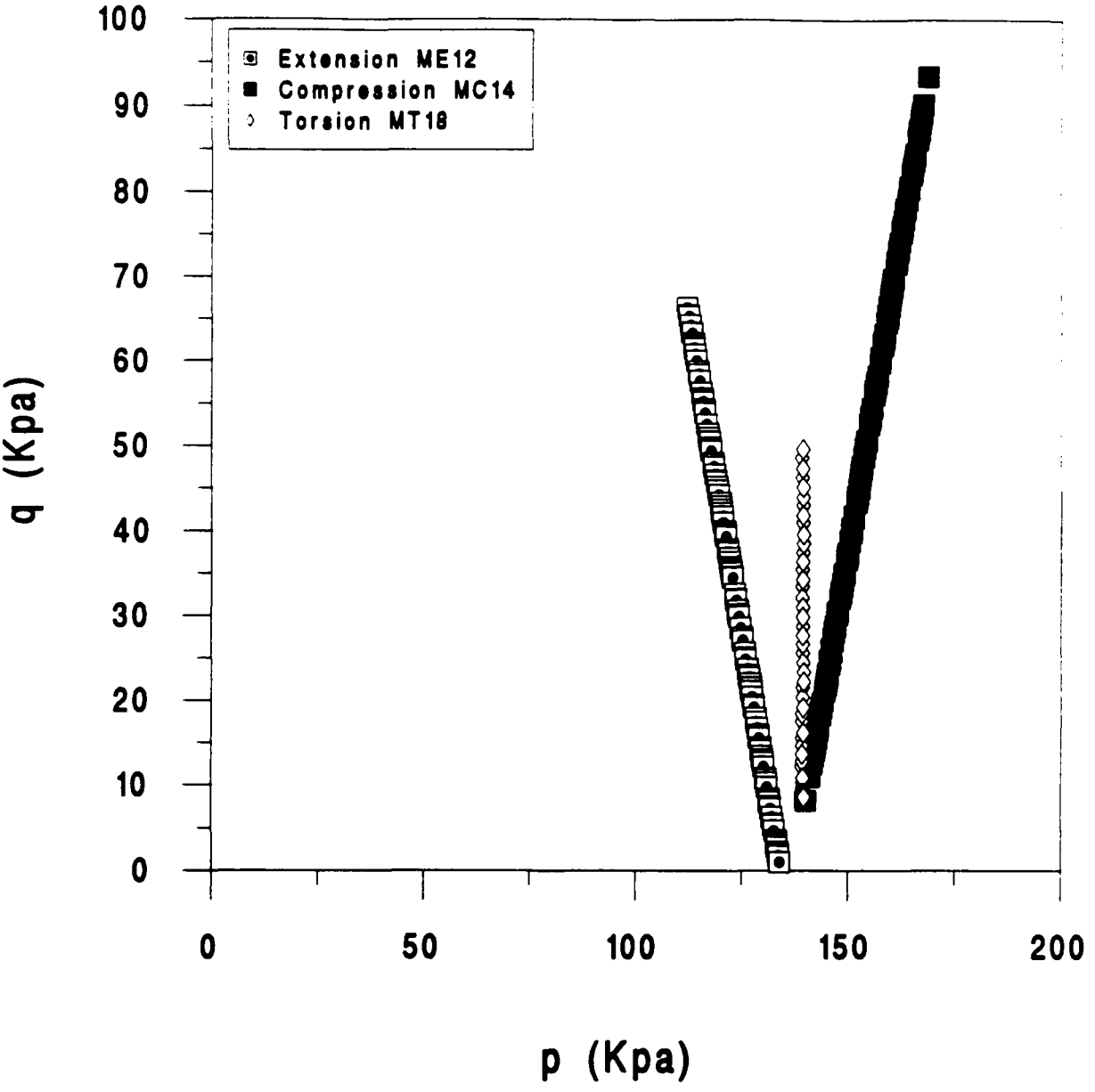

Fig. 27. Stress paths in q-p stress plane for three monotonic proportional tests composed of particles with equal diameters.

(a)

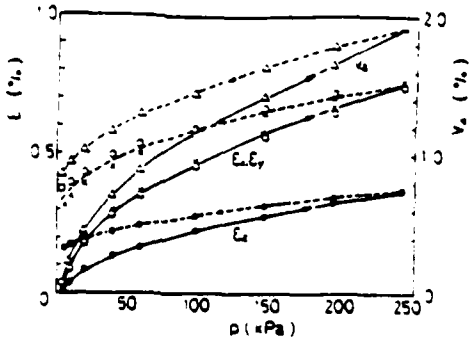

(b)

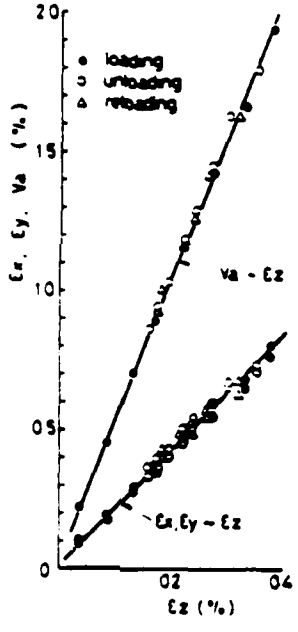

Figure 28 Stress-Strain curves for isotropic compression tests (a) and Relations between strains under isotropic compression tests (b), (after Haruyama, 1981).

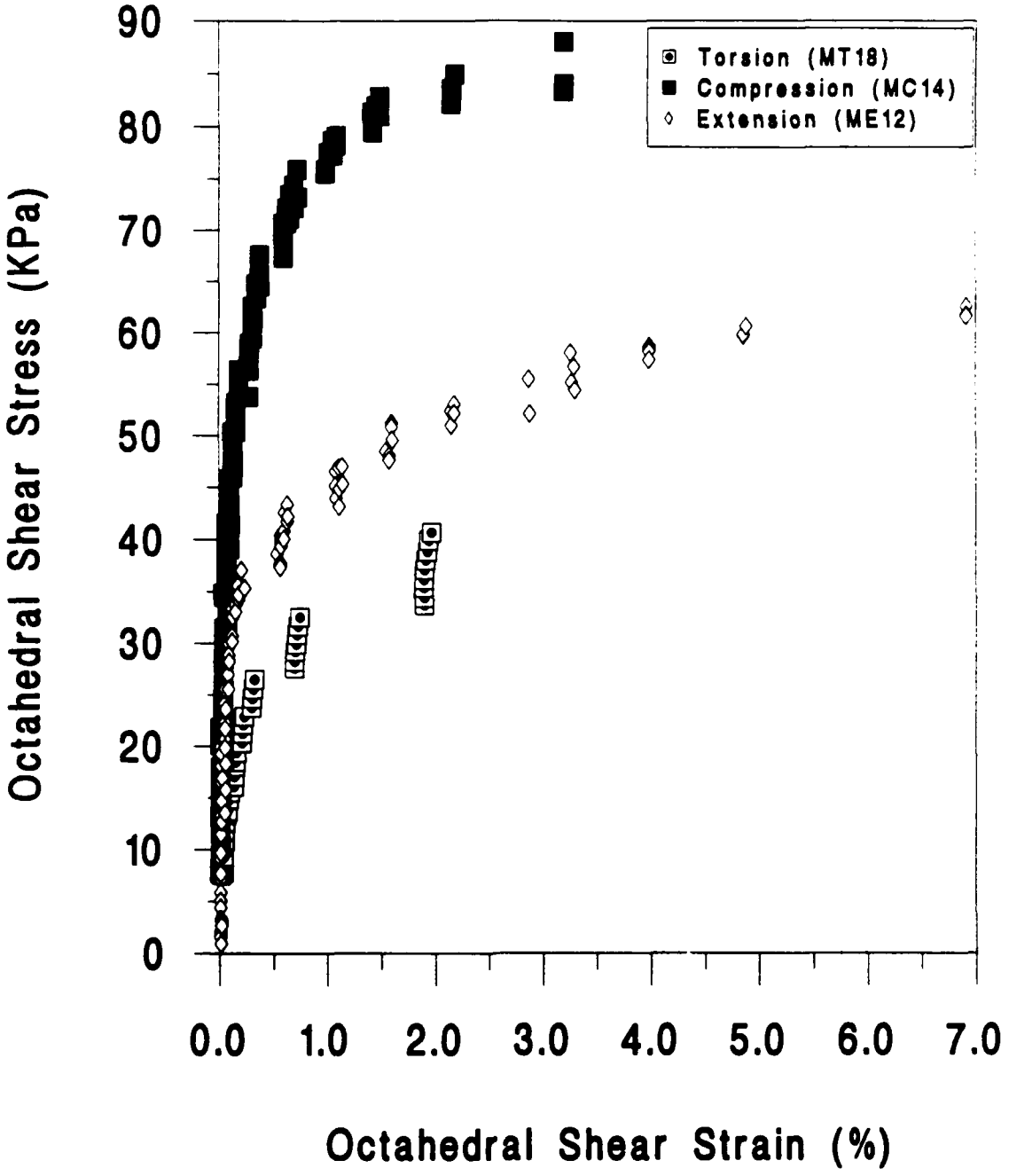

Fig. 29. Comparison of the behavior of monosized glass bead specimens under three inclinations of principal stress

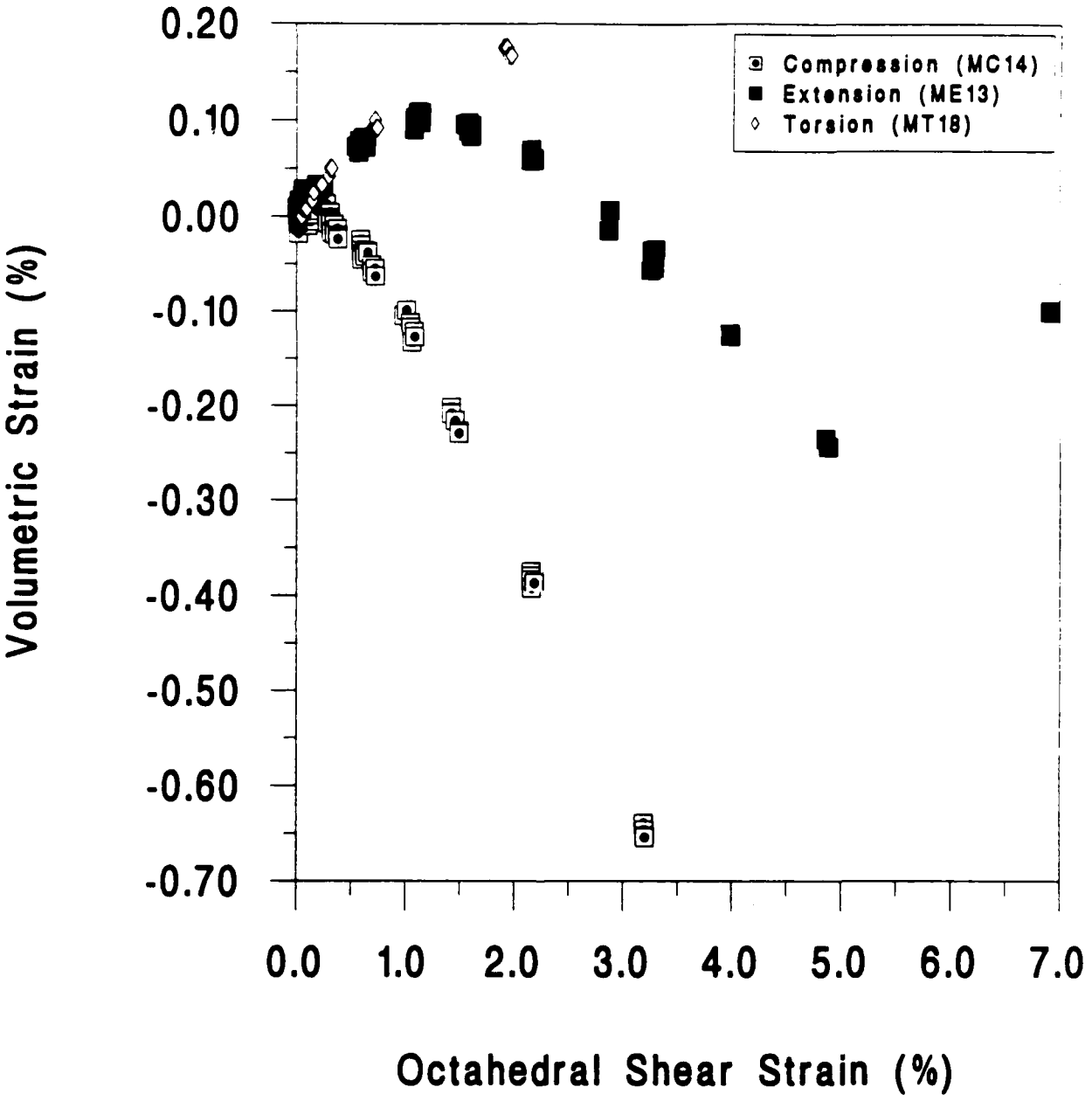

Fig. 30. Comparison of the volumetric strain response of 1-sized glass bead specimens under three inclinations of principal stress.

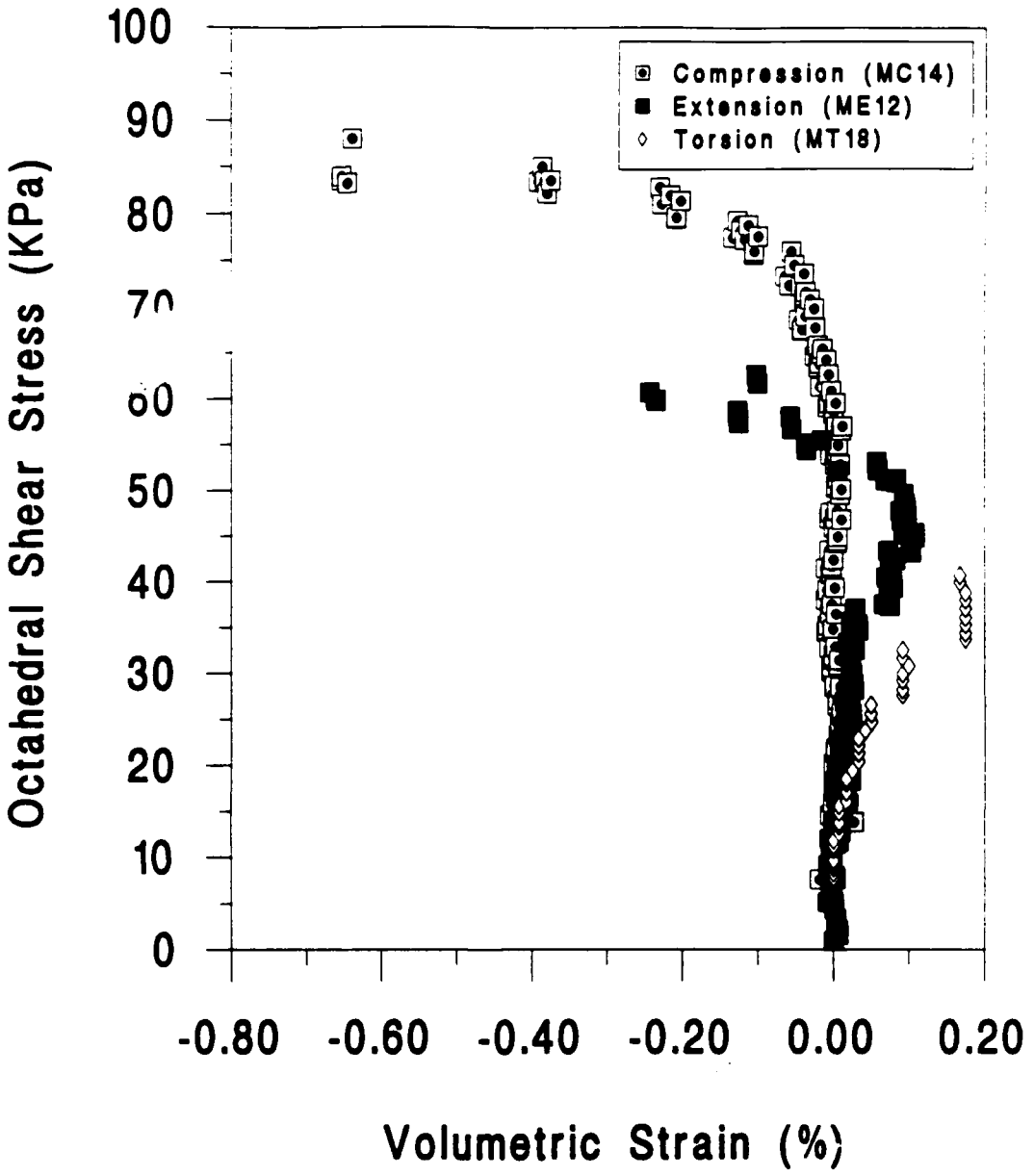

Fig. 31. Comparison of the volumetric response of monosized glass bead specimens under three inclinations of principal stress

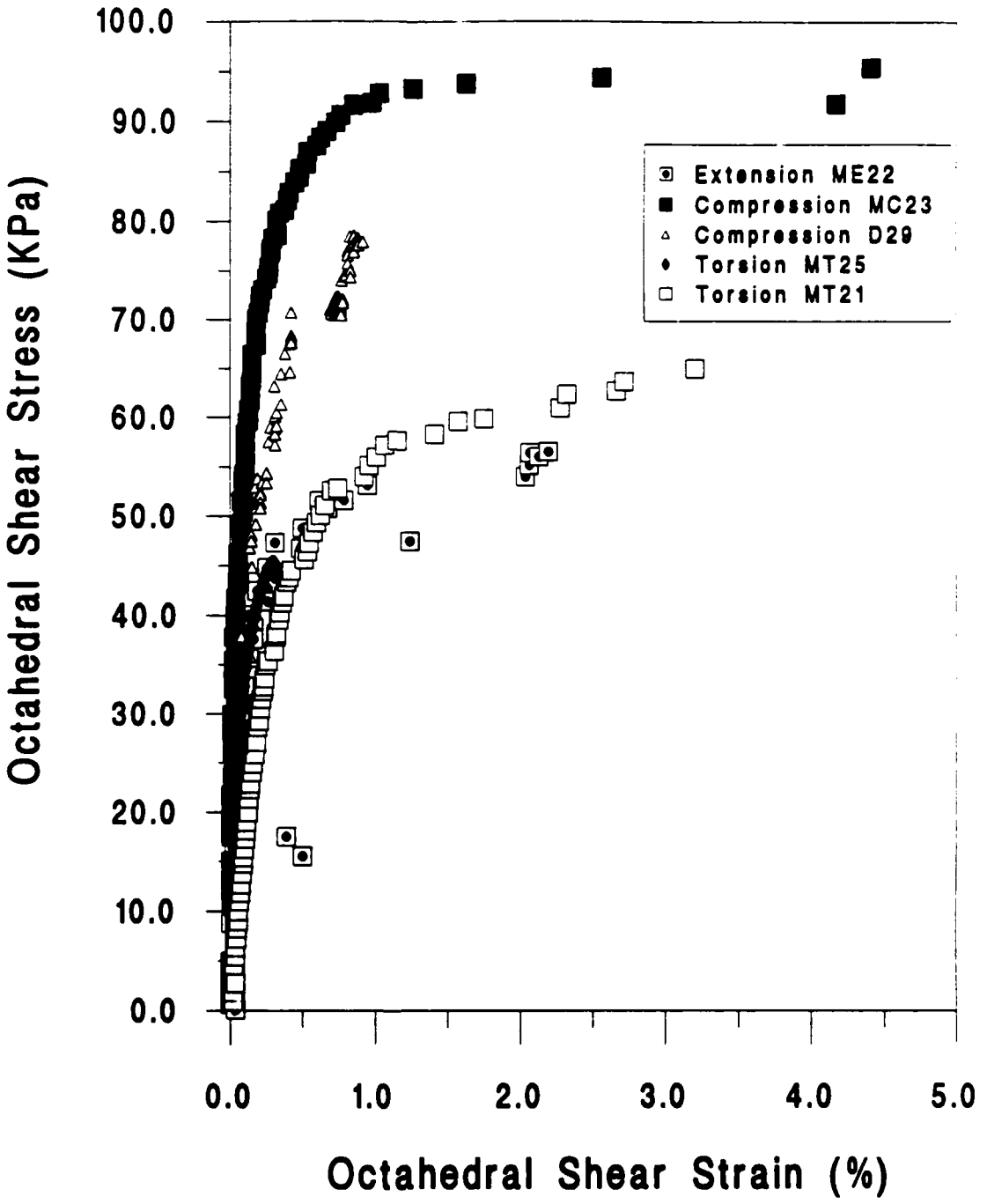

Fig. 32. Stress-strain curves from monotonic compression, extension and torsional shear tests on a mixture of glass beads prepared by undercompaction. Mean stress constant 138 KPa.

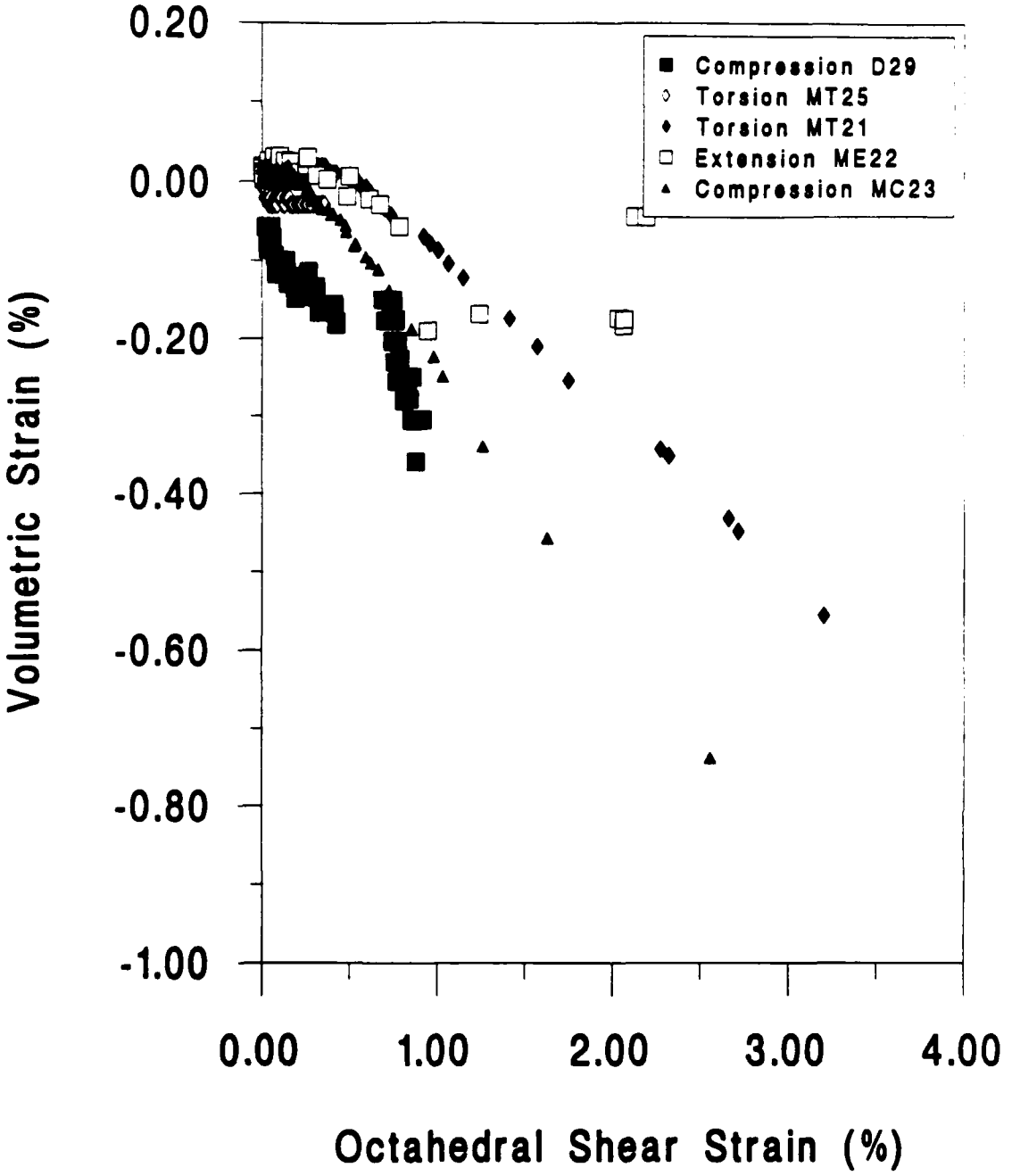

Fig. 33. Volumetric strain vs octahedral shear strain for specimens composed of mixture 2 sheared in compression, extension and torsional shear. Mean stress constant at 138 KPa.

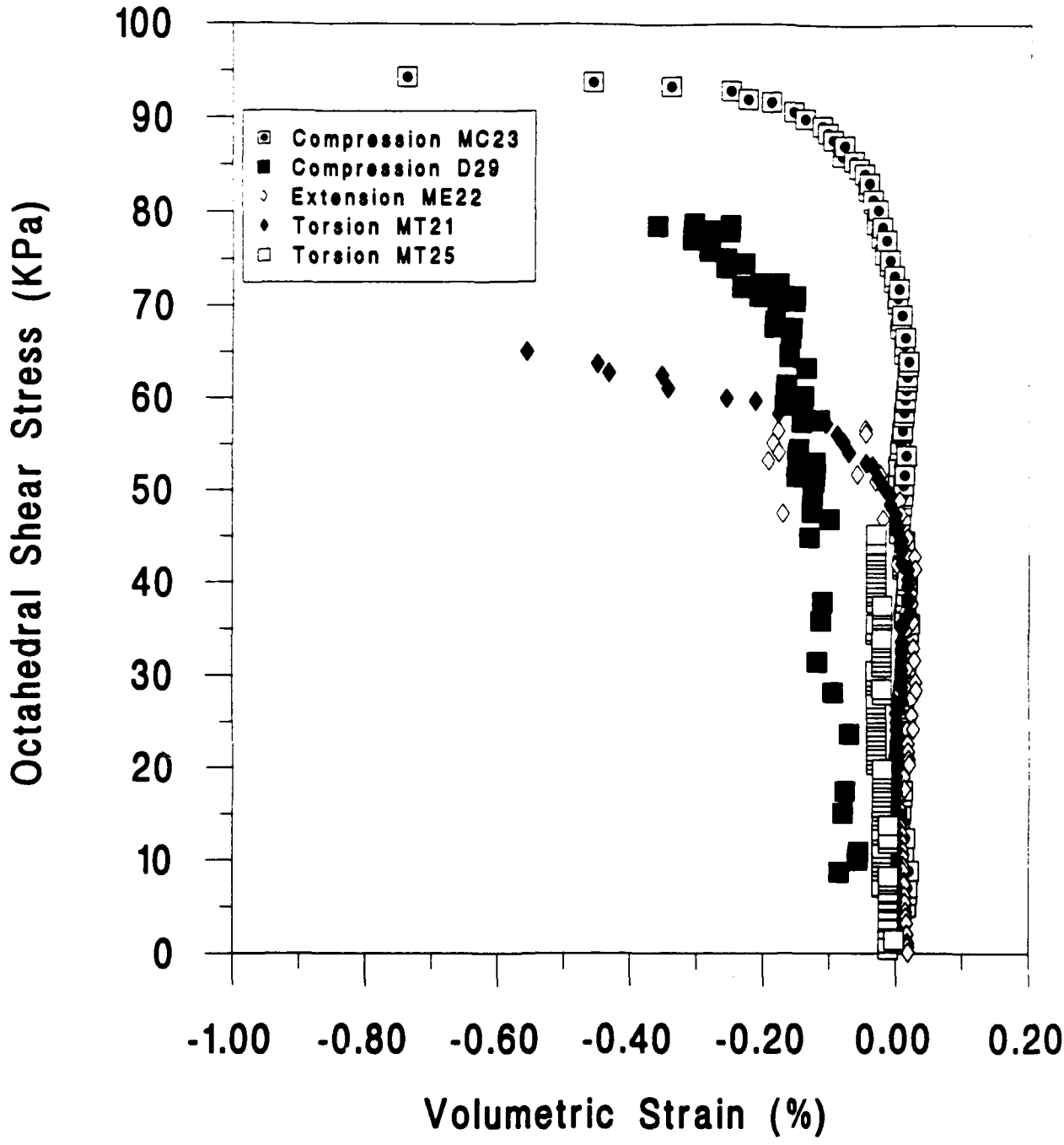

Fig. 34. Variation of volumetric strain with octhedral shear stress for compression, extension and torsional shear tests. Mean stress constant at 138 KPa. Samples composed of particles with wide range of diameters and prepared by undercompaction.

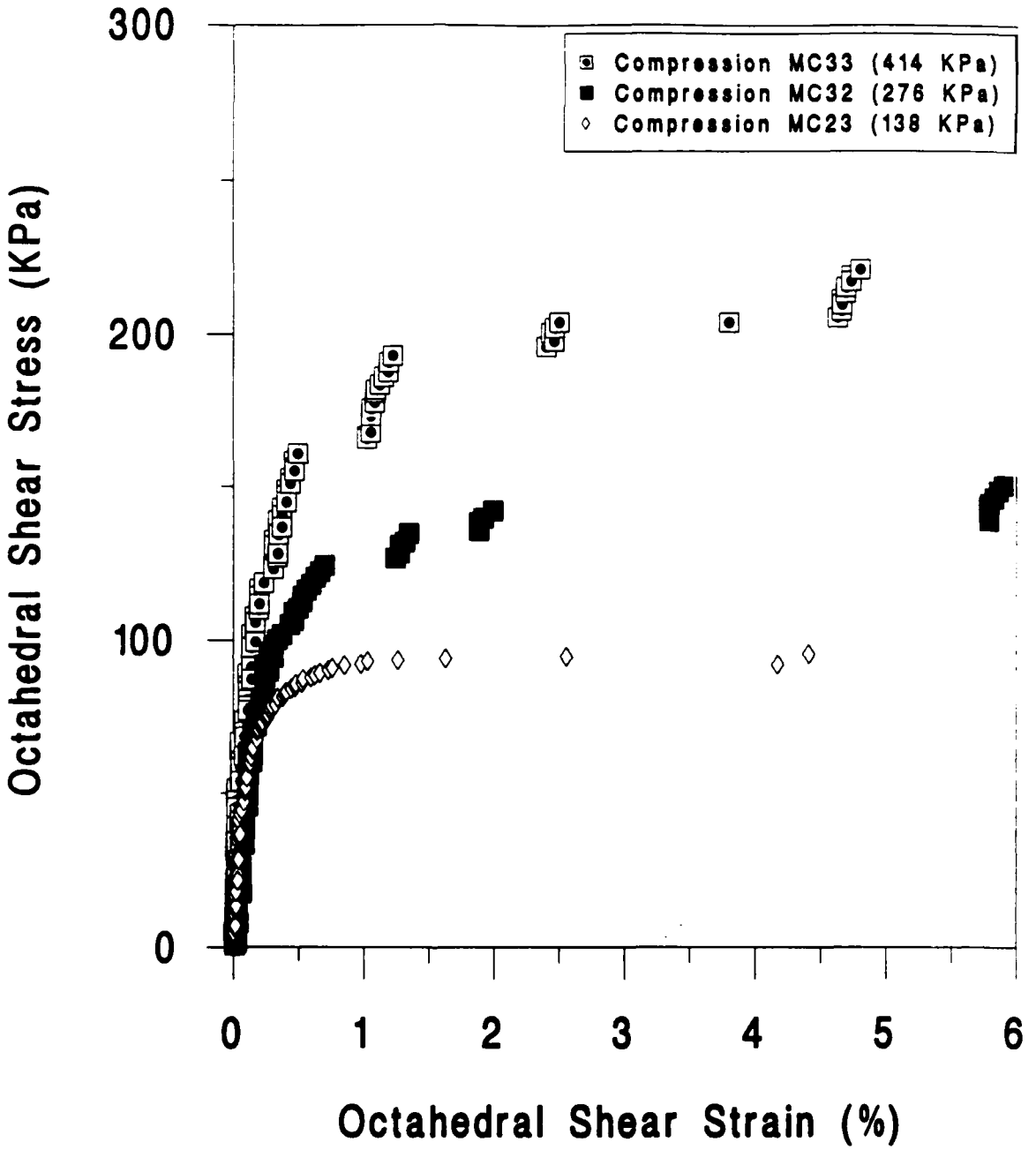

Fig. 35. Stress-strain curves obtained by compression under constant mean stress on specimens consolidated at three different confining pressures. Samples prepared by undercompaction and composed of glass beads with a wide range of diameters

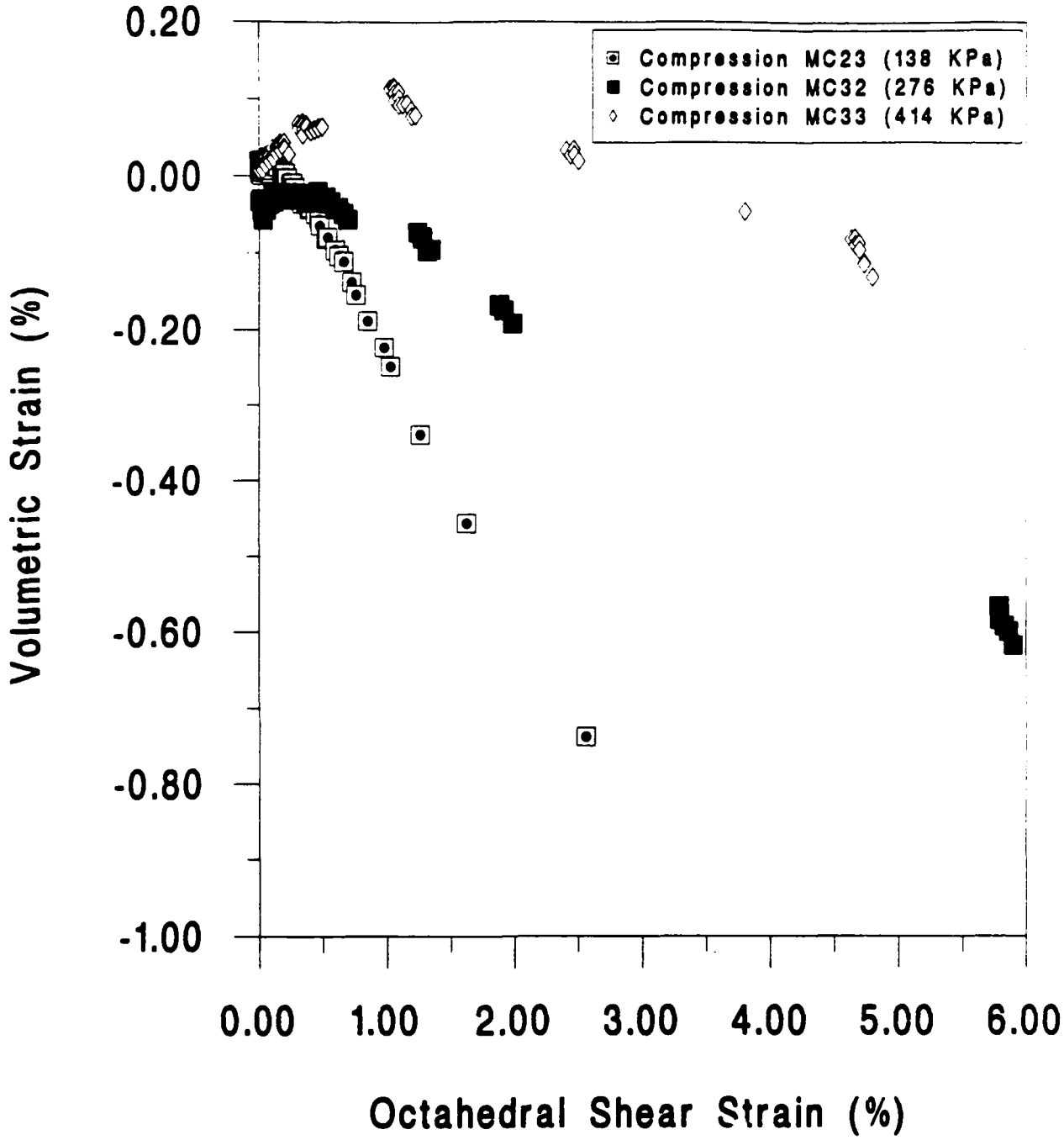

Fig. 36. Volumetric versus shear strain curves obtained from compression under constant mean stress for specimens consolidated at three different confining pressures. Samples composed of glass beads with a wide range of diameters and prepared with undercompaction.

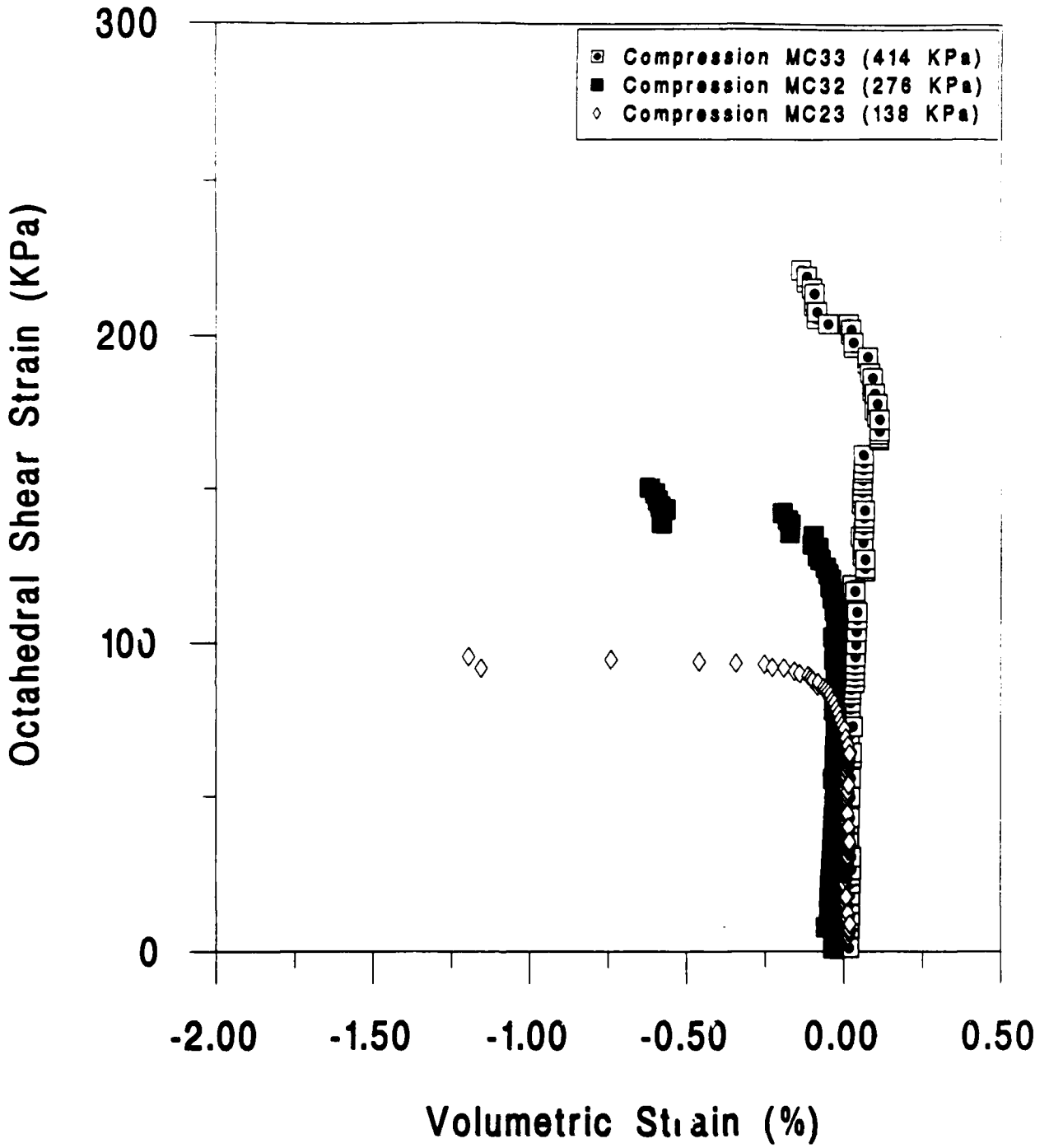

Fig. 37. Volumetric strain - octahedral shear stress curves obtained from compression under constant mean stress for specimens consolidated under three different confining pressures. Samples composed of glass beads with wide range of diameters.

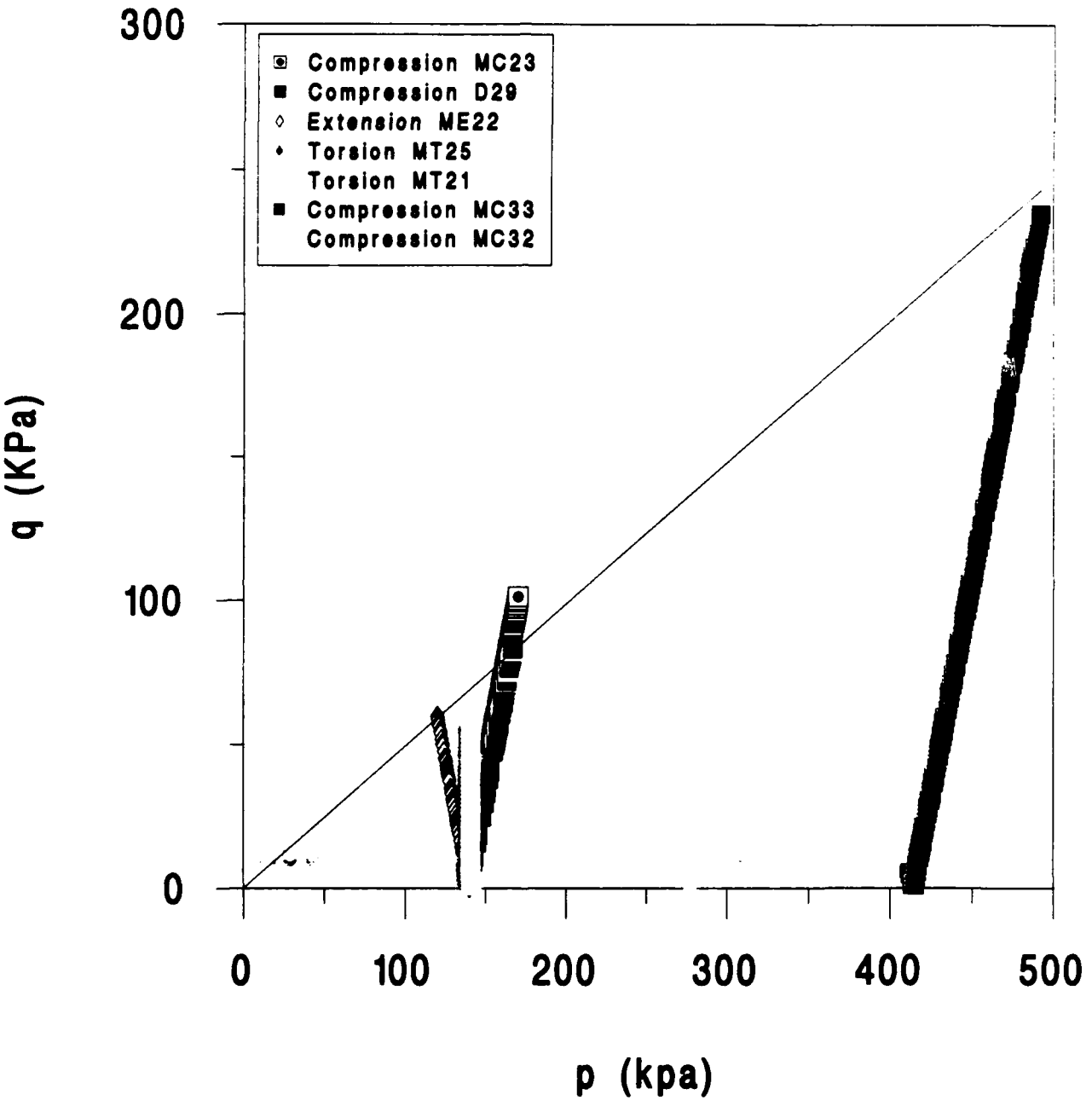

Fig. 38. Stress paths on p-q plane for specimens composed of glass beads with a wide range of diameters and prepared by undercompaction.

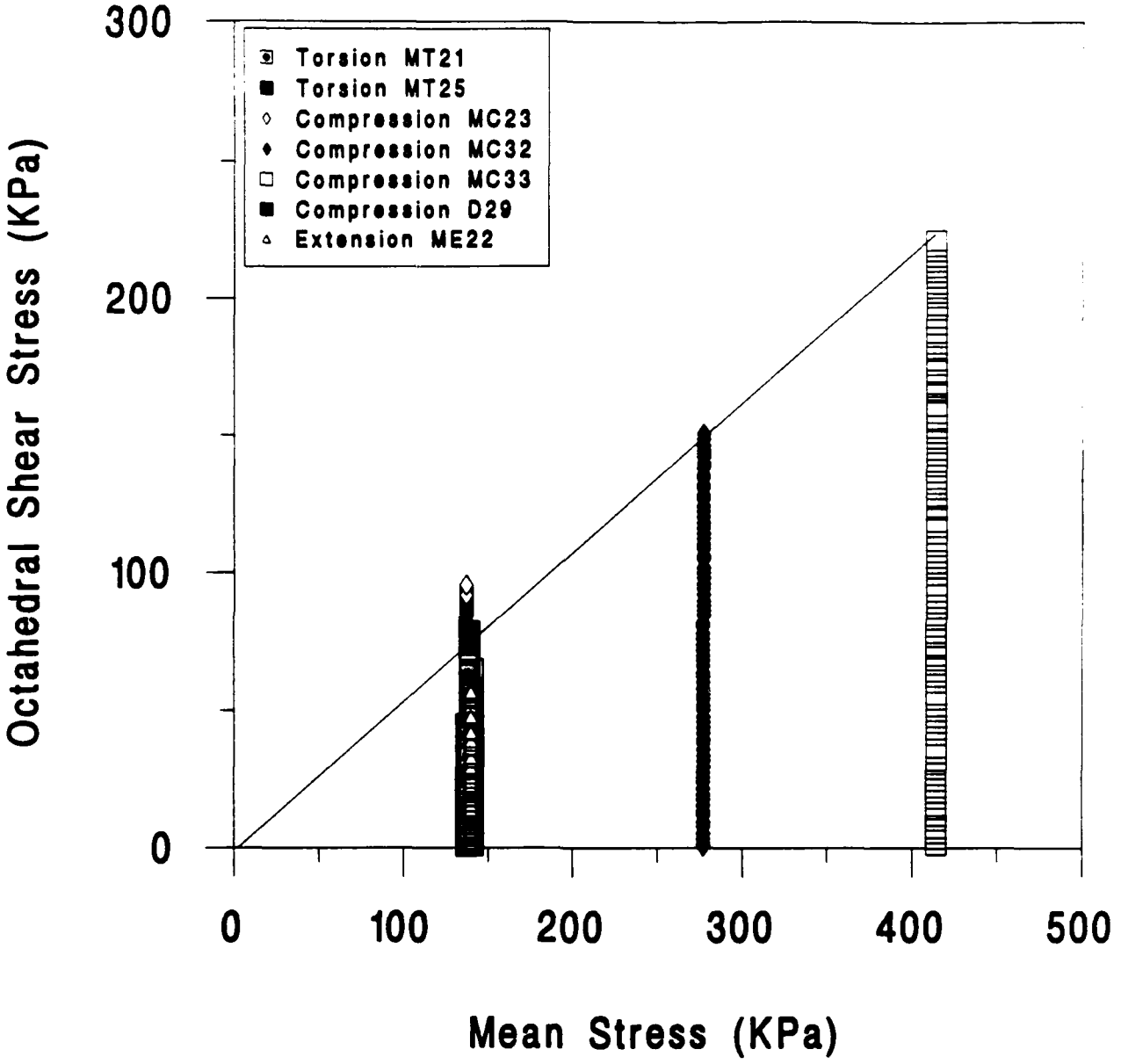

Fig. 39. Stress path on octahedral stress plane for specimens composed of glass beads with wide range of particle diameters and prepared by undercompaction.

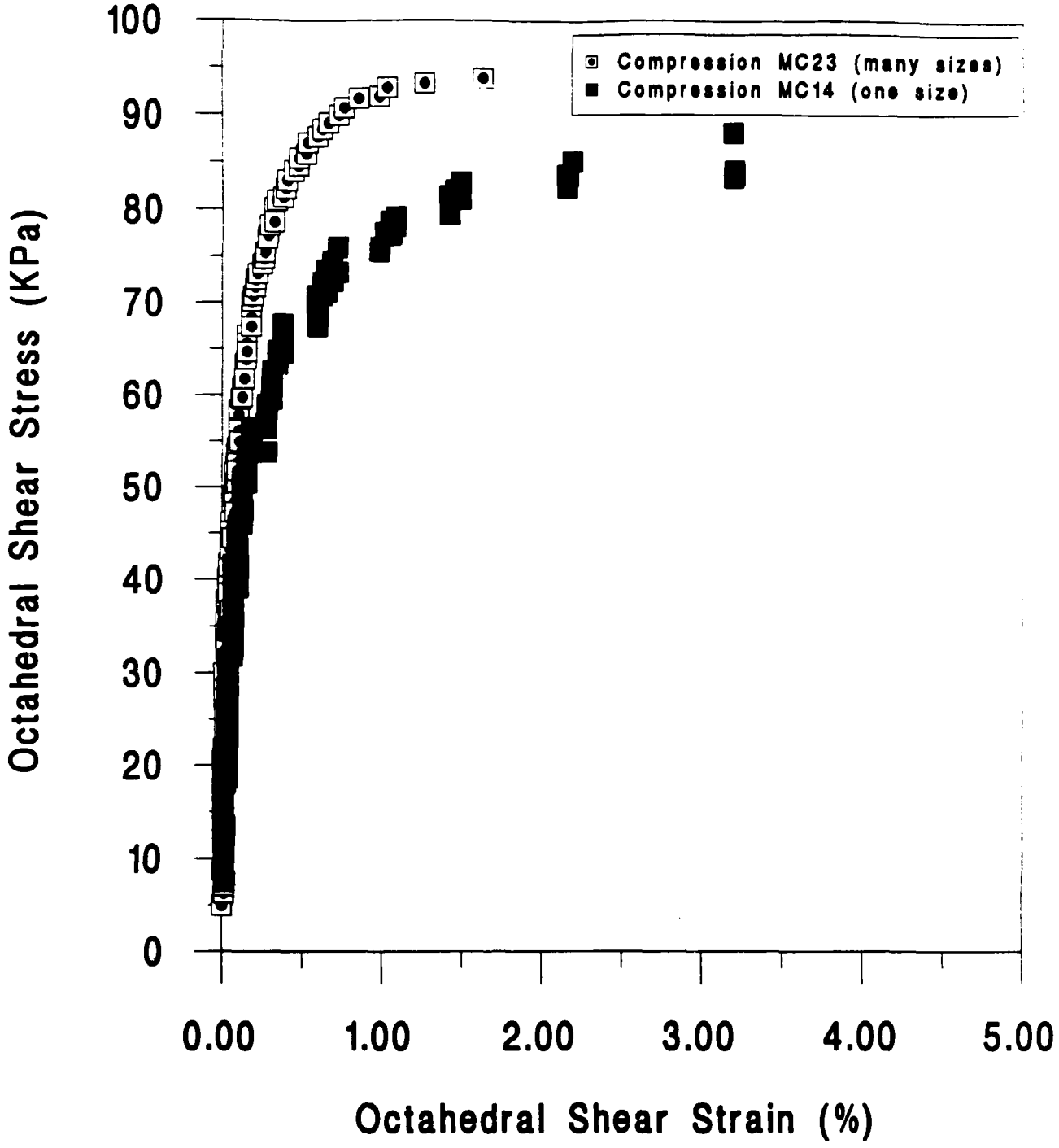

Fig. 40. Comparison of the stress-strain response under compression between specimens composed of: ii) one and iii) many particle sizes. Loading under constant mean stress.

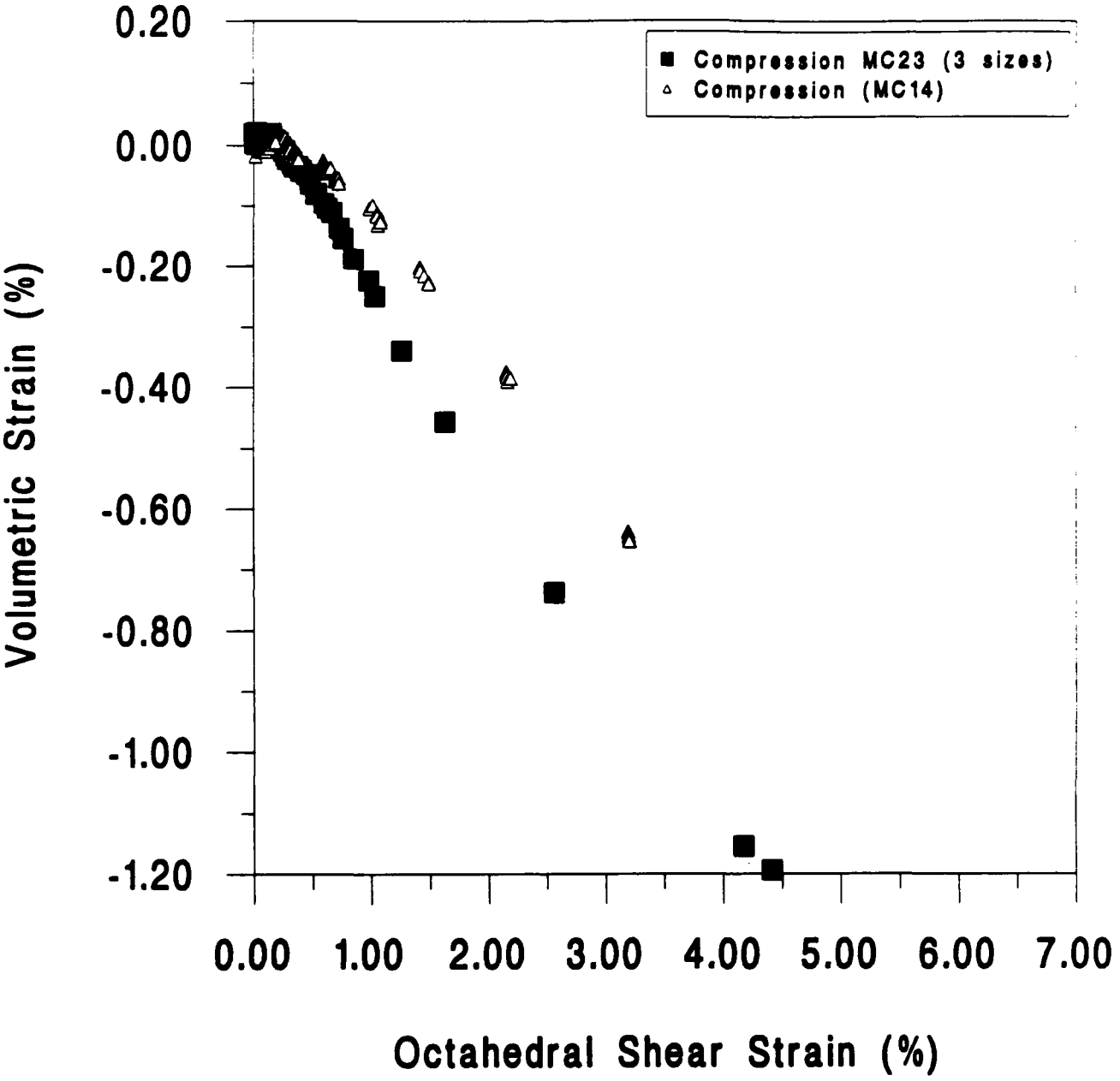

Fig. 41. Comaprison of the volumetric response under compression between specimens composed of 1 and 3 particle sizes. Loading under constant mean stress (138 KPa)

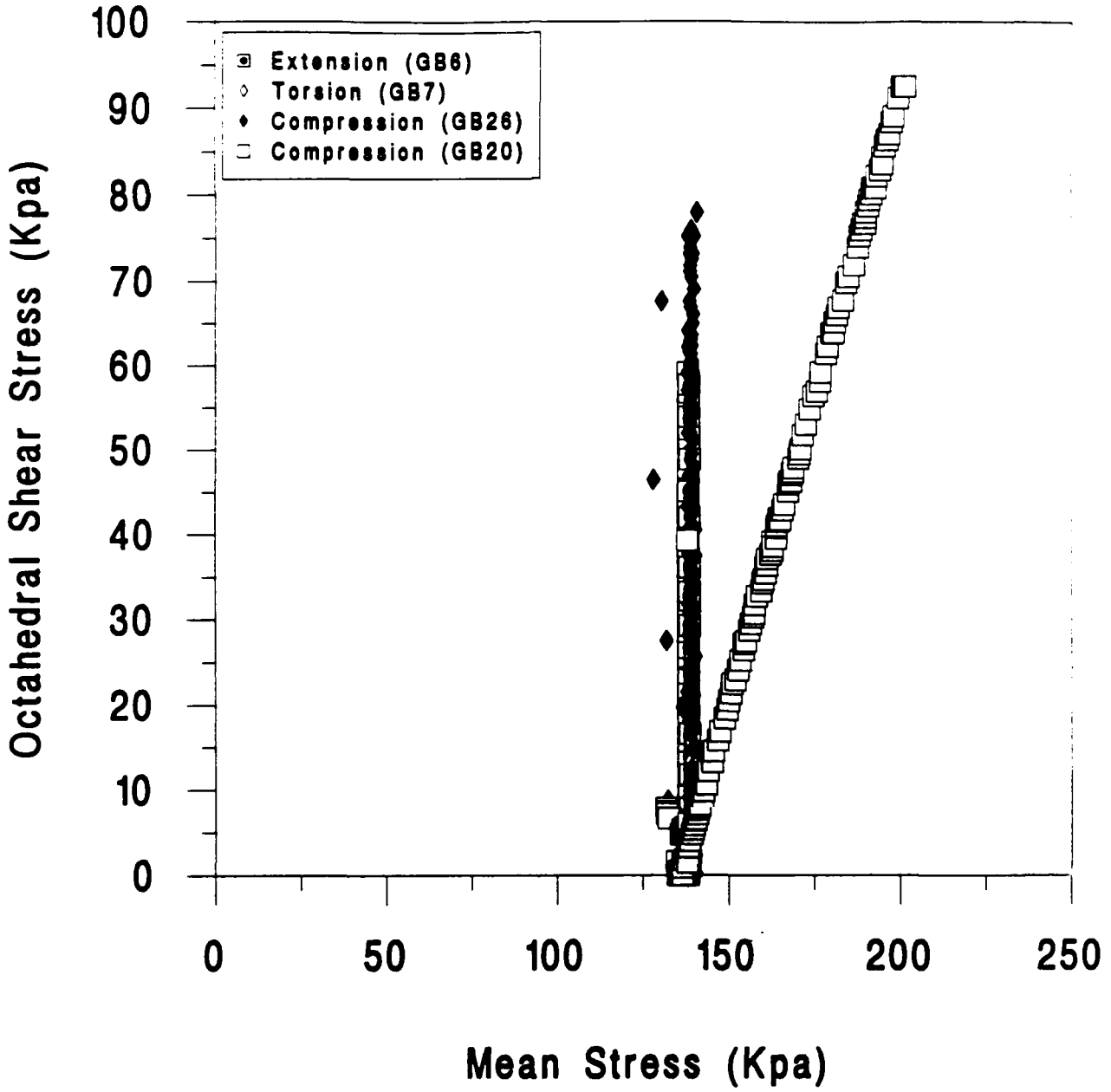

Fig. 42. Stress paths on octahedral stress plane for experiments composed of glass beads with many diameters and prepared with dry pluviation.

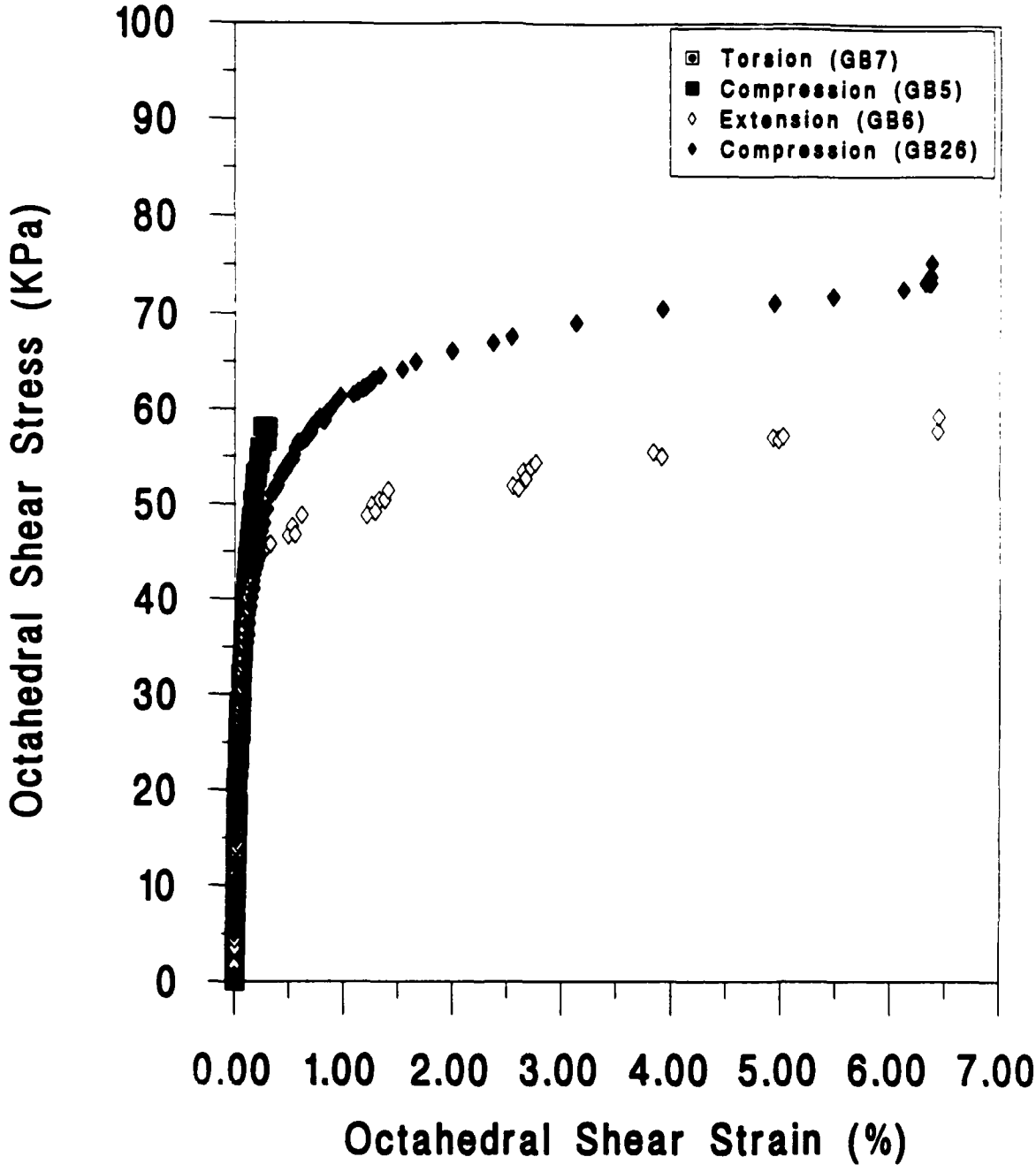

Fig. 43. Octahedral Stress-Strain Curves obtained from compression, extension and torsional shear experiments under constant mean stress. Specimens with many particle diameters and prepared by dry pluviation. Compression test GB5 had a low B-parameter.

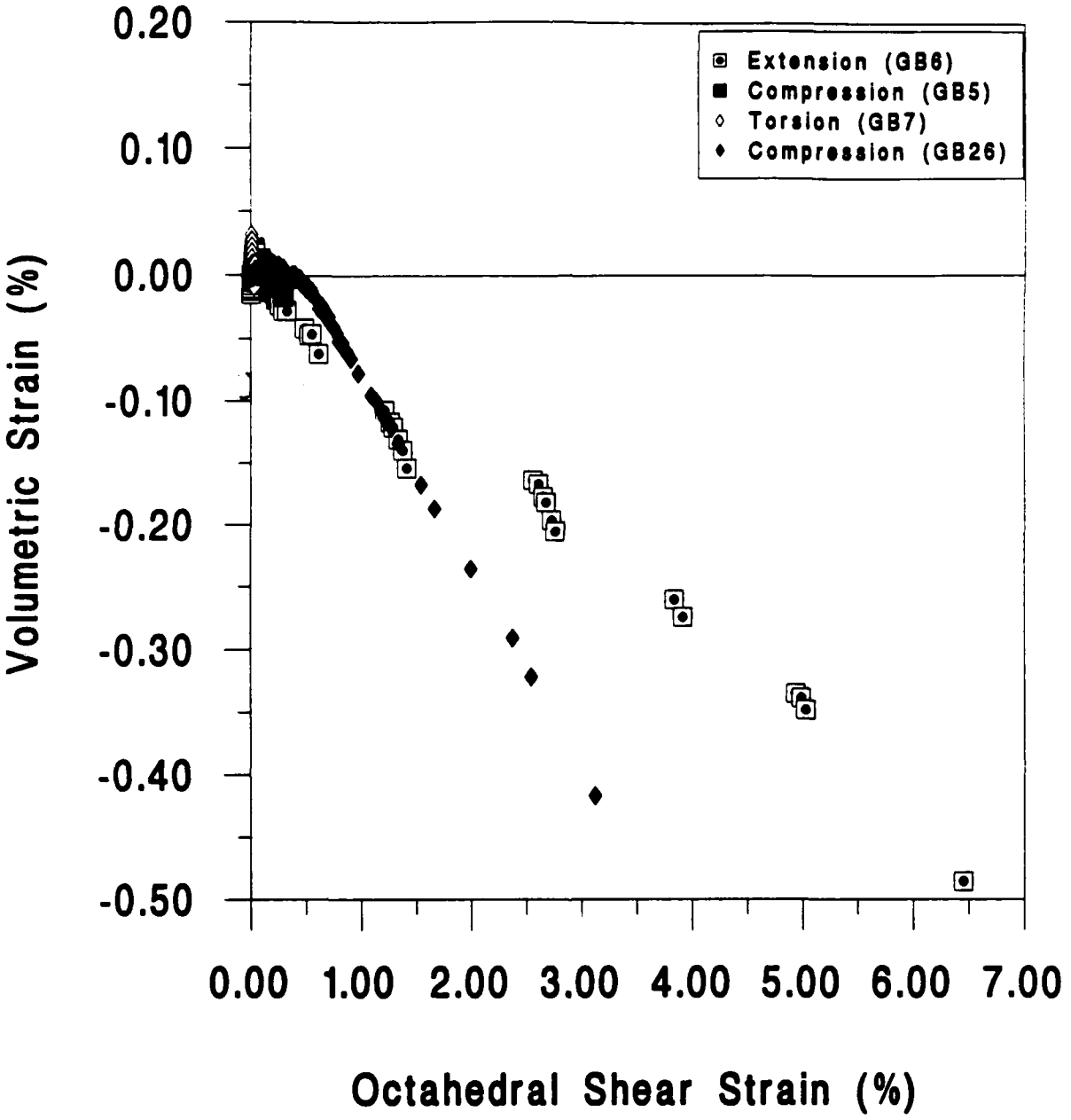

Fig. 44. Volumetric Strain vs. Octahedral Shear Strain curves obtained from compression, extension and torsional shear tests under constant mean stress. Specimens composed of many particle diameters and prepared by dry pluviation.

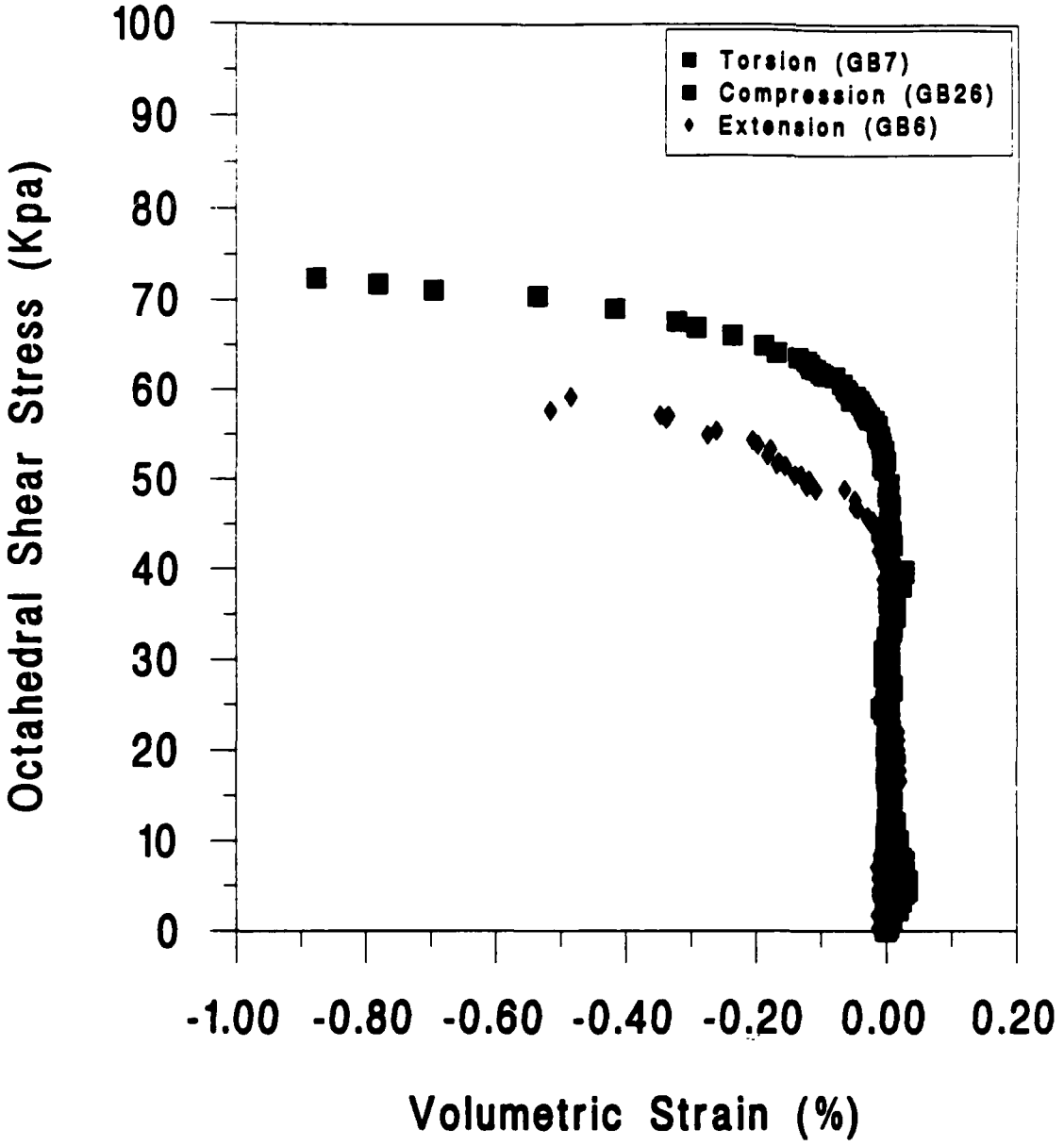

Fig. 45. Volumetric strain versus octheadral shear stress curve obtained from compression, extension and torsional shear experiments under constant mean stress (138 KPa). Specimens composed of particles having a range of diameters and prepared by dry pluviation.

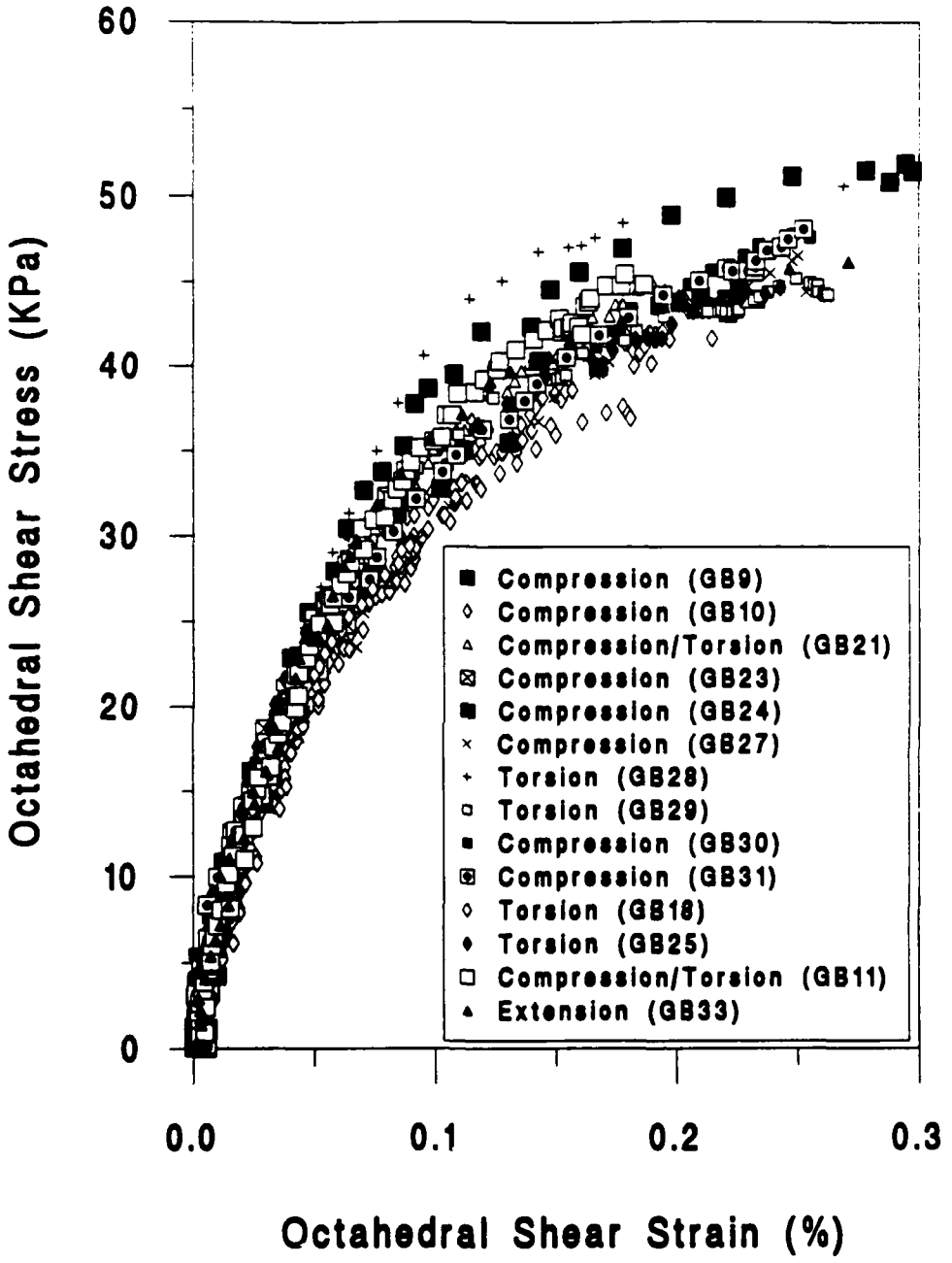

Fig. 46. Octahedral shear stress-strain curves obtained from the monotonic portion of all cyclic tests on specimens prepared by pluviation.

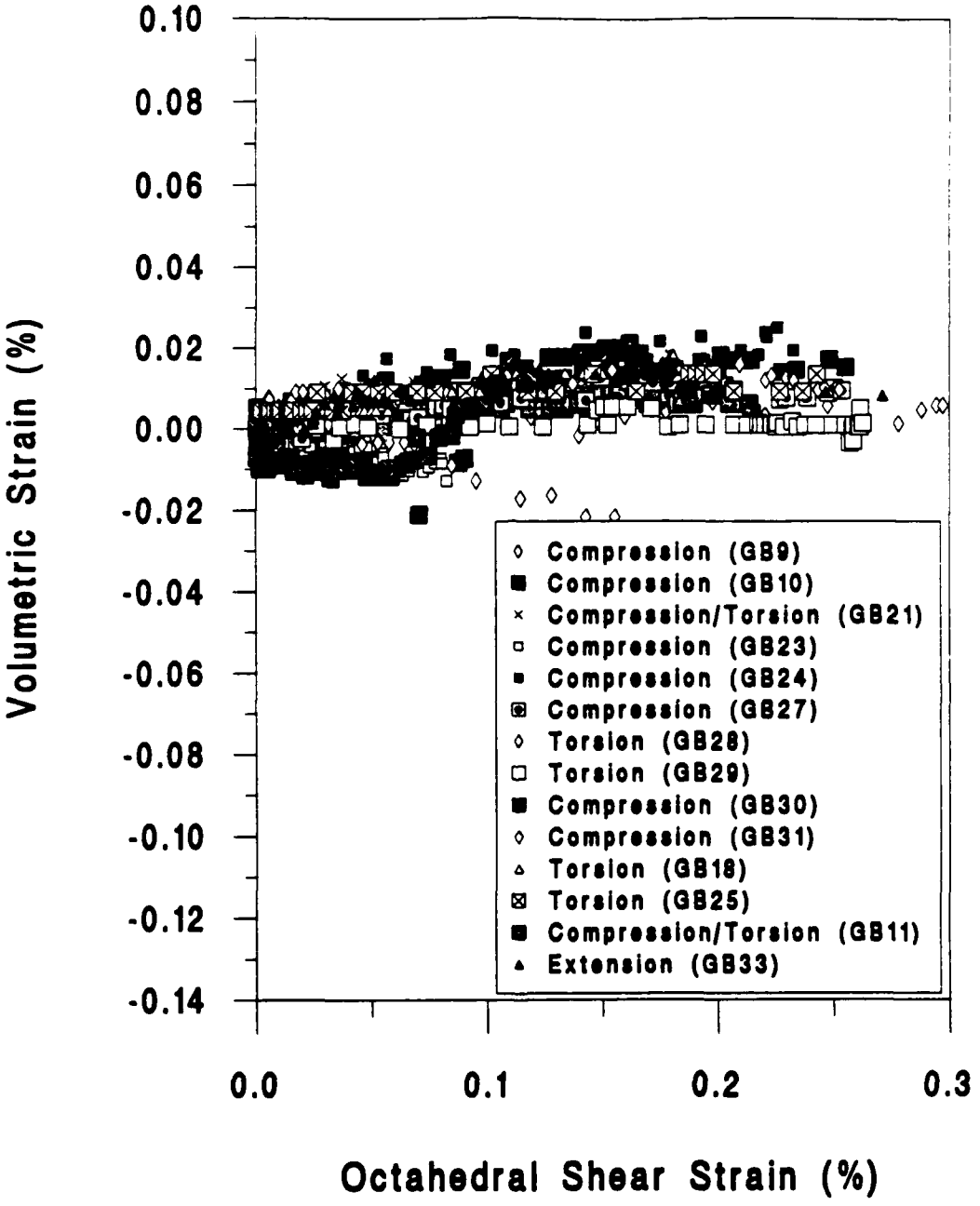

Fig. 47. Variation of volumetric strain with octahedral shear strain observed in the monotonic portion of all cyclic tests for specimens prepared by dry pluviation.

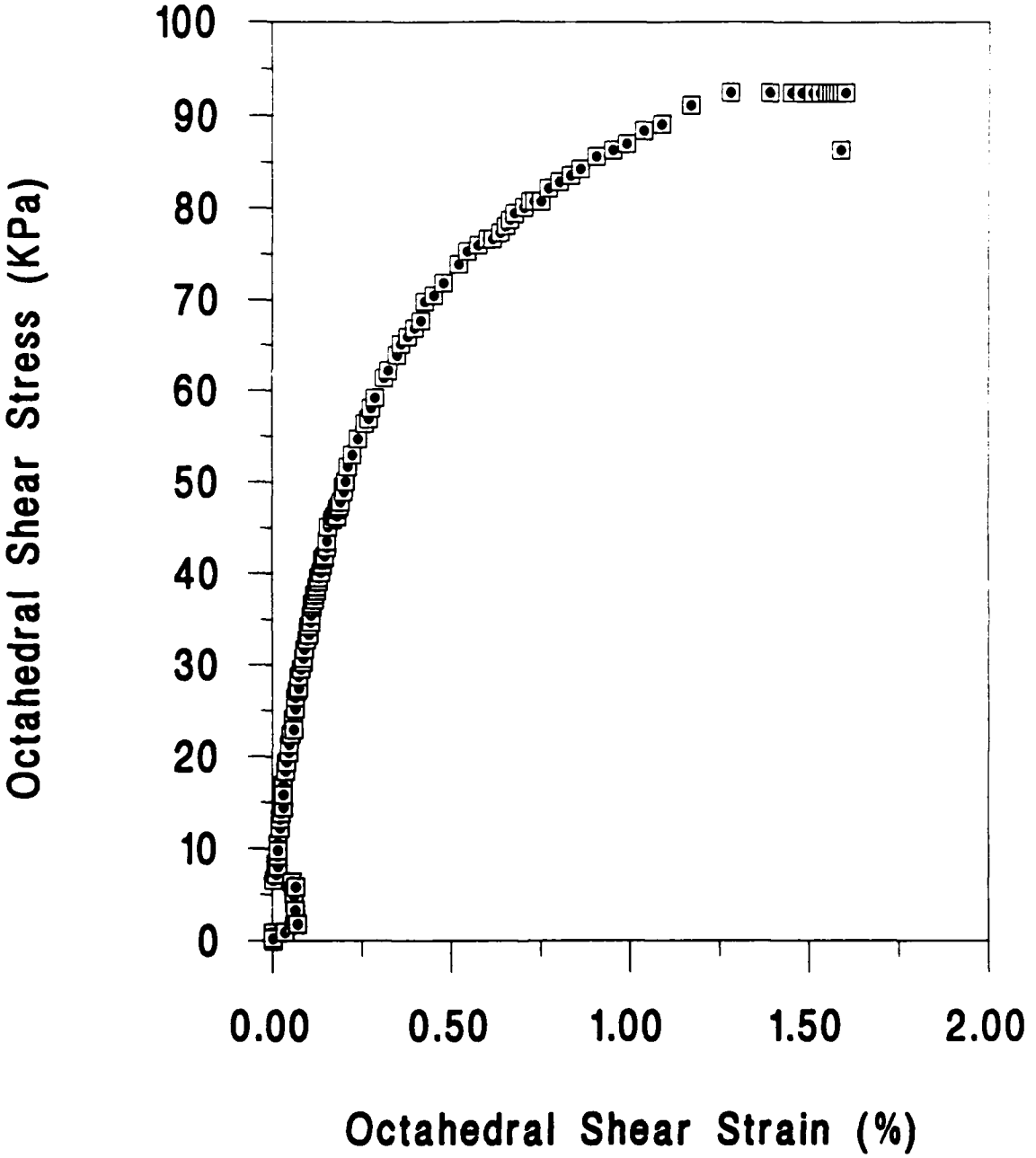

Fig. 48. Octahedral Stress-strain curve obtained from triaxial compression test GB20. Mean stress was varaible.

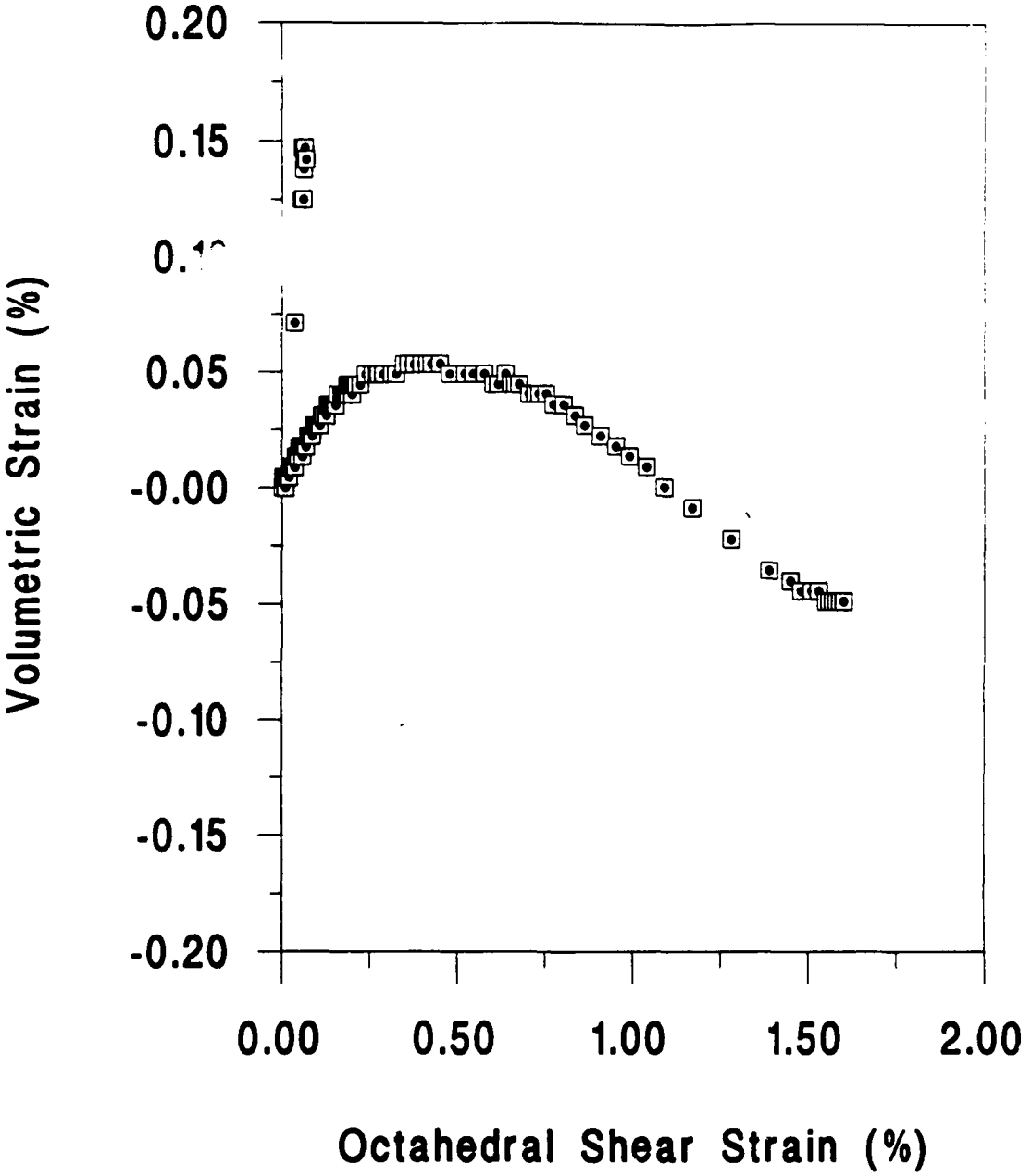

Fig. 49. Volumetric vs octahedral shear strain curve for triaxial compression test GB20. Mean stress was not kept constant. Specimen prepared by dry pluviation.

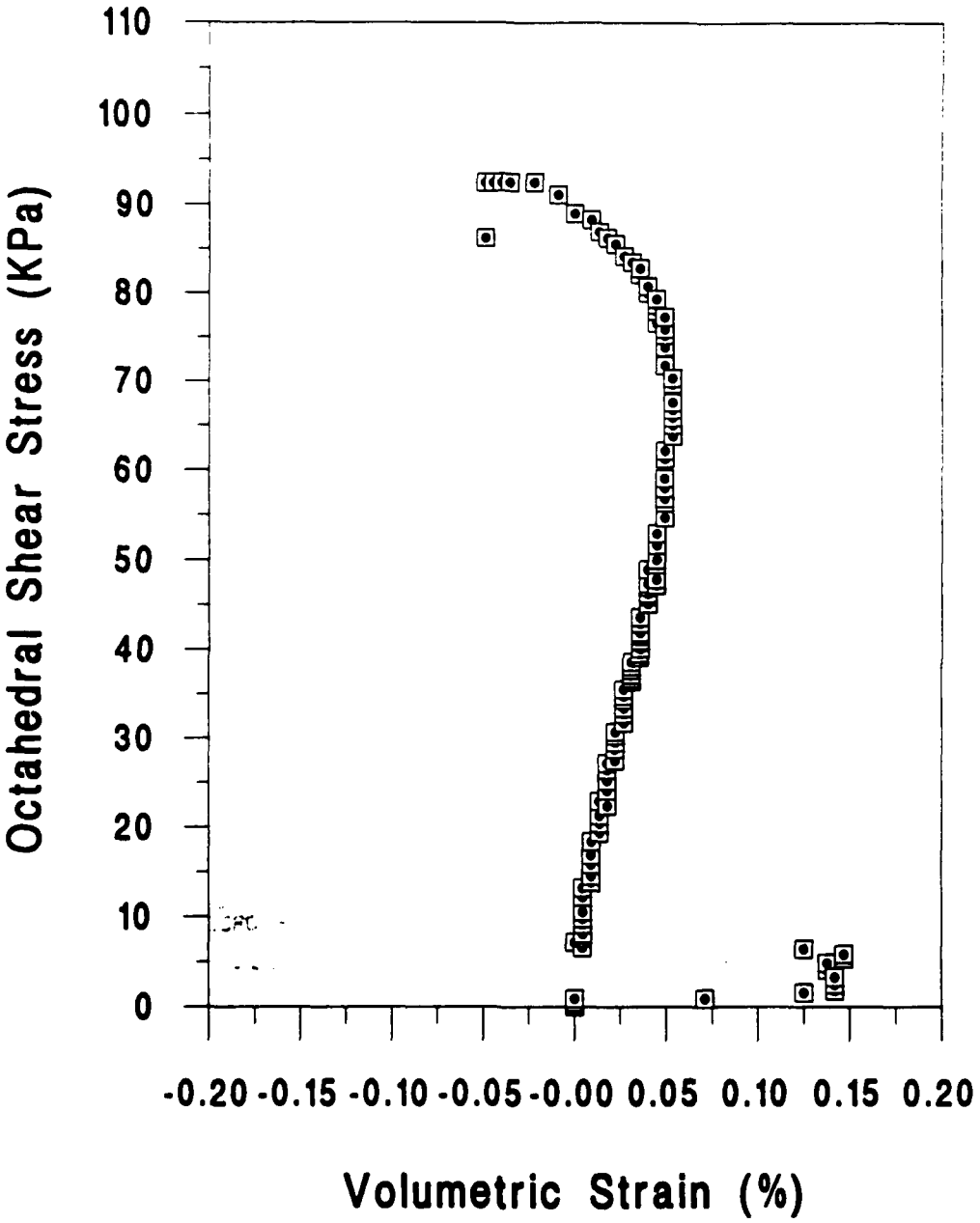

Fig. 50. Octahedral shear stress vs volumetric strain curve for triaxial compression test GB20. Mean stress was not kept constant. Specimen prepared with undercompaction.

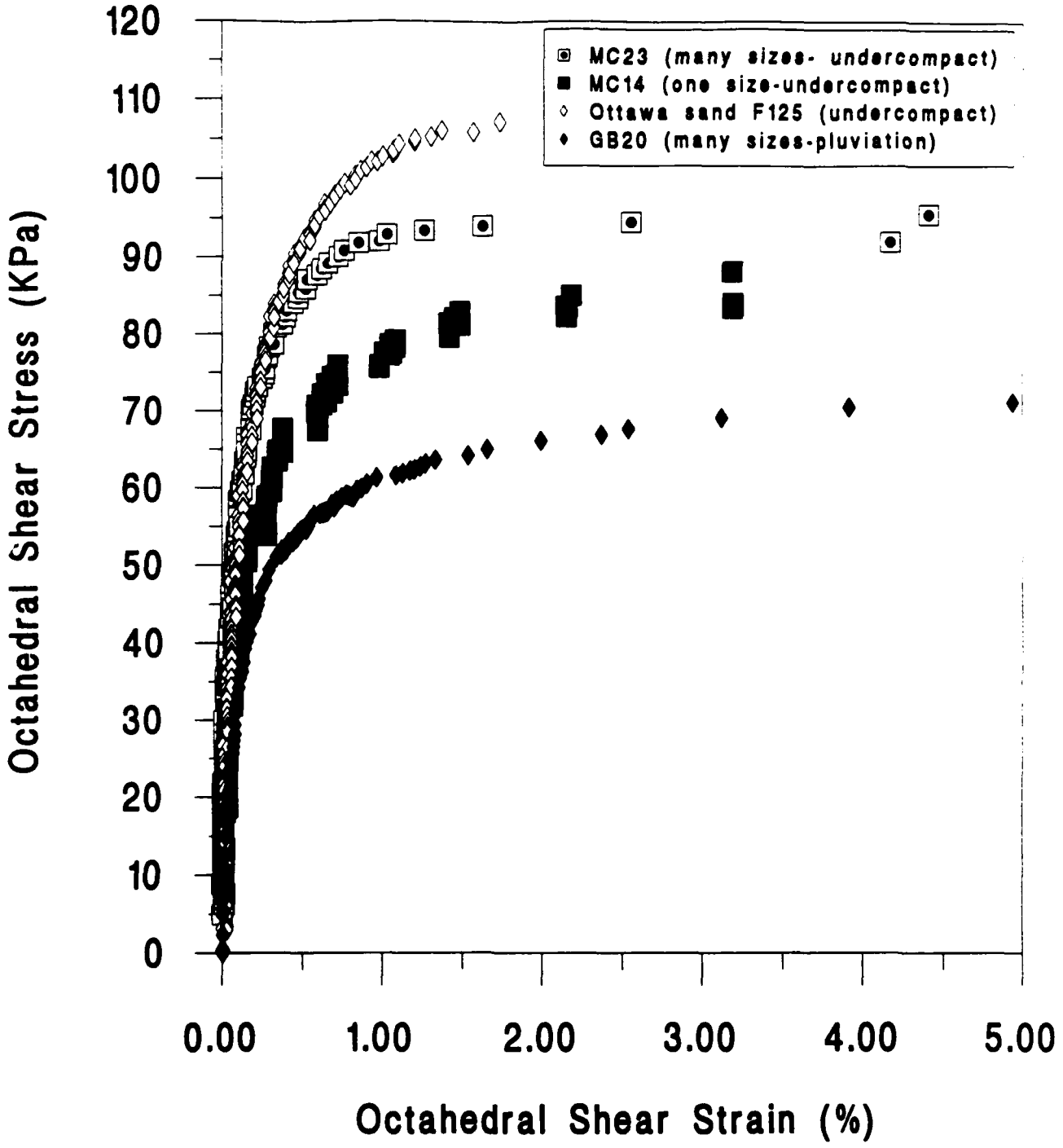

Fig. 51. Comparison of the stress-strain response under compression between specimens composed of: i) Ottawa sand, ii) many and iii) one particle sizes prepared either by undercompaction or pluviation. Loading under constant mean stress (138 KPa).

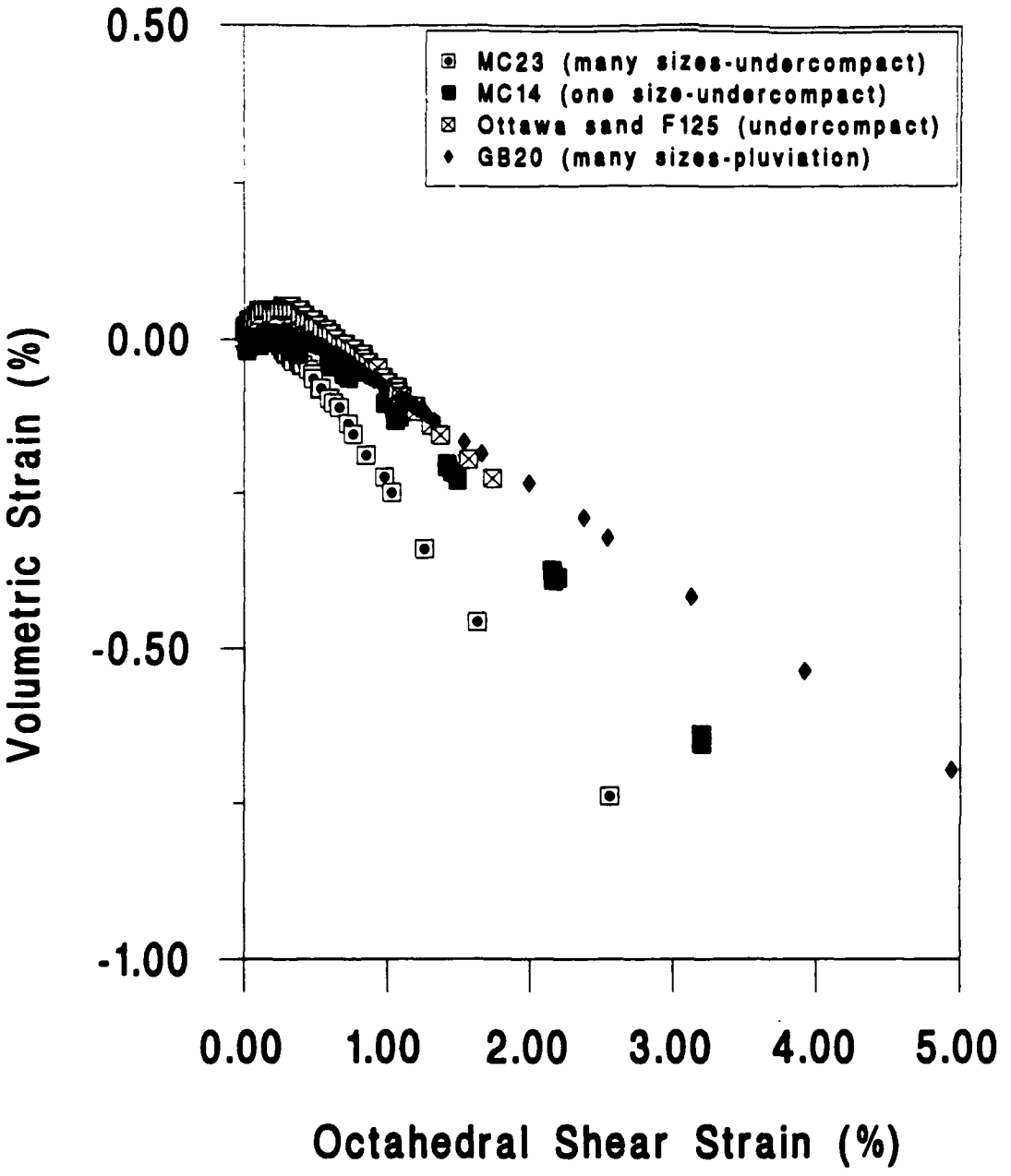

Fig. 52. Comaprison of the volumetric response under compression between specimens composed of: i) Ottawa sand ii) one and ii) many particle sizes prepared either by undercompaction or pluviation. Loading under constant mean stress (138 KPa).

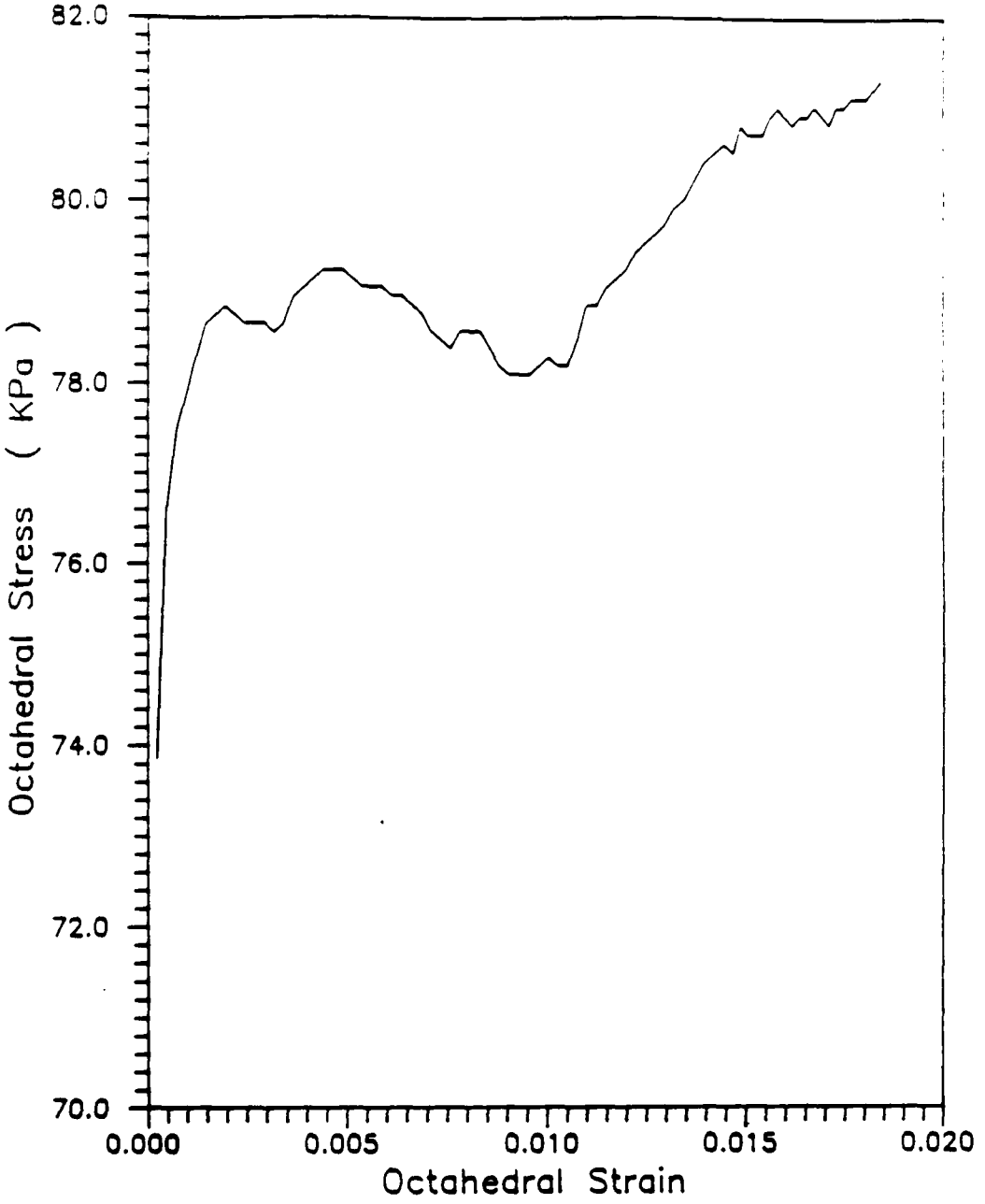

Figure 53 Octahedral shear stress versus octahedral shear strain from compression simulation test under constant mean stress on 531 particle array. (σ_c = 130 KPa)

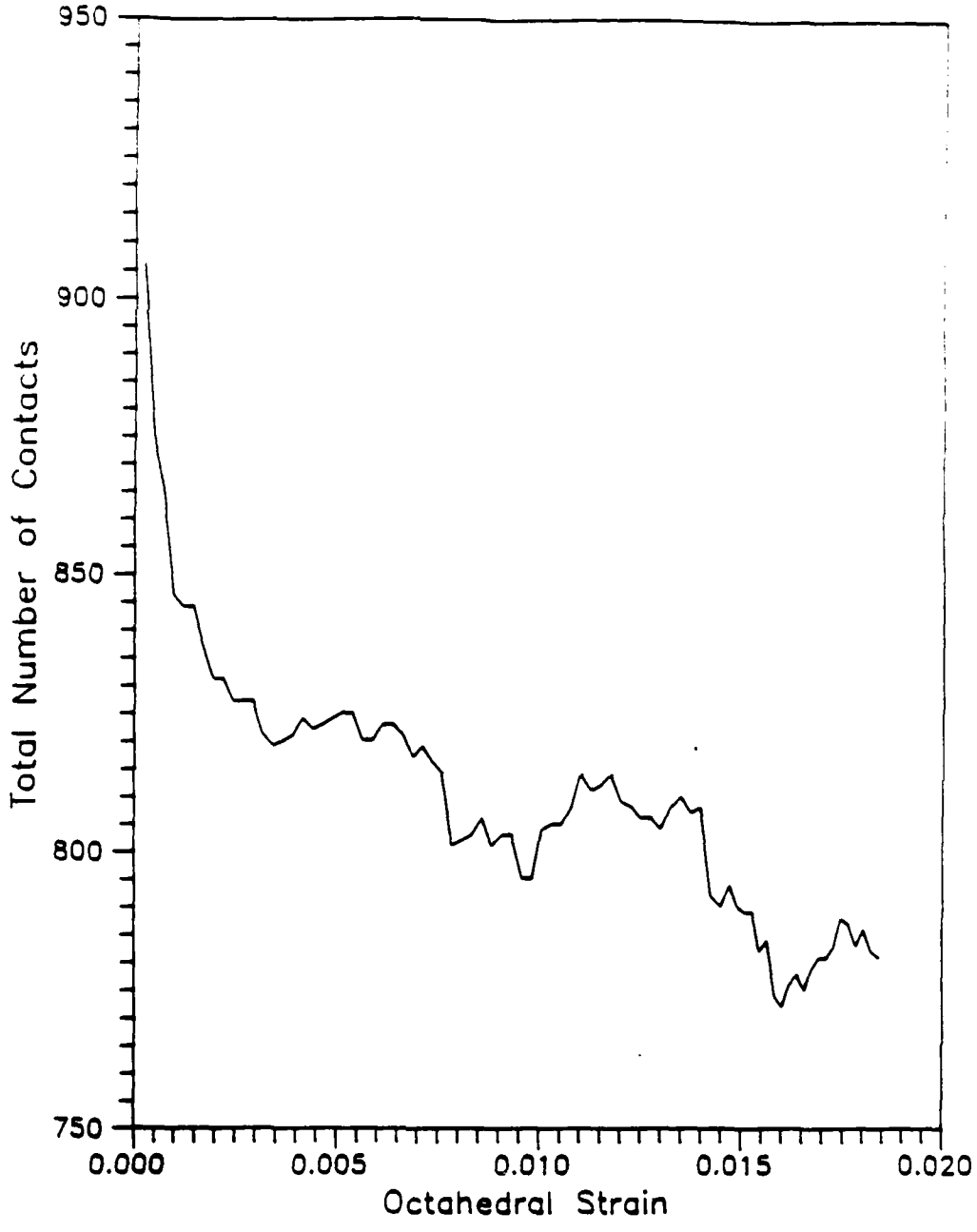

Figure 54 Variation of total number of contacts with octahedral shear strain from the numerical simulation on the 531 particle array.

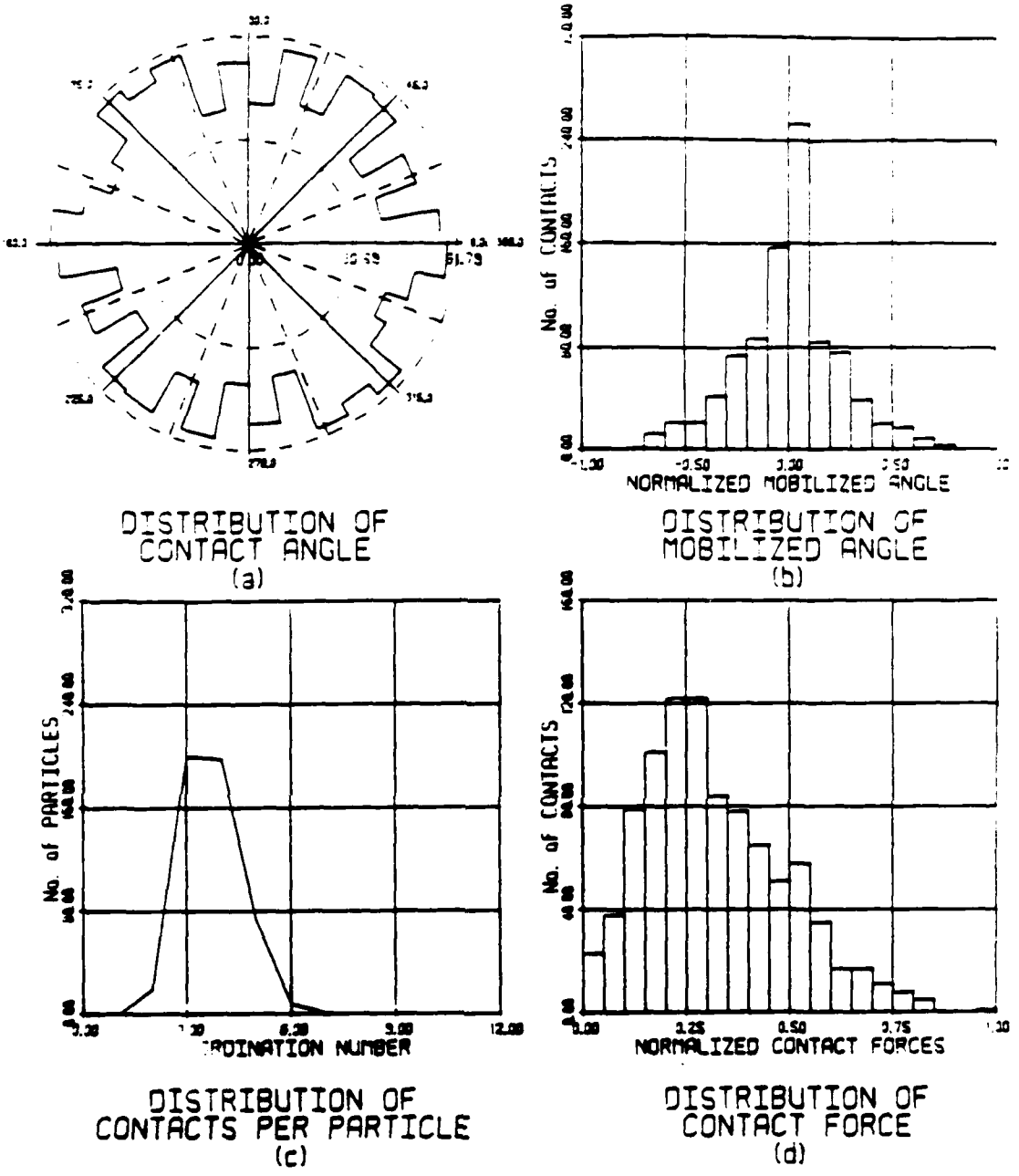

Figure 55 Micromechanical statistics of the numerical simulation on 531 particle array at the end of the isotropic consolidation.

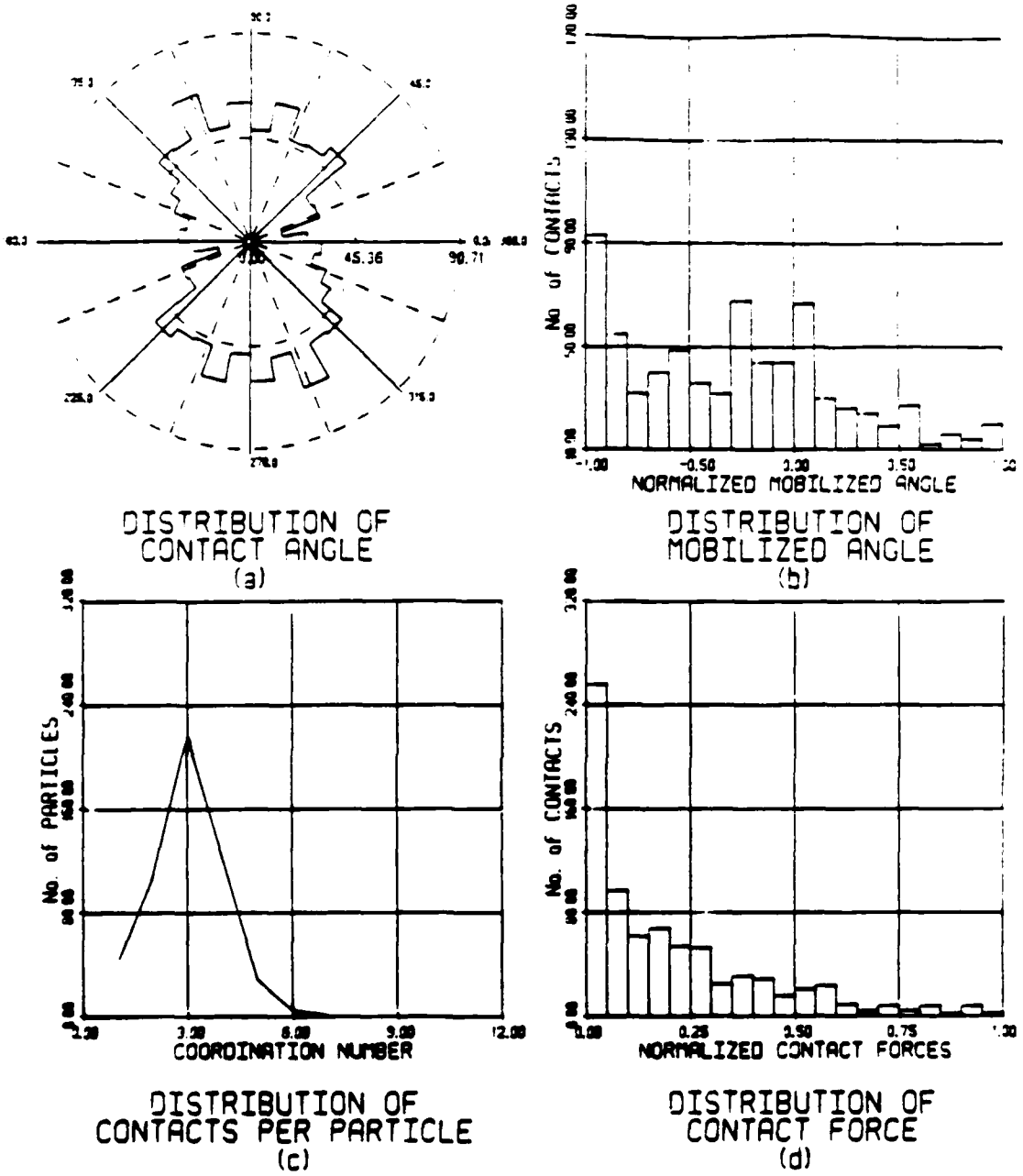

Figure 56 Micromechanical statistics of the numerical simulation on 531 particle array at the end of the shearing phase.

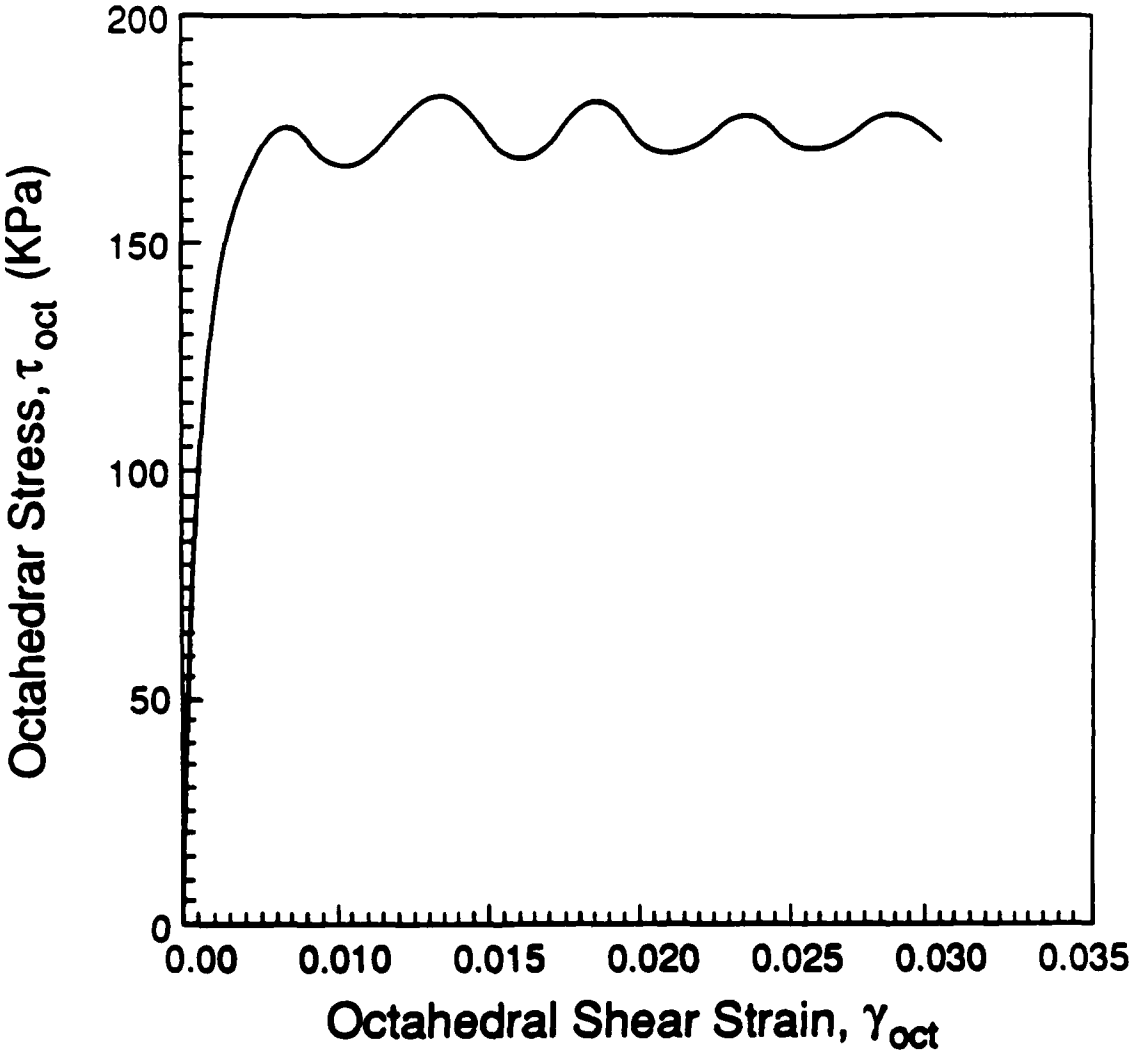

Figure 57 Octahedral shear stress versus octahedral shear strain from compression simulation under constant mean stress (σ_c = 130 KPa) on 477 equal particle array, (after Petrakis and Dobry, 1989).

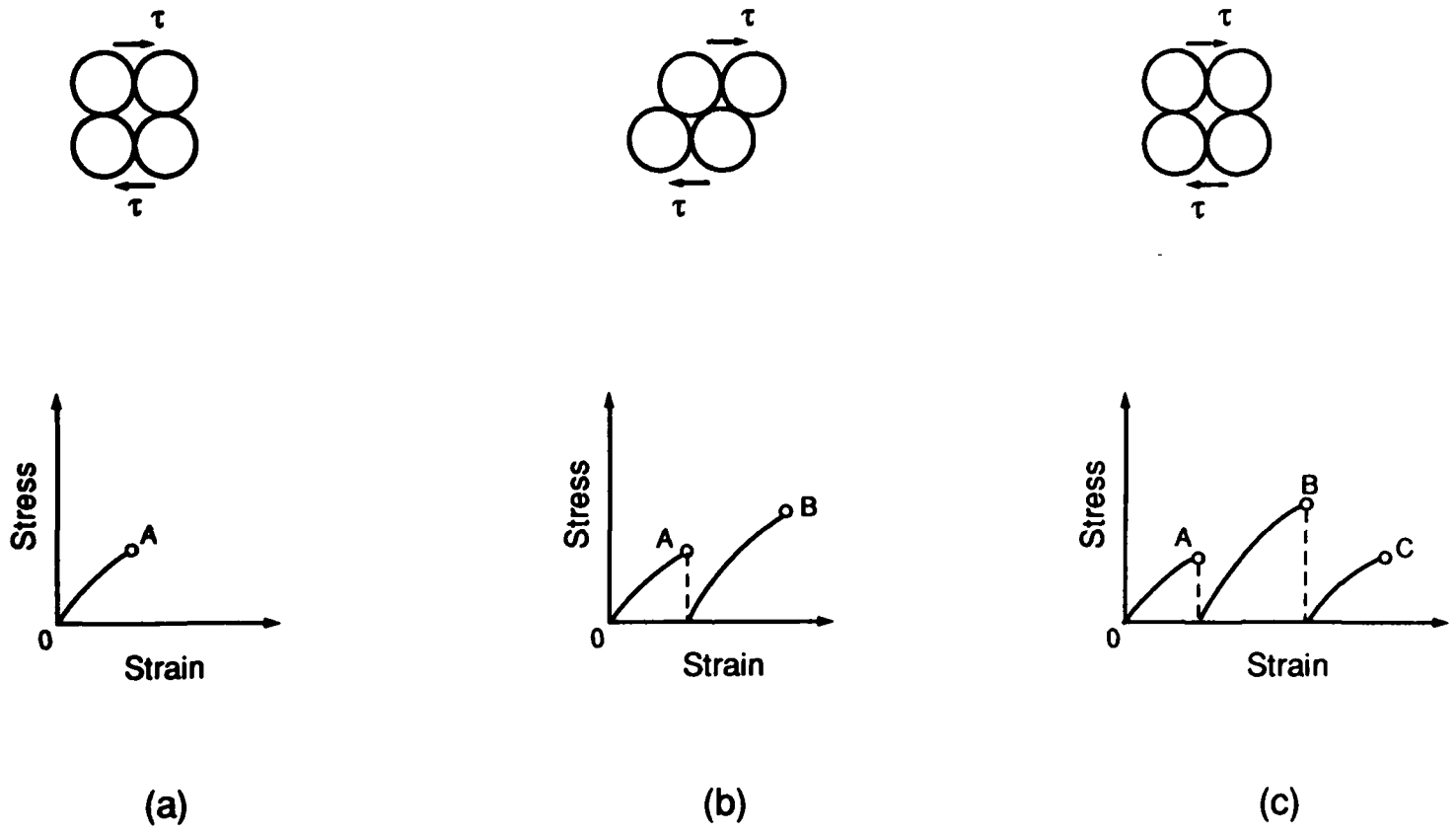

Fig. 58. Simplified microstructural changes during shearing of a simple cubic array. Initial simple cubic array until failure at point A (a). Subsequent new packing (point A to point B) (b). New simple cubic array (c).

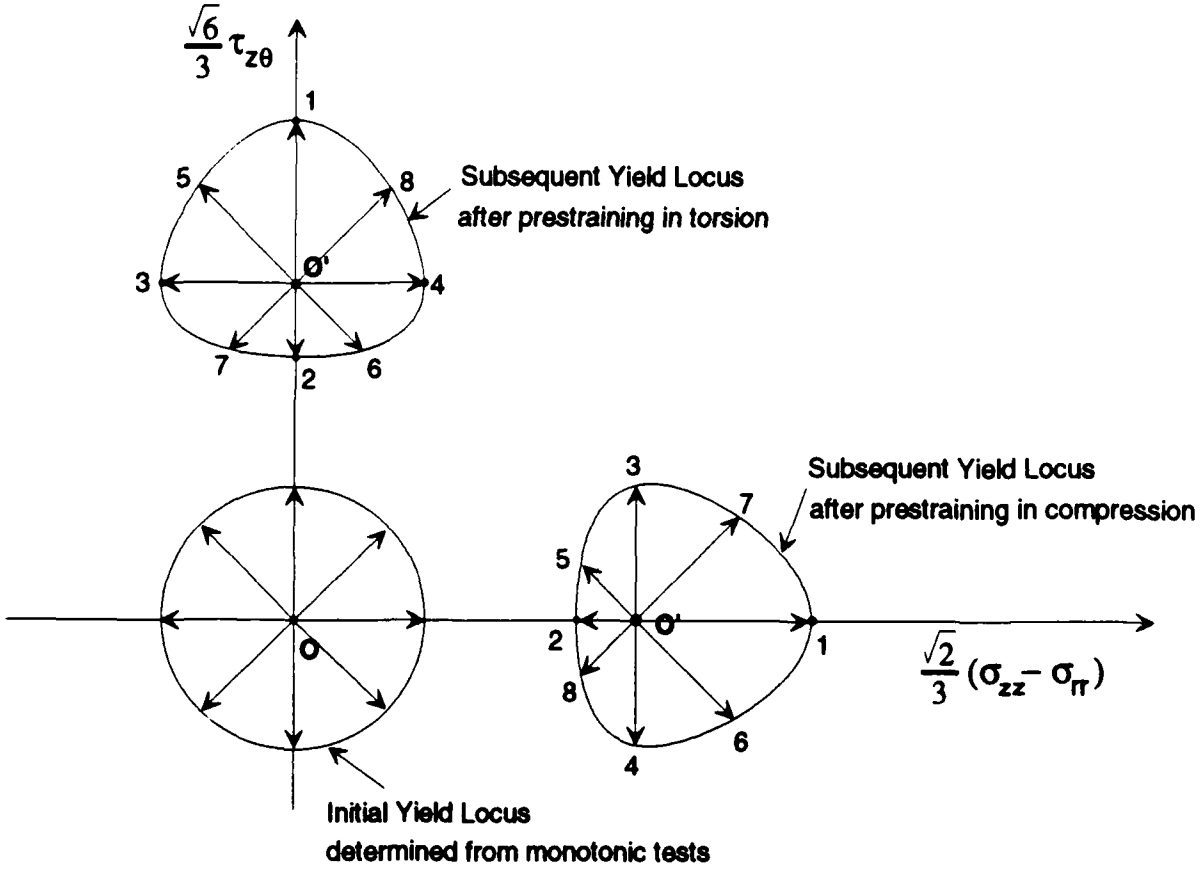

Fig. 59. Loading sequence followed for determining the initial and subsequent yield loci of granular media.

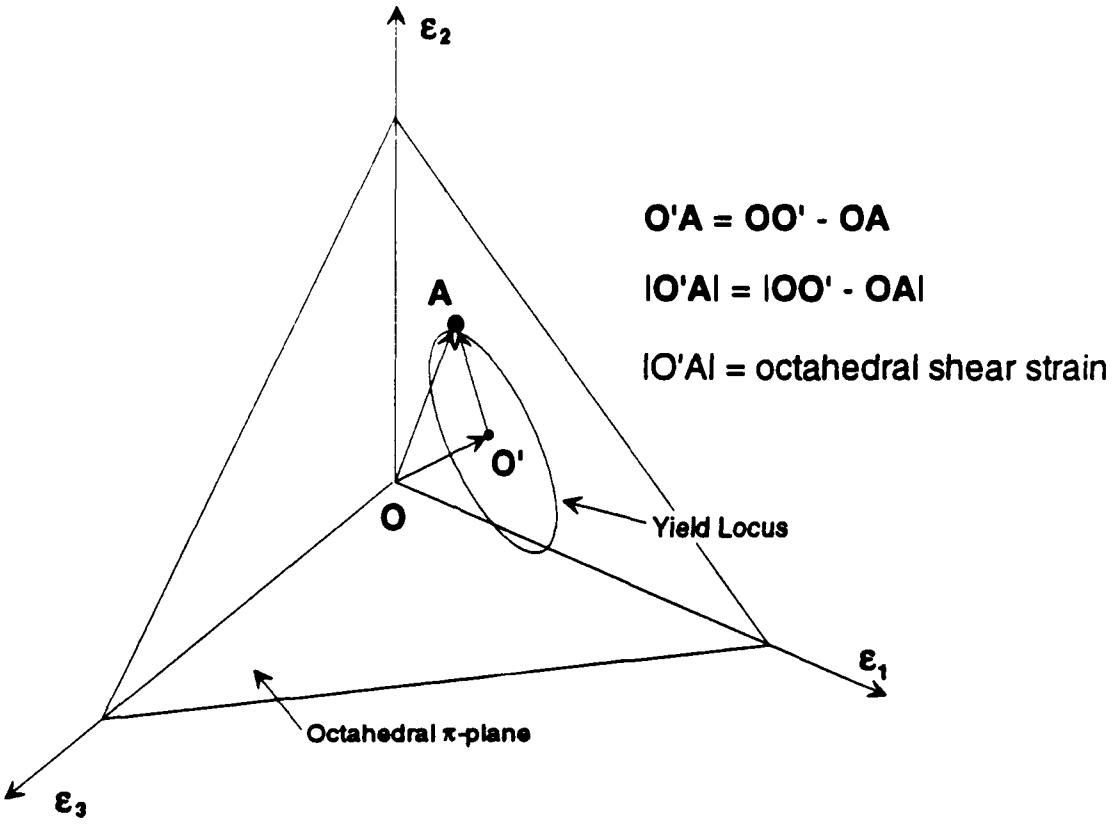

Fig. 60. Definition of yield surface based on octhedral shear strain criterion

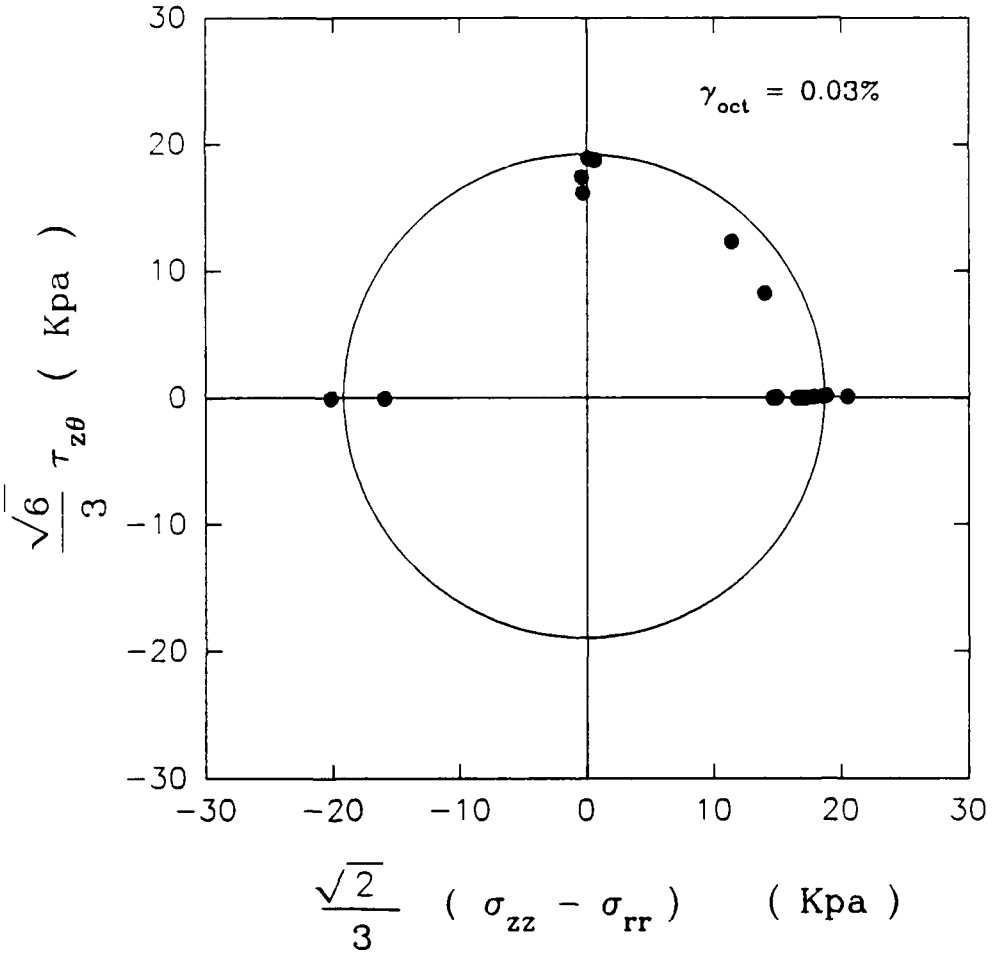

Fig. 61. Initial Yield locus determined from all monotonic proportional experiments

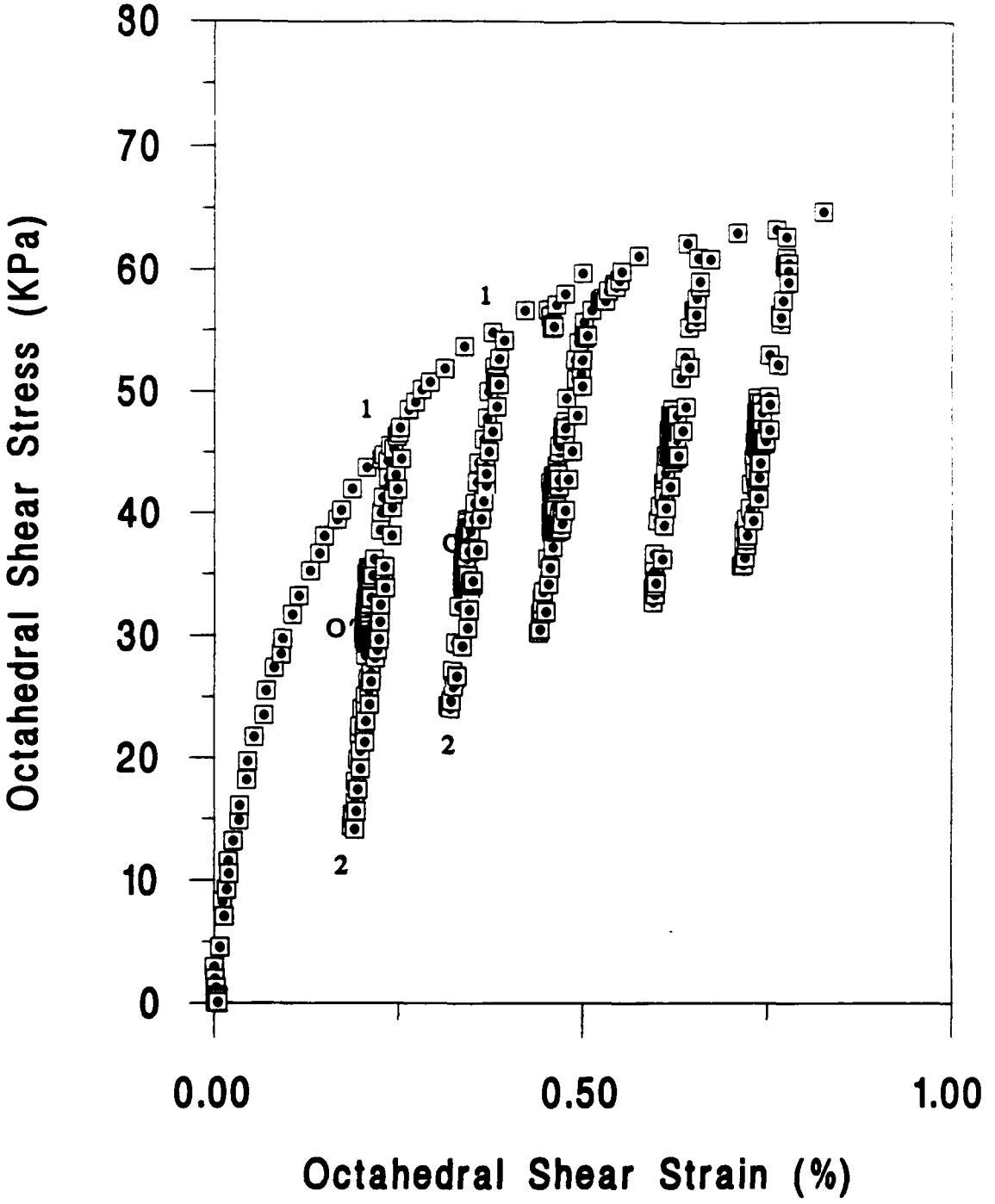

Fig. 62. Octahedral shear stress strain curve obtianed from probe test GB27 after prestraining in compression. Four points per yield locus investigation. Mean stress constant (138 KPa).

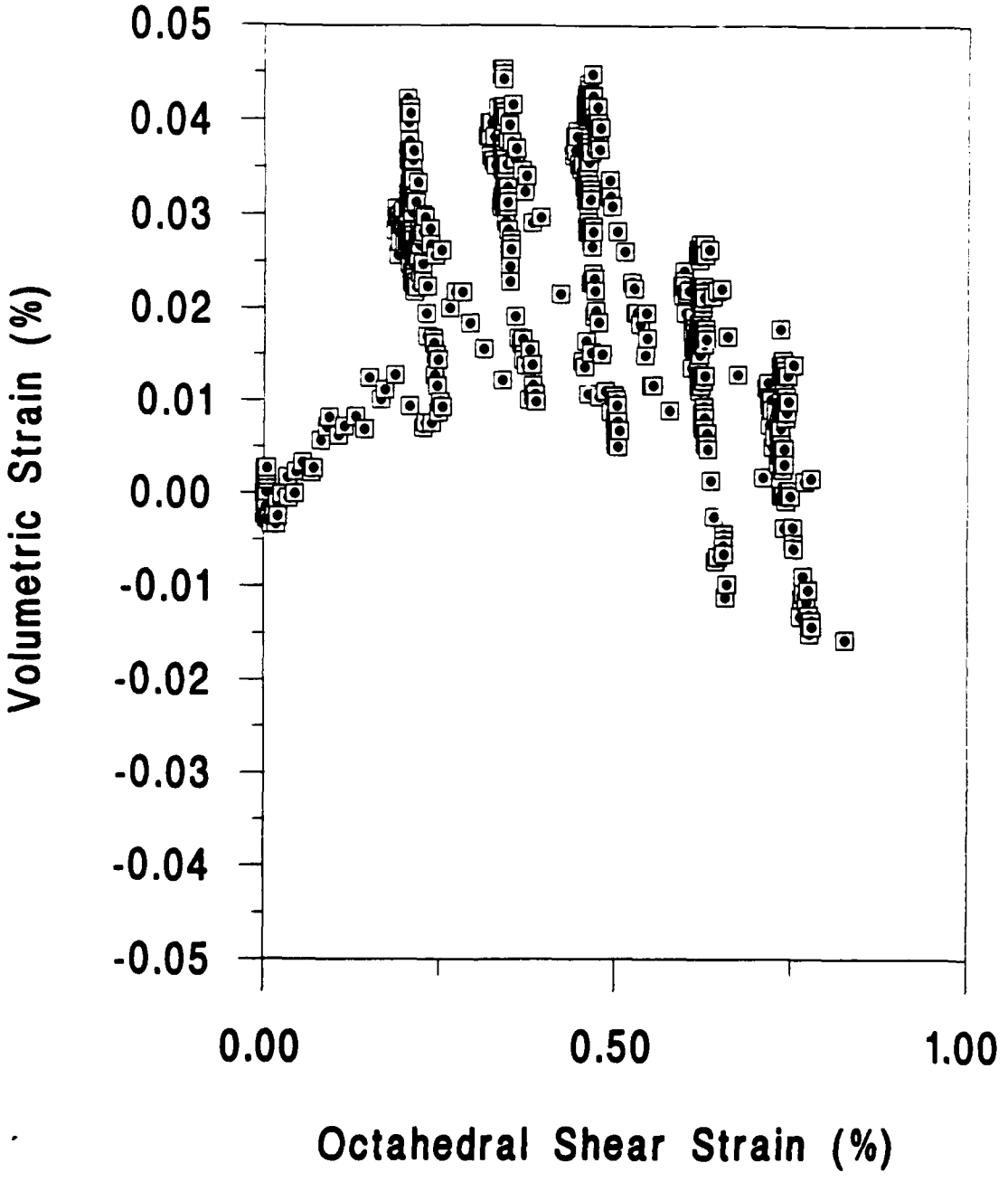

Fig. 63. Volumetric strain vs Octahedral shear strain curve obtained from probe test GB27 after prestraining in compression. 4 points per yield surface investigation.

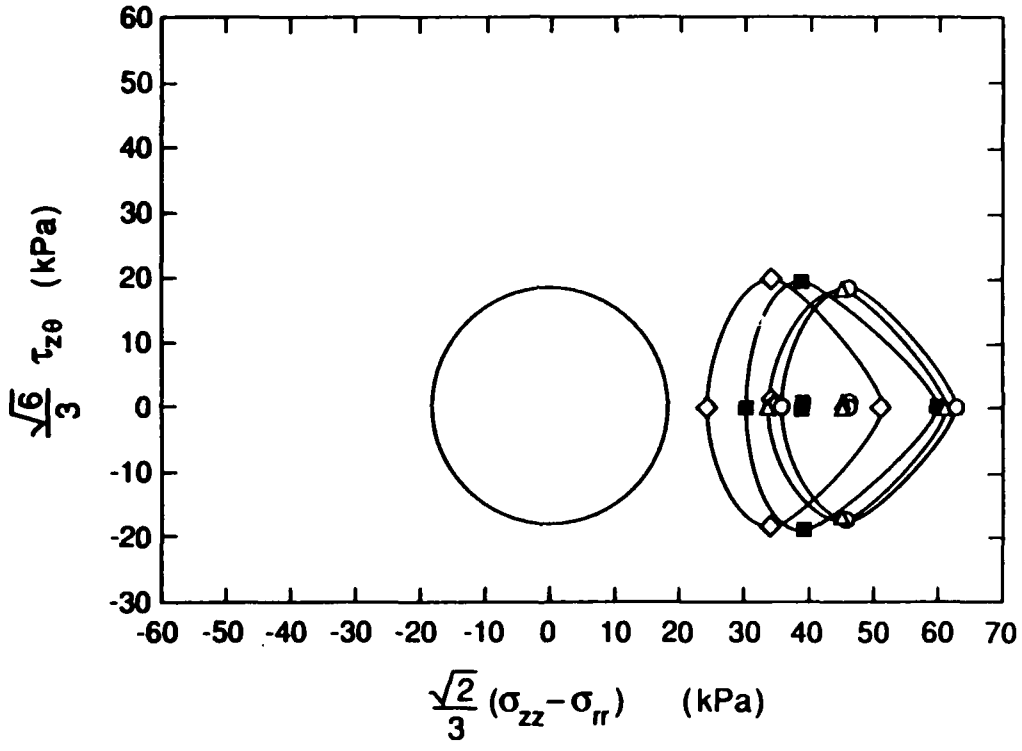

Fig. 64. Initial and subsequent yield loci determined after prestraining in compression (test GB27)

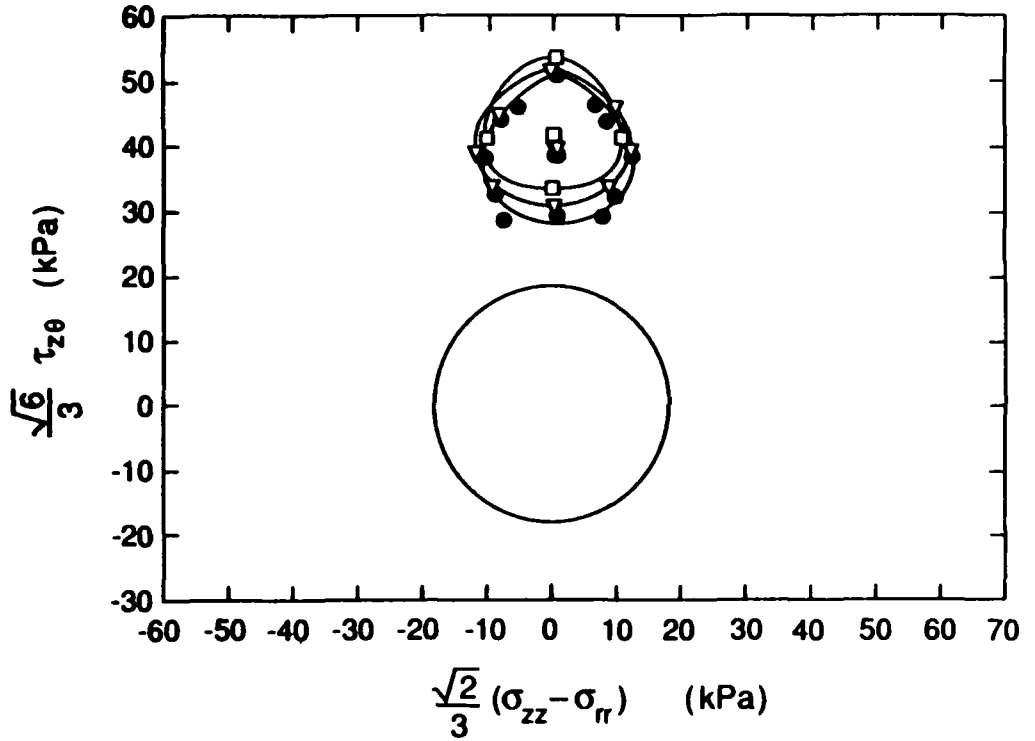

Fig. 65. Initial and subsequent yield loci determined after prestraining in torsion (test GB28)

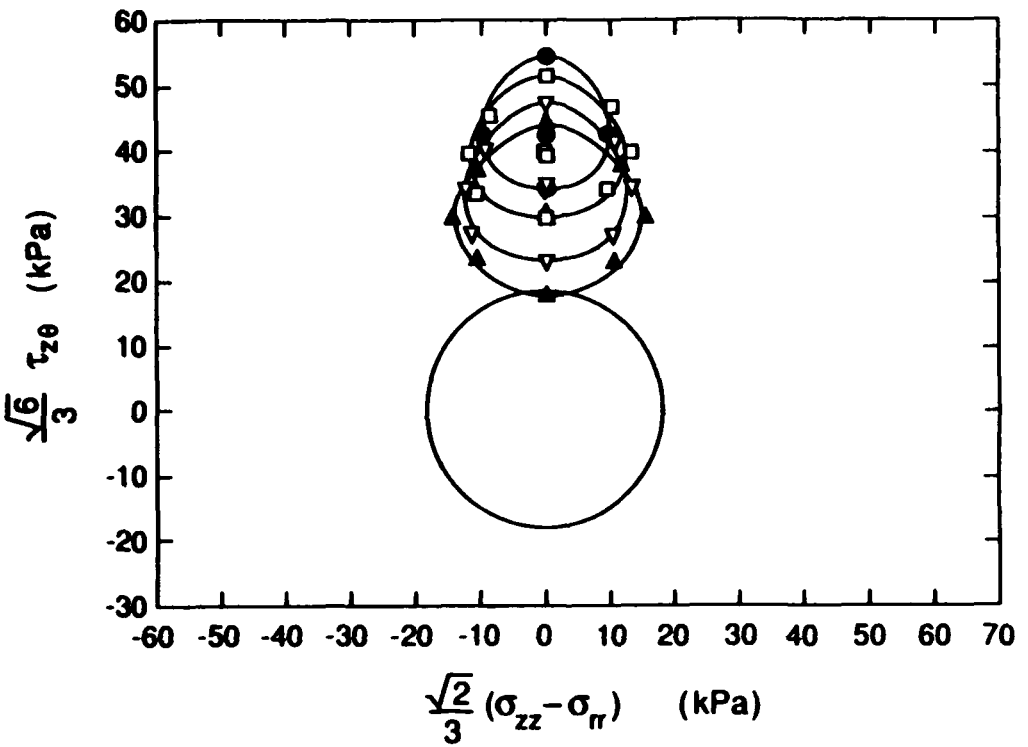

Fig. 66. Initial and subsequent yield loci determined after prestraining in torsion (test GB29)

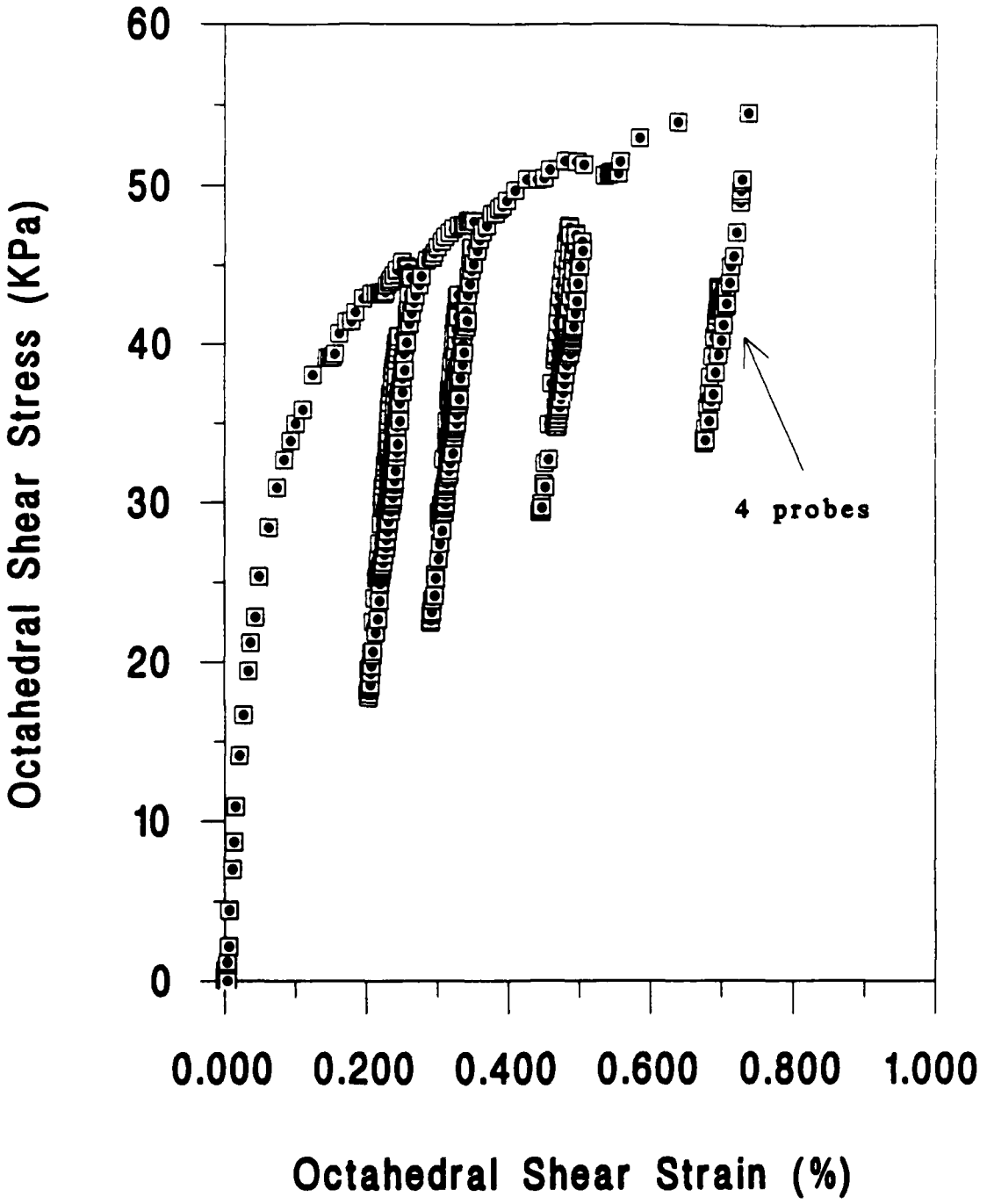

Fig. 67. Octahedral shear stress-strain curve obtained from probe test GB29 after prestraining in torsion. Either eight or four probes per yield locus investigation.

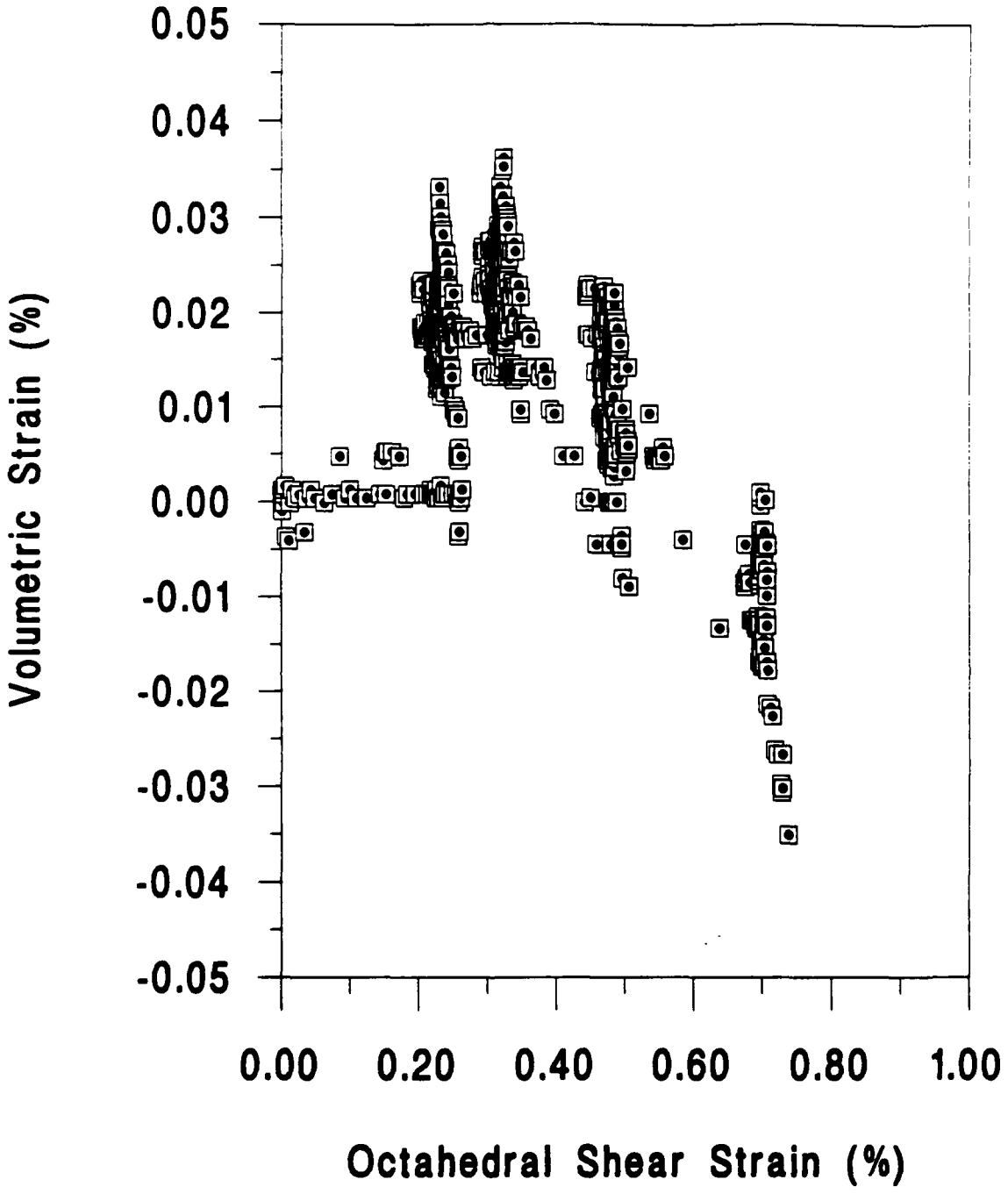

Fig. 68. Volumetric strain vs octahedral shear strain obtained from probe test GB29 after prestraining in torsion. Either eight or four points per yield locus investigation.

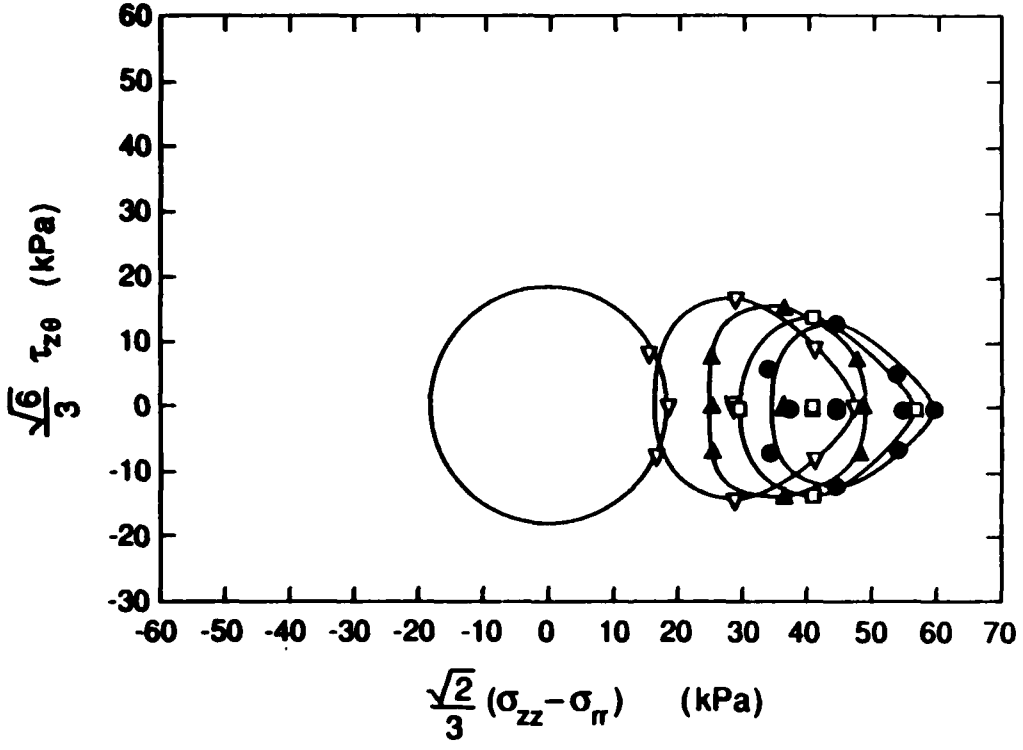

Fig. 69. Initial and subsequent yield loci determined after prestraining in compression (test GB30)

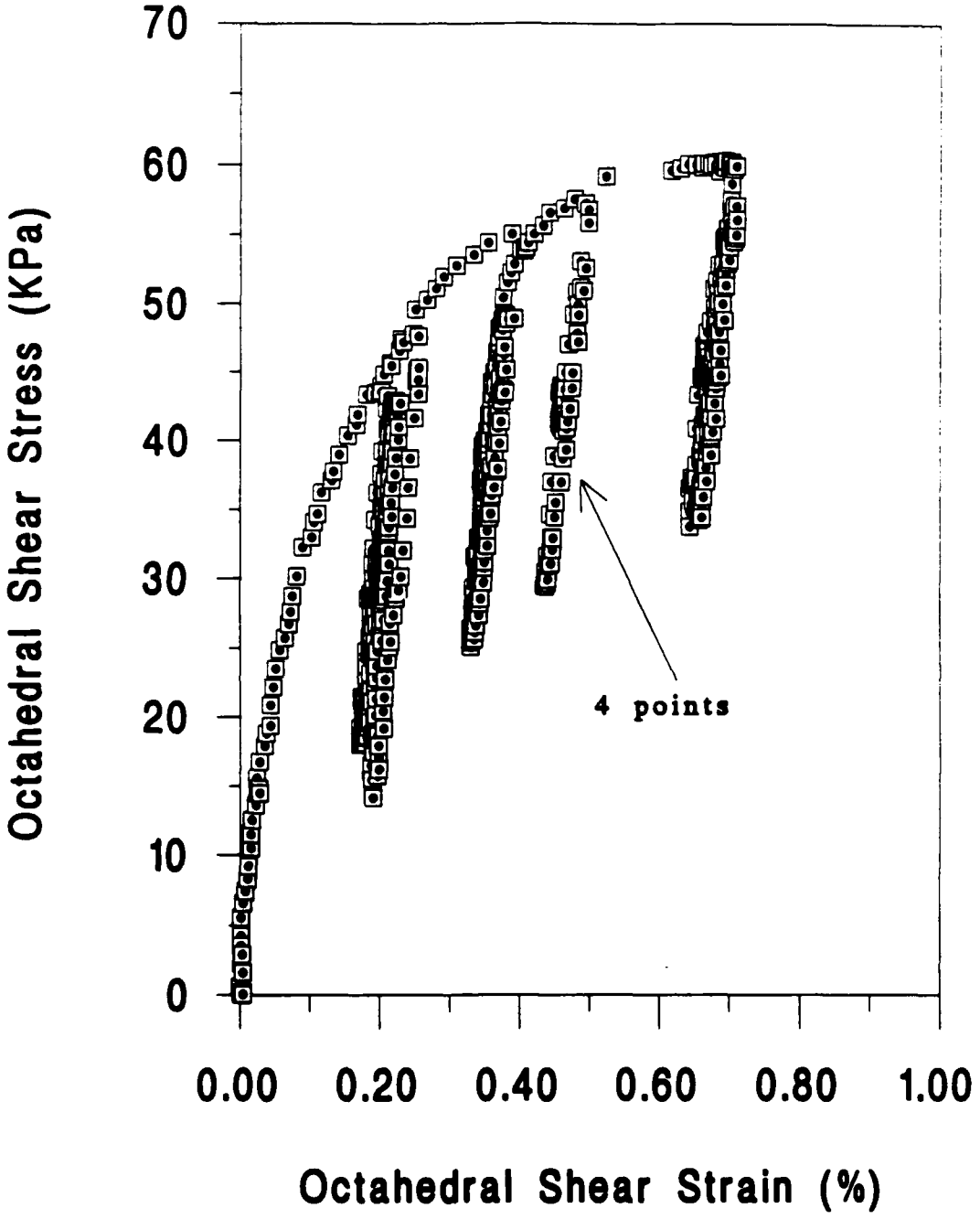

Fig. 70. Octahedral shear stress strain curve obtained after prestraining in compression from probe test GB30. Either eight or four points per yield surface investigation.

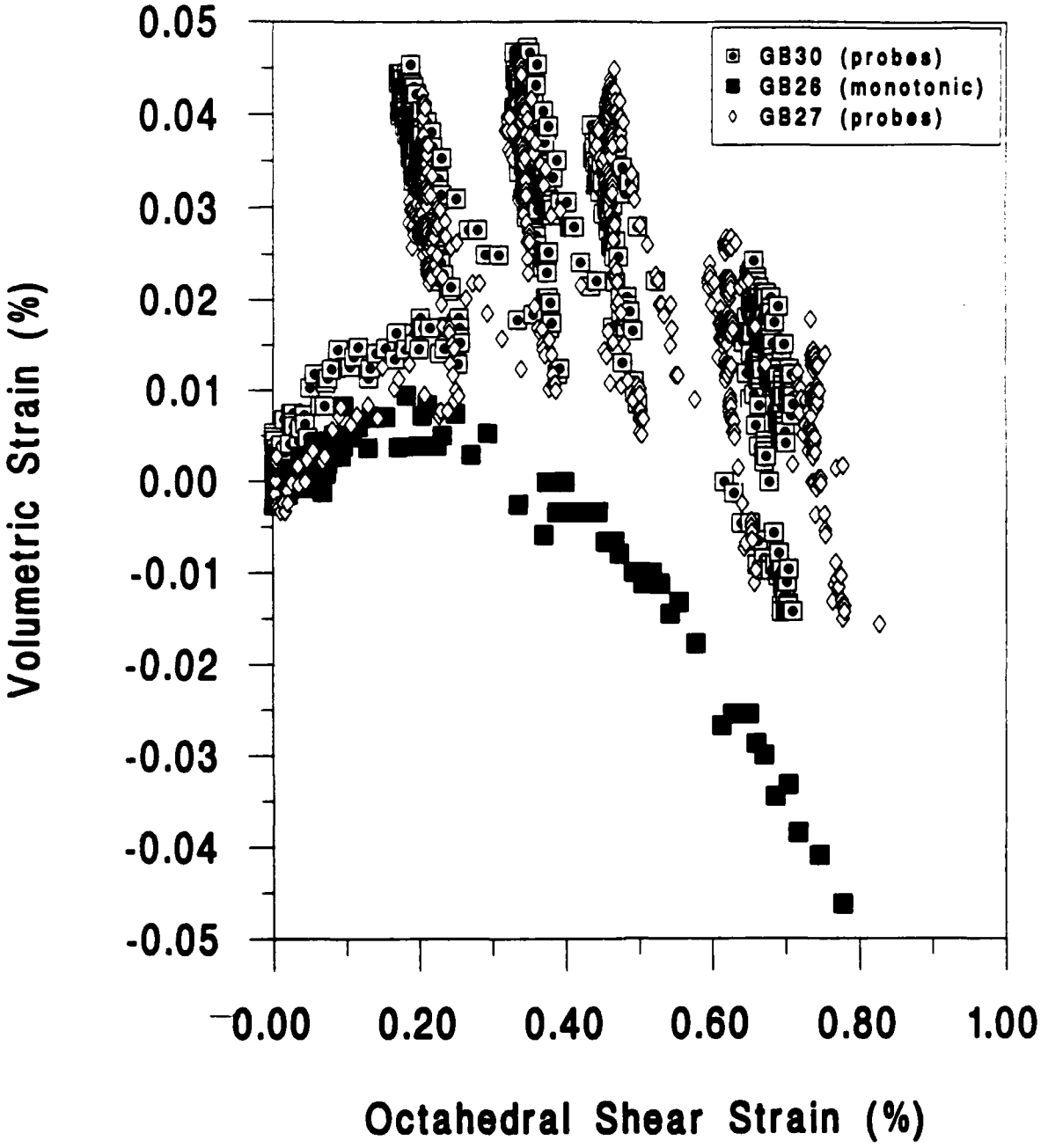

Fig. 71. Comparison between the volumetric strains caused by proportional monotonic and probe tests prestrained in compression.

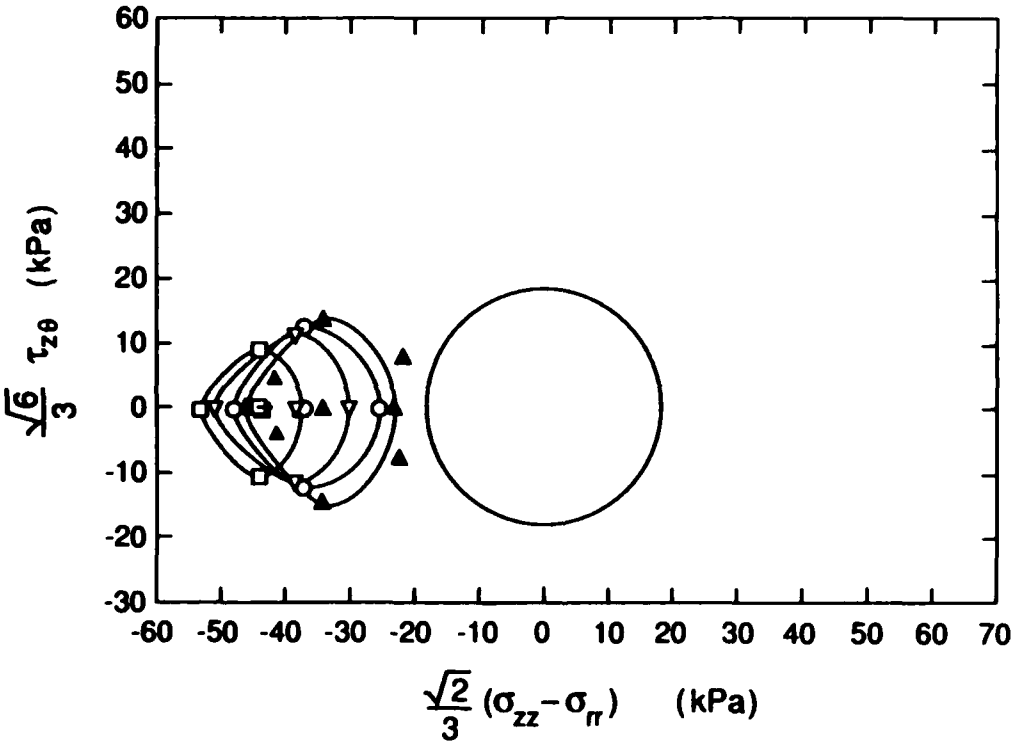

Fig. 72. Initial and subsequent yield loci determined after prestraining in extension (test GB33)

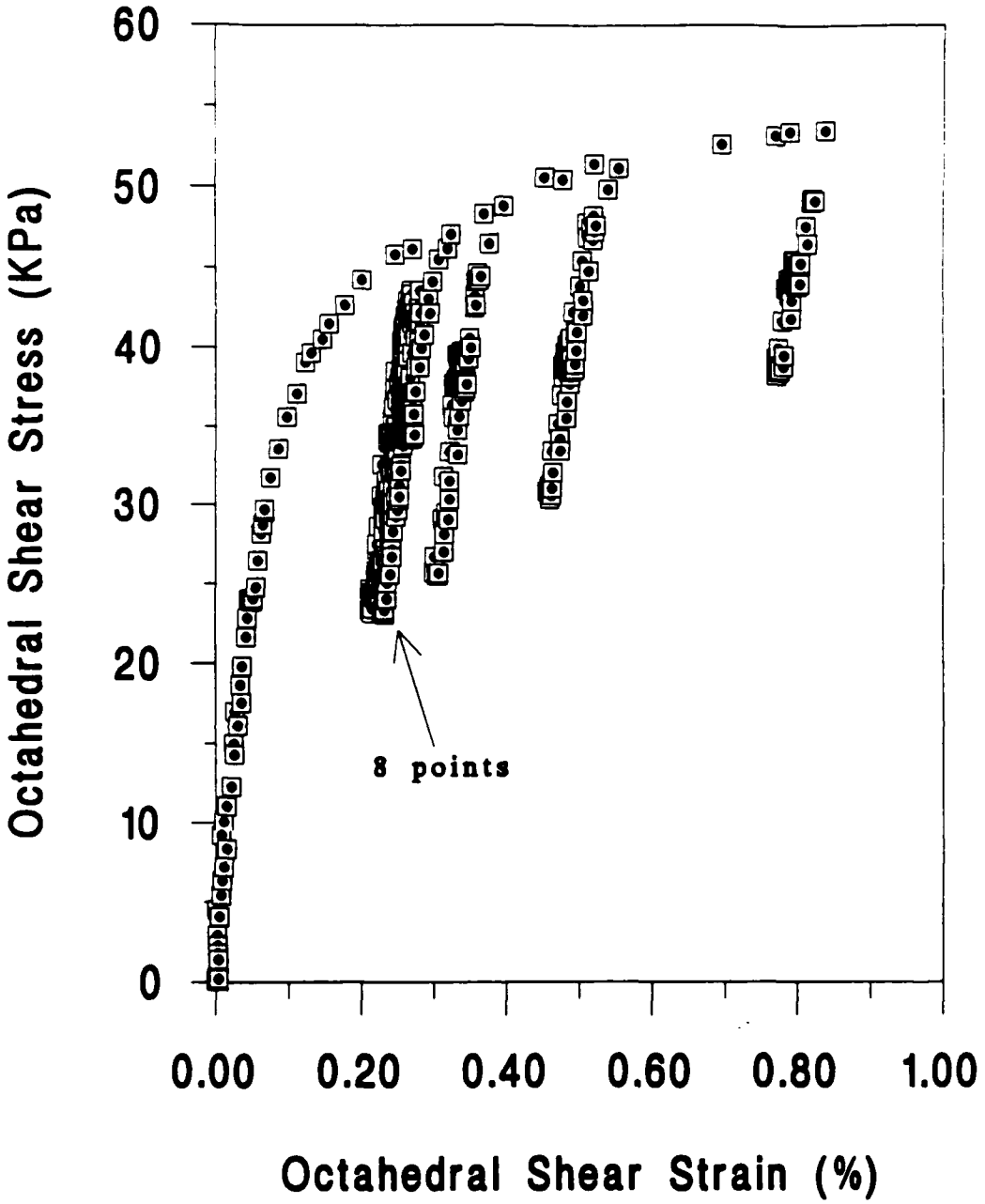

Fig. 73. Octahedral shear stress-strain curve obtained from probe test GB33 after prestraining in extension. Either four or eight investigations per yield locus.

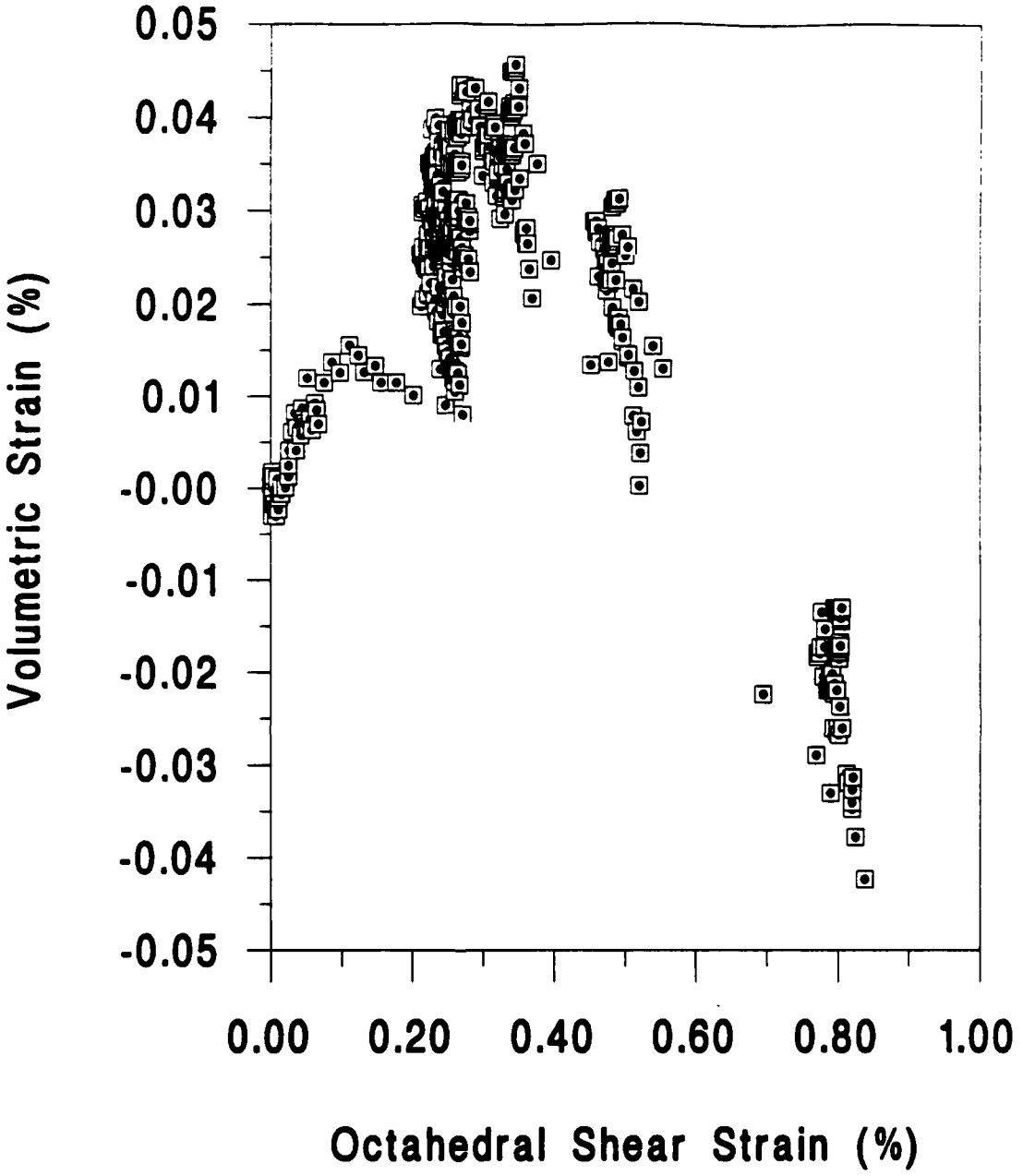

Fig. 74. Volumetric strain vs octahedral shear strain obtained from probe test GB33 after prestraining in extension. Either four or eightpoints per yield locus investigation.

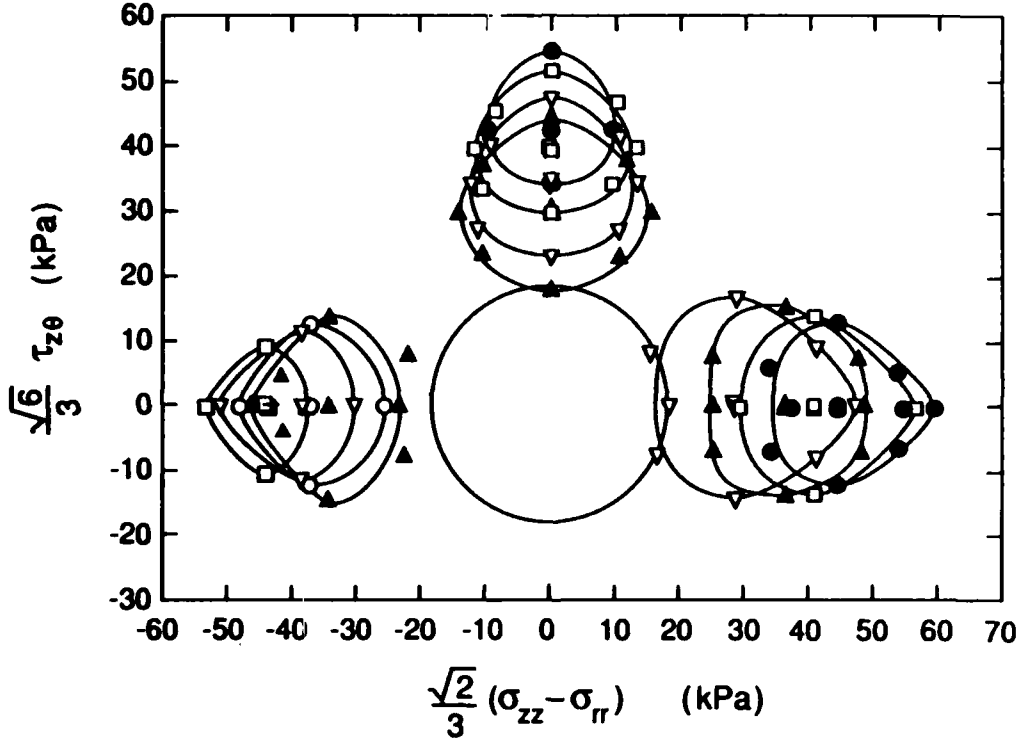

Fig. 75. Initial and subsequent yield loci for tests GB29, GB30, GB33

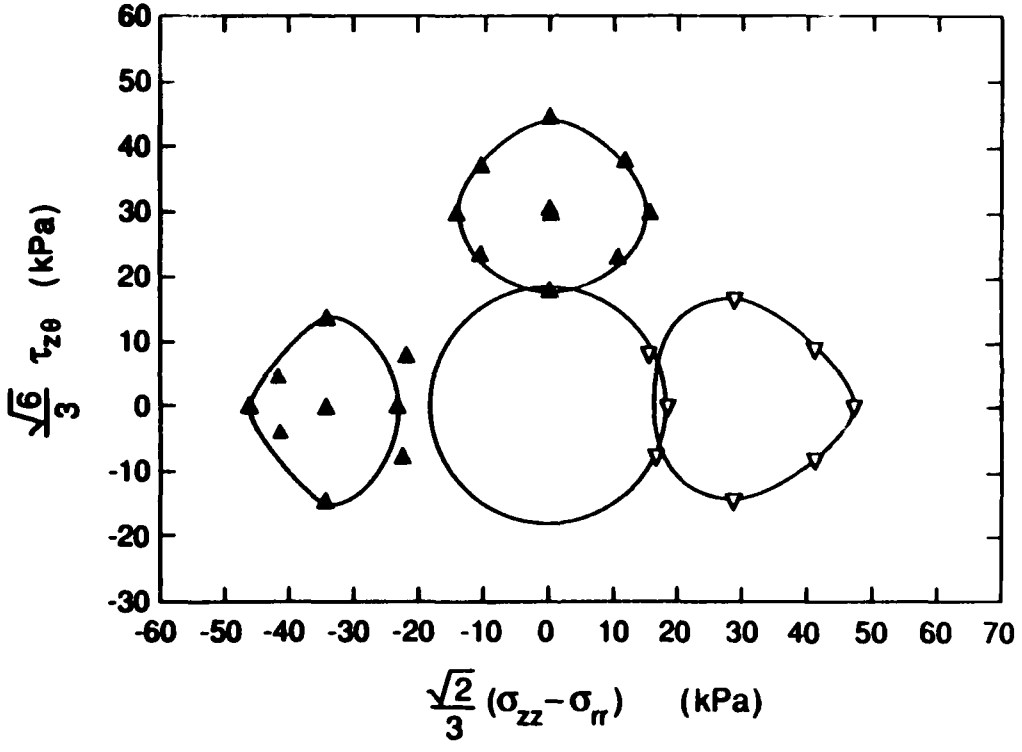

Fig. 76. Initial and first subsequent yield loci (after prestraining to γ_{oct} = 0.25%) for tests GB29, GB30, GB33